ABSTRACT

NORMAN, MICHAEL JAMES. Connectivity and Contraction in Cytoskeletal Networks. (Under the direction of Dr. Julio Monti Belmonte).

The cytoskeleton is a network of filaments and associated proteins inside each cell whose ability to contract and propagate forces is the fundamental mechanism behind cell morphology, division and migration. Fibers located near the inner membrane of a cell provide structure for the cell, determining its shape and function. Motor proteins can attach to fibers and, by consuming energy, walk along fibers, generating force that can reorganize fiber networks. The local interactions are well understood, but how those interactions translate into the global behavior of the cell is a long-standing question.

In this thesis, we examine how network geometry and connectivity contribute to global behaviors. We use intuition gained by studying the local fiber-motor rearrangement interaction known as polarity sorting to build a theoretical framework aimed at identifying conditions under which a disordered network can undergo contraction and whether this contraction results in multiple isolated structures or one structure incorporating all elements of the network. The key idea is quantizing the connectivity formed by direct geometric intersections between individual fibers and motors. We show that this interconnectivity is a function only of fiber and motor densities and the associated length distributions.

We validate our predictions with agent-based computer simulations and a new metric capable of distinguishing between contraction outcomes. All results are independent of filament rigidity, making our findings applicable to both actin and microtubule networks. Other potential fiber properties such as dynamic growth are also shown to be irrelevant. We then discuss how those outcomes are affected by the introduction of crosslinking proteins, which, despite not actively generating forces of their own, can promote global contractility at small doses even for

networks made of short and/or rigid filaments. We explore the effect of spatial boundary conditions on contraction behavior. Finally, we show that our results can be applied to systems with fiber turnover, which are of particular importance to the early development of organisms.

We then adapt our connectivity approach to the construction of cytokinetic rings, which are vital structures for cell division. Working with the Carvalho experimental group, we are able to predict the conditions under which cytokinetic rings are formed and identify the role crosslinker variants have in the formation and maintenance of cytokinetic rings.

We conclude that geometry and connectivity metrics developed through simple physical intuition are powerful tools for studying the biologically complex network of the cytoskeleton. Our results can be applied to a diverse set of environments and structures and provide a baseline for future theoretical and experimental explorations of other contraction mechanisms.

Connectivity and Contraction in Cytoskeletal Networks

by
Michael James Norman

A thesis submitted to the Graduate Faculty of
North Carolina State University
in partial fulfillment of the
requirements for the degree of
Doctor of Philosophy

Physics

Raleigh, North Carolina
2025

APPROVED BY:

Julio Monti Belmonte Committee Chair	Mary Elting
Nicolas Buchler External Member	Alexander Kemper

BIOGRAPHY

Michael Norman is a PhD student working under Julio Belmonte in the Physics department at North Carolina State University. They have previously received a Master of Science in Physics from the Georgia Institute of Technology and a Bachelor of Science in Physics and Math from the University of Michigan, Ann Arbor. Their research interests are the geometric and mechanical properties of biological networks, and their professional interests are in university level physics education. Before enrolling at NC State, they taught introductory physics full time for three years and hopes to return following the completion of this degree program.

TABLE OF CONTENTS

LIST OF TABLES

LIST OF FIGURES

Chapter 1 Introduction to the Cytoskeleton

1.1 Introduction

The ability of cytoskeletal networks to generate contractile forces is fundamental to proper cellular function. This biological network of fibers, molecular motors and crosslinking proteins dictate fundamental features and behaviors of cells, such as morphology, migration and division. (An image of the cytoskeleton can be seen in **FIG 1.1**) In order to function, a sufficiently dense collection of cytoskeletal components generate force and construct large scale structures capable of propagating those forces across the cell. On a microscopic level, the method through which a single myosin motor consumes energy and generates force on a single fiber is relatively well understood. The method through which these randomized local forces lead to predictable global behaviors is not.

The primary goal of this work is to investigate the geometric conditions of the network that allow for the translation of local forces into global contraction through a mechanism known as polarity sorting. We present a theory about how the densities of fibers and motors can determine the appropriate connectivity of a network. New metrics will be developed to measure the state of a network and determine numerically whether a network has undergone contraction. Our predictions will be tested using simulated cytoskeletal networks built using the software CytoSim. Ultimately, we will show that the interconnectivity of fibers and motors is predictive of

the ability of a semi-2D network to restructure a randomly ordered collection of fibers into large scale structures such as asters and contract semi-1D networks such as cytokinetic rings.

In this introductory chapter we will discuss previous work done studying the relationship between force generation, network connectivity and contractile behaviors. We will then describe the three broad categories of components we identified as crucial for network contraction, the details of how forces are generated, and the type of connectivity required to drive structure formation. In the following chapters, we detail the theory we created to predict contractility, the methodology used to simulate networks, the tools we created to measure systems and test predictions, and the results of such tests. We detail how our idea of connectivity can be adapted to the study of cytokinetic rings through collaboration with experimentalists. Finally, we discuss how this work can be used as a baseline for future research into other contraction mechanisms.

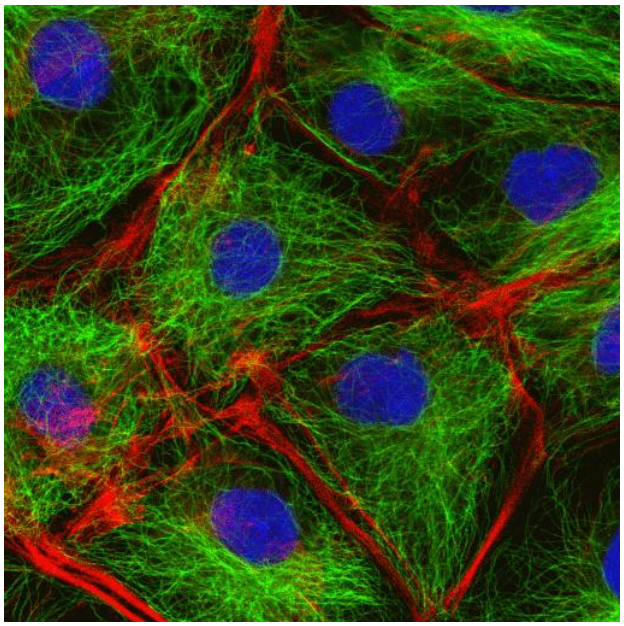

FIG 1.1: The Cytoskeleton *An image of a collection of animal cells. Stains are used to distinguish between components with actin in red, microtubules in green and the nucleus in blue. Images collected by Mark Shipman, James Blyth and Louise Cramer, Laboratory for Molecular Cell Biology, University College London, UK.*

1.2 Cytoskeletal Components

1.2.1 Fibers

The fundamental proteins that constitute a cytoskeletal network are the fibers, which can be found throughout the interior of all cells and are particularly dense in the cell cortex, which is the thin layer of actin fibers that sits beneath the cell membrane. Fibers provide the structure of the network and many cell behaviors depend on the interactions between the fibers, the cell membrane and individual proteins that can bind to the fibers (Doherty et al 2008). The structure of the fiber network provides the foundation for a cell's overall external morphology, which dictates the role the cell has as part of a larger organism. A large collection of well-ordered fibers is necessary for many cell functions. Lamellipodia and filopodia are protrusions made of ordered fibers that allow the cell to sense and move in its environment. In the final stage of mitosis, fibers throughout the cortex migrate towards a central cytokinetic ring that then constricts, physically separating a cell into two daughter cells.

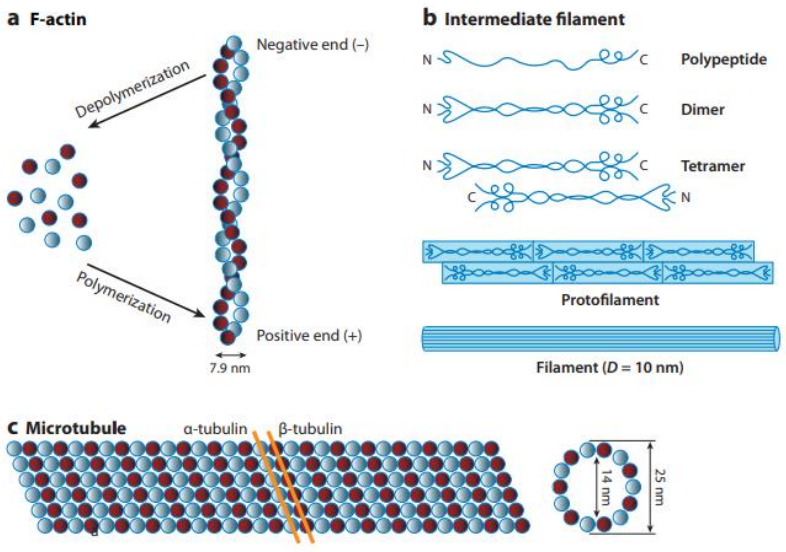

FIG 1.2: Cytoskeletal Fibers *Modelled structure of the broad categories of fibers in the cytoskeleton. Taken from Mofrad, M. R. (2009).*

As seen in **FIG 1.2**, fibers can be divided into three categories: actin, microtubules and intermediate filaments (Mofrad 2009). For our purposes, the defining features of actin are a relatively high flexibility (with a rigidity of $0.075\ pN\mu m^2$ (Gittes et al. 1993)) and geometric polarization. Actin fibers (or F-Actin) are formed by the polymerization of G-Actin monomers into a twisted chain up to several microns long. Each G-Actin contains a structural polarity and will only bind with each other (+) end to (-) end. This creates an overall polarity for the entire fiber (**FIG 1.3**), which can be sensed by proteins bound to the fiber. While polymerization and depolymerization of F-actin happens at both ends, G-Actin monomers typically bind to the chain at the barbed end (+) and unbind at the pointed (-) end. Actin is one of the most abundant types of protein in a cell and there is a large collection of other proteins that can bind to actin which are the focus of a large body of research (Winder et al 2005).

FIG 1.3: Simplified Fiber *The most fundamental representation of a fiber used in the presentation of theory, displaying the extended 1D nature of a fiber with a barbed (+) end on the right and pointed (-) end on the left.*

Microtubules are hollow tubes made of a spiral of dimers made of **α** and **β** tubulin monomers. Like actin, they are geometrically polarized. They primarily grow and shrink at the positive end and often undergo a rapid depolymerization of the entire fiber from the plus end known as catastrophe (Gardner et al 2013). For our purpose, their defining feature is a rigidity multiple orders of magnitude higher than that of actin (with a rigidity of $22\ pN\mu m^2$ (Gittes et al. 1993)).

Intermediate fibers have a rigidity between actin and microtubules. These fibers possess a large range of properties and roles within the cell. One key distinction from actin and microtubules is the fact that these fibers are not geometrically polarized and cannot serve as a medium for molecular motors to slide them and generate forces. Therefore, we will not explicitly be considering this type of fiber throughout this work.

1.2.2 Motors

While fibers form the structure of the cytoskeletal network, they are passive objects that cannot generate work or drive their own organization. This role is played by a large collection of binding proteins. Molecular motors drive motion both microscopic and macroscopic throughout a body. Cytoskeletal motors that are free floating in the cytoplasm can stochastically bind to and

unbind from nearby fibers and use the energy released during the hydrolysis of captured ATP to perform work by pushing the fiber a few nanometers behind the motor (Bustamante et al 2004). As shown in **FIG 1.4**, a motor monomer consists of a long tail domain and a head domain capable of binding to a fiber. Two tail domains coil to form a dimer, which forms a legs-like structure capable of walking along the fiber. The function of the motor is then typically defined by the purpose of the tail domain. For many motors, multiple motor tail domains twist together to form a bipolar motor bundle capable of walking along multiple fibers simultaneously (**FIG 1.4B**). The crucial parts of this geometry can be modelled as in **FIG 1.5**. Later in this chapter, we detail how this is the primary method for cell wide force generation and network restructuring. For other classes of motors, the tail is instead capable of capturing and carrying cargo. This role is crucial for transporting material between the cell membrane and nucleus (Ross et al 2008).

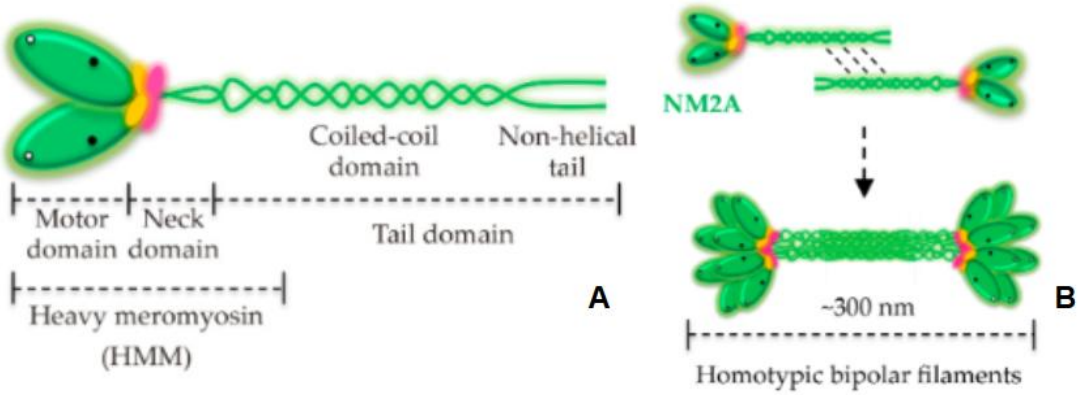

FIG 1.4: Non-Muscle Myosin II *Modelled structure of Non-Muscle Myosin two. (A) Myosin dimer, with two binding heads and intertwined tail domains. These heads work together to take steps along a fiber. (B) The tail domains of many dimers are wrapped together to form a fiber bundle with heads concentrated on both ends joined by a bare zone. Images adapted from Brito, C., & Sousa, S. (2020).*

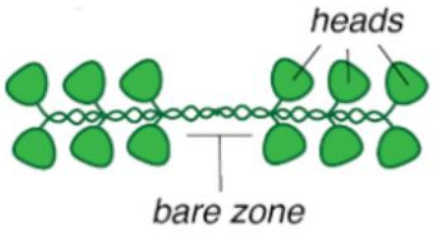

FIG 1.5: Simplified Motor *The fundamental representation of molecular motor, used in the presentation of theory displaying independent motor heads attached to a straight backbone with a bare zone in the middle.*

This work will focus on the force generating potential of motor bundles. There are three broad categories of motors with a variety of geometries that walk along cytoskeletal fibers: myosin, kinesin and dynein. Myosin alone has a large number of subcategories (Hodge et al 2000, Odronitz et al 2007) with a wide range of structures, behaviors and functions. This work will take as a model protein the bundled Non-Muscle Myosin II type motor, with a focus on its ability to bind to multiple separate fibers and walk towards the barbed end. This is a very common motor type found in a wide collection of cell types and is of particular importance to the large-scale structure formation we are interested in (Brito et al 2020). Kinesin and dynein have different structures and purposes within the cell, such as the ability to carry cargo or walk towards the pointed end. We will not consider them in this work since our goal is to examine the effects of the geometric, not biochemical, properties of motors.

1.2.3 Crosslinkers

The other category of binding protein we will consider is the crosslinker. Much like the molecular motors, crosslinkers can be found throughout the cytoplasm and will bind to nearby

fibers. Crosslinkers do not consume energy and do not move while attached. Crosslinkers typically have two binding domains and, when bound to a pair of fibers, they can provide local stability allowing for certain types of contraction and long-term global stability to cytoskeletal structures created by the interaction between fibers and motors. The structure and exact function of crosslinkers vary widely across the large collection of crosslinker types, but their contribution to contraction is dependent on other network components and microscopic contraction mechanisms. As discussed in the next section, we will primarily discuss a mechanism where crosslinkers play a minor role. Therefore, we will work with a simple generic model where two binding heads are connected by a short, stiff spring. Chapter 6 will briefly discuss how different crosslinker geometries can affect the contraction of structures like the cytokinetic ring.

1.2.4 Other Associated Proteins

There are many other proteins potentially present in a living cell that serve a wide variety of functions. Nucleating proteins like formin are required to collect and bind G-actin monomers into a full actin fiber. The Arp2/3 complex binds to an existing actin and begins the growth of a new fiber at set angle, creating a large, ordered branching actin network. This process is crucial for structures like lamellipodia, which are needed for directed cell migration. Many different proteins are needed to regulate the growth and size of fibers. Actin capping proteins are able to bind to the barbed end and stop all further growth. Proteins like severin are capable of severing actin fibers, meaning an ordered network can be rapidly disassembled and prepared to contract again. Similar to how crosslinkers can bind fibers to other fibers, many proteins exist that bind

fibers to other cell structures. Moesin and ezrin connect fibers to the cell membrane, which is crucial to translating internal network behavior into external cell behavior.

All these proteins play a role in the creation and maintenance of cytoskeletal networks but are not directly related to contractile behavior. We will ignore the individual contributions of these proteins. When needed, the end result of their functions will be built directly into our simulation models. For example, when working with fiber dynamics, we will create fibers of a given length without actually polymerizing them. Instead of individual proteins driving the collection or loss of individual monomers, the fibers will simply increase or decrease in size. Since our focus is on the geometry of the network, the loss of biochemical detail should not affect our results.

1.3 Methods of Local Force Generation

The methods through which the combination of fibers, motors and crosslinkers are capable of generating local forces are relatively well understood. How motors translate their walking motion into the motion of attached fibers depends on the geometry, organization and biophysical properties of the components. When the network is highly organized, translation of local behavior into global contraction is well understood. While common in muscle tissue, most cells lack this definitive structure, and fibers are allowed to move freely in multiple dimensions. In these disordered networks, the relationship between local and global behaviors is not clear. In this section, we will describe the local methods of force generation in order to lay the foundation of how we will explore the relationship between network connectivity and contractile behavior.

1.3.1 Sarcomeric Contraction

In muscle tissue, fibers and motors are highly organized into a regular structure called a sarcomere, which effectively constrains fibers to slide in one dimension (**FIG 1.6**). The barbed end of each fiber is attached to a Z-line, while the body is bound by a motor bundle. As motors step, due to the strict organization, they pull the pointed ends of fibers towards one another. This pulls adjacent Z-lines with them. When repeated over more identical structures, causes large-scale contraction of the muscle. Through this process, the local interaction of fibers and motors generate local forces which are translated into global behavior.

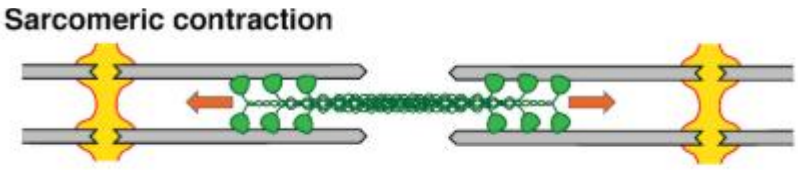

FIG 1.6: Sarcomere Schematic *Diagram of a sarcomere, which uses highly organized fiber and motor interactions to generate long range forces. All motors walk together towards the yellow Z-lines, sliding the fibers together. When repeated over many copies, full muscles contract allowing macroscopic organisms to apply forces on their environment.*

1.3.2 Polarity Sorting

The simplest contraction mechanism, and the primary interest of this work, capable of restructuring a diffuse, disordered network of fibers is known as polarity sorting (Kruse et al 2000). This mechanism can be found in a large number of biological systems, including networks composed of microtubules (Surrey et al 2001) and actin (Wollrab et al 2019). Polarity

sorting can occur if the motors in the network possess the property known as end dwelling. Upon reaching the end of the fiber, the motor head will remain bound to the fiber instead of automatically unbinding. Without end dwelling, the motor will detach from the fiber as soon as it reaches its end.

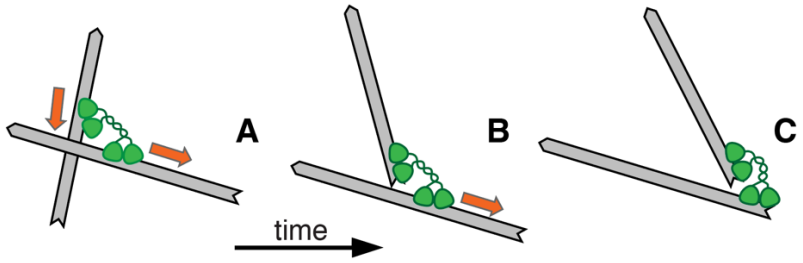

FIG 1.7: Polarity Sorting Schematic *A diagram showing the stages of polarity sorting. (A) A motor binds to two fibers at some point along their lengths. Each motor domain walks towards the end of its fiber. (B) One domain has reached the end of the fiber and dwells there while the other continues to walk. This configuration pulls the ends of the two fibers together until (C) both fibers have reached the end of their fibers. Overall, this motion tends to pull fibers together and when repeated over a large network will contract all fibers into a similar location.*

FIG 1.7 shows the time evolution of a pair of fibers bound to the same motor undergoing polarity sorting. Initially the fibers are uncorrelated in both position and orientation, only needing to be close enough for a single motor to bind to both. The two independent motor heads walk towards the end of their respective fiber until one end is reached. The motor head will dwell there keeping the fibers connected as the other continues to move. Since the fibers are geometrically polarized, this movement draws the same ends of the two fibers together as well as rotating the fibers so that they are more parallel than the initial state. Once all walking has been exhausted the fibers are now correlated in both position and orientation. Even if the motor detaches from one or both of the fibers, the fibers position will remain sorted if fiber diffusion timescales are longer than the sorting process.

If the network is sufficiently dense and connected, these sorted fibers will be able to form a motor bound pair with a new neighbor and the sorting process will begin again. This will bring the new fiber into alignment with both of the original fibers. When repeated over an entire network, most fibers in the network will be simultaneously sorted with their neighbors. The barbed ends of all fibers will end up in a similar position.

The exact result depends on the boundary conditions of the space. In an open, flat space the end result is a structure known as an aster, a disk-like structure of fibers with each pointed radially inward towards a common center. (Spaces with periodic boundary conditions are discussed in Chapter 2.5, and the behavior of fibers restricted to the surface of a cylinder is discussed in Chapter 6.) The radius of these asters will approximately cover the area of a circle with radius equal to the length of the fibers, i.e., $\pi {L_F}^2$, where L_F is the average fiber length. Since all fiber have been sorted in a similar position as their neighbors, the resulting structure will be more compact than the initial disordered network. Specifically, the initial area covered by the fibers must be sufficiently bigger than the area covered by the aster. Thus, polarity sorting is a mechanism that turns the local forces generated by a walking motor protein into a system-wide organization and contraction of the network's fibers.

As stated, global sorting will only occur when the network is sufficiently connected. Determining what exactly it means to be sufficiently connected is the ultimate goal of this work. Focusing on this mechanism is reasonable since both microtubule networks (Zemel et al 2008, Rao et al 2018) and actin networks (Wollrab et al 2019) are known to contract through the polarity sorting mechanism.

1.3.3 Buckling

The next contraction mechanism, known as buckling (Costa et al 2002, Li et al 2017), requires more conditions to be met in order to function. Firstly, the fibers must be flexible. This means buckling is common in actin systems, not in microtubule ones, making it less universal than polarity sorting. Secondly, buckling can occur if crosslinkers are present in addition to fibers and motors. It is also possible to drive buckling when motors of differing speeds are simultaneously present in the network.

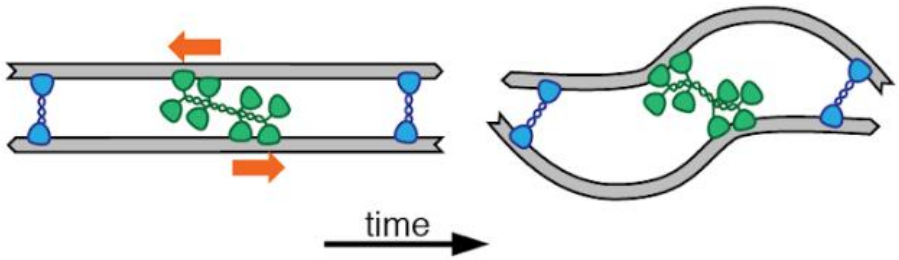

FIG 1.8: Buckling Schematic *A diagram showing the stages of buckling. Contraction through buckling can occur when a pair of flexible, antiparallel fibers are bound by both a motor and crosslinkers. The two motor heads walk in opposite directions, thus pushing the fibers in opposite directions. However, since the fibers are prevented from sliding by the crosslinkers, the force is instead used to bend the fibers, ultimately decreasing the distance from the ends of the fibers.*

FIG 1.8 shows the time evolution of the buckling process in the presence of crosslinkers. Beyond the basic behavioral conditions of the individual components, geometric conditions must also be met. The process requires a pair of fibers with opposite orientations to be bound by multiple crosslinkers as well as a motor. As with polarity sorting, the motor heads will attempt to walk towards the barbed ends of their respective fibers. Since the fibers are antiparallel, this will

tend to slide the fibers over each other in an attempt to sort the barbed ends together. However, the presence of the bound crosslinkers means the relative orientations and positions of the fibers are locked in place and no sliding can occur. The force instead will become compressive on parts of the fiber while expansive on the others. Since fibers can bend but not stretch, if the fibers are flexible, the structure will buckle. This will bring the ends of the fibers closer together, ultimately decreasing the size of the local structure. As with both sarcomere contraction and polarity sorting, if one or both of these fibers are bound to another fiber in the appropriate configuration, the process will repeat again and again, and the local contraction will propagate to become global contraction across the entire network. The end result of buckling tends to lack the predictable aster structure of polarity sorting since the exact amount and direction of buckling will be dependent on the particular positioning of the fibers, motor and crosslinkers in the buckling structure which cannot be predicted or controlled. This makes studying buckling in a systematic way significantly more difficult than analyzing polarity sorting. In Chapter 7 we briefly discuss preliminary attempts to expand this work to buckling.

If the fibers are inflexible, the force will be used to stall the motor movement instead. No shortening of the structure will occur and thus no local or global contraction can take place. In this case the crosslinkers will tend to lock in whatever organization, or lack thereof, the system originally started with.

1.3.4 Filament Disassembly

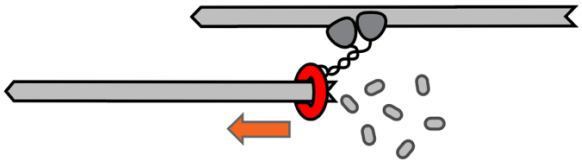

FIG 1.9: Filament Disassembly Schematic *A diagram showing the process of contraction driven by filament disassembly. As a fiber shortens as it disassembles, an end binding crosslinker tracks the end, dragging the other fiber it is connected to with it.*

A third known way for generating local contraction comes from harnessing the energy released during filament disassembly (Pollard et al 2003, Bun et al 2018). This process is unique in that it does not require the presence of a motor. Instead, it requires the presence of an end binding crosslinker that is able to track the end of a shrinking fiber while being attached to another fiber.

FIG 1.9 shows the process of filament disassembly. This configuration requires a fiber to be connected to depolymerizing fiber by a specific type of crosslinker attached to the end of that fiber. As the depolymerizing fiber shrinks, the specific end bound crosslinker remains bound and tracks the position of the disassembling end. This process drags the other fiber with it, sliding it towards the pointed end of the depolymerizing fiber. As with the other mechanics, this brings the fibers closer together and, when repeated over many such configurations in the network, can drive global network contraction. Given the lack of motors and the geometric features that are the focus of this work, we will not discuss this mechanism further except to discuss how it could be integrated with the study of the other mechanism for contraction in a disordered network in future research.

Table 1.1: Summary of Local Contraction Mechanisms *A summary of the required elements for the three local contraction mechanisms in a disordered network with crucial behaviors in bold. *Crosslinkers can be effectively replaced by a second motor type with a distinct walking speed.*

Mechanism	Fiber Rigidity	Fiber Dynamics	Motor End Dwelling	Crosslinker Presence	Crosslinker End Tracking
Polarity Sorting	Either	Optional	**Required**	Optional	Optional
Buckling	**Flexible Only**	Optional	Optional	**Required***	Optional
Disassembly	Either	**Required**	None Present	**Required**	**Required**

1.4 Previous Work

Many researchers have been interested in the connection between local interactions and global behavior. As we have noted, this connection is still poorly understood for disordered networks. There have been a diverse collection of tools and approaches that have been used to understand this contraction. In all cases, local force generation due to an interaction between fibers and motors can only translate into global contraction if the action is repeated over many units all being pulled together. This suggests that the connectivity of the network is important. Connectivity further suggests that percolation theory and graph theory are natural approaches to studying these networks. The importance of direct interaction between cytoskeletal components means agent based models could be helpful. In this section we will discuss the work previous researchers have performed, what is missing and how we can construct a theory to fill in the gaps.

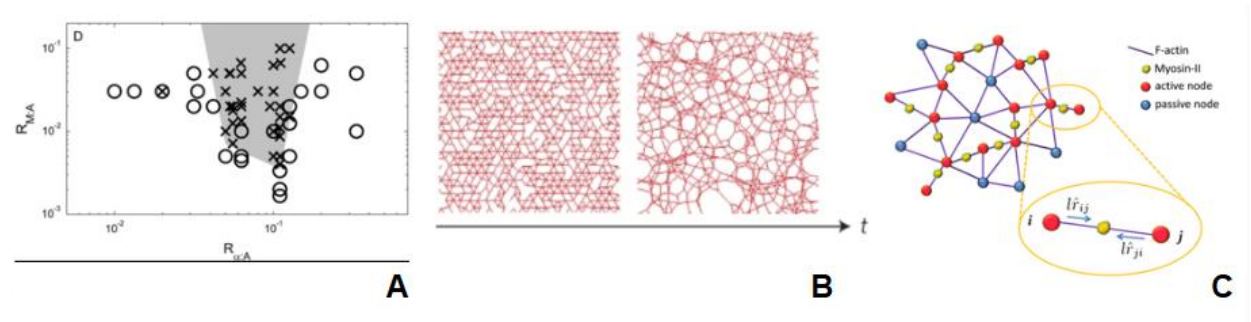

FIG 1.10: Examples of Previous Work *Examples of previous work studying the role of connectivity in cytoskeletal behavior. (A) Taken from Bendix et al 2008, a set of experiments showing when a network contracts based on motor (y-axis) and crosslinker (x-axis) densities. (B) Taken from Alvarado et al 2013, a regular triangular grid showing the role percolation plays in network contraction. (C) Taken from Wang et al 2012, a graph theory approach that highlights how local interactions between components can influence macroscopic properties.*

Connectivity is the key idea of both this work and many previous experiments. Fibers must be directly connected to motors in order to generate force and indirectly connected to other fibers in order for those forces to propagate across the network and drive global behavior. Many experiments have measured the role of connectivity using *in vitro* reconstituted actomyosin networks with carrying combinations of actin, myosin and crosslinkers. Bendix et al 2008 and Alvarado et al 13 found that global contraction occurs when a sufficient number of motors are present and crosslinkers are within a specific range (**FIG 1.10A**). Too few crosslinkers lead to disconnected network, while too many crosslinkers create rigid networks that cannot be reorganized.

The detailed behavior of components is also important to create connectivity. Thoresen et al 2013 showed that motor properties like length and stall force influence their ability to bundle actin. Köhler et al 2012 demonstrated that crosslinker type is crucial. Low concentrations of polar crosslinkers like fascin can lead to reliable network contraction, while apolar crosslinkers like cortexillin required much higher concentrations. Ennomani et al 2016 showed that rings

made of organized actin bundles readily contract, while those made from disordered actin required the assistance of crosslinkers.

These works are largely experimental but are occasionally coupled to models that attempt to explain the observed behavior. However, these tend to be limited in scope and are hard to compare experiments directly. The importance of connectivity is frequently discussed but rarely ever explicitly and rigorously defined. Many simply rely on component concentrations, primarily that of crosslinkers. Few directly measure how fiber variations, both in concentration and length, influences network behavior, while many assume crosslinkers are essential. However, Linsmeier et al 2016 showed that actomyosin networks can contract without the presence of any crosslinkers, highlighting how connectivity arises directly from fiber-motor interactions.

Any attempt to add rigor to the idea of connectivity leads to percolation theory. This field of study provides mathematical tools to understand when pathways through a network are available. As network fills with components or bonds, the ability to move from object to object becomes higher. Eventually a threshold is reached where a network quickly transitions from a state where most objects are isolated to one where most objects are connected to each other. The idea to apply percolation theory to biological networks is a longstanding one. Forgacs 1995, inspired by biological signaling, was the first to speculate that connectivity and percolation could be an important factor in cytoskeletal behavior and force propagation across cells. He recognized the difficulty applying a mathematical approach heavily reliant on regular grids to derive useful results to a system inherently disordered as a cytoskeletal networks.

Alvarado et al 13 attempted to explain their experimental results with a regular triangular grid (**FIG 1.10B**) to little success before producing an overview of the attempts to explore the role of connectivity with traditional percolation theory in Alvarado et al 2017. They showed that

this approach was more successful in explaining macroscopic material properties more than the behavior of the cytoskeleton itself. Work such as Sheinman et al 2012 and Kumar et al 2023 used cubic and hexagonal grids, respectively, to examine how the density of components could influence elasticity and stress propagation. Wang et al 2024 used a triangular grid with anisotropic connectivity to show direction dependent percolation thresholds that may reflect how more structed actin networks behave. Stress fiber formation was studied using square lattices in Ueda et al 2023, revealing the significant role fiber length distribution plays in network connectivity and force propagation.

All these cases require regular grids and some level of abstraction of how sites and edges are filled. No work attempts to account for the direction interaction between two different objects, like fibers and motors. Nedrelow et al 2018, Lee et al 2021 and Lwin et al 2022 all attempt to study dual networks where two objects coexist, though in all cases they examine two different types of fibers, one more rigid than the other, and focus on macroscopic properties more than cytoskeletal behavior. No existing work captures a network where the interaction between two distinct components is fundamental.

Attempts to move away from regular grids relied on even more abstraction of the components themselves. Works like Zeng et al 2012 and Wang et al 2012 create 3D models of a cell uses techniques of graph theory (**FIG 1.10C**), where fibers becomes nodes and motor activity bonds between those nodes. These models do a good job of capturing the ability of interactions to influence network behavior but cannot capture network dynamics. Agent based models like Frolov at al 2024 capture these dynamics and highlight the importance of motor activity to contraction. However, they are not able to develop a theory predictive of their results.

Finally, Bueno et al 2023 use a mean field approach that can accurately predict percolation thresholds but lose all information about the components themselves.

1.5 Expanding Upon Previous Work

As the above works show, the mechanisms that connect local interactions to global behavior are still a topic of great interest. Many try to explain the relationship using the ideas of connectivity and percolation, but there remain many important gaps in these approaches. Of most concern, there is no consistent or rigorous definition of connectivity. Some groups focus primarily on crosslinker density, overlooking that motors provide crosslinking alongside walking activity. Groups that do include motor activity in their definition of connectivity overlook the importance of the fibers themselves. Work that includes concentrations of components abstract those components away and thus cannot capture the importance of protein properties like the length distribution of the components. Percolation theories rely on rigid grids which provide insight to macroscopic material properties but cannot capture direct interactions between or the dynamics of components.

Designing experiments that capture all the variation of concentration of three different components alongside with all the variations in the structure of the components themselves would be impractical. A theoretical approach is crucial to understanding the relationship between local interaction and global behavior. Taking inspiration from the physics of the local contraction mechanisms, we can design tools that define connectivity and use it to predict contractile behavior. By focusing on the geometry of the network, we will be able to account for both component concentration and structural properties like length distributions. In the following

section, we will provide the baseline approach to our theory of connectivity before fully detailing the mathematical approach and hypothesizing about the contractile behavior of the network.

1.6 Proposal and Scope of this Work

In this work, we present a theory that attempts to keep in as much about the local physical activity of the necessary components while being general enough to account for a wide variety of outcomes. The tradeoff is we will limit our scope to understanding as much as possible about the polarity sorting mechanism while leaving the other contractile mechanisms out. We will work in two dimensions only, which is a reasonable approach given the very thin, flat nature of the cellular cortex where many of the most interesting actin cytoskeletal behaviors occur. We will also spend most of this work looking at systems driven by fiber and motor interactions only. As previous work has shown, crosslinkers are not always necessary for contractile activity.

Our primary focus will be the type of connectivity that arises from the geometric intersection between a fiber and motor in a randomly disordered network. These crossings can be observed in experiments (**FIG 1.11**) and form the basis for our theoretical approach to network connectivity (**FIG 1.12**). Though their roles in force generation may be different, we will begin by treating fibers and motors symmetrically when attempting to classify the connectivity of the system. Our key insight is that the only network pieces that can propagate information will be chains that alternate between fiber and motor objects. This is a novel approach to a percolation problem, thus traditional tools of the field have not proved helpful for this work. Instead, we will pull as much intuition out of the piece we understand the most: the local physical interaction

between fiber and motor. This will allow us to define what local structures must be present in the system to drive contraction and what the probability of those configurations must be.

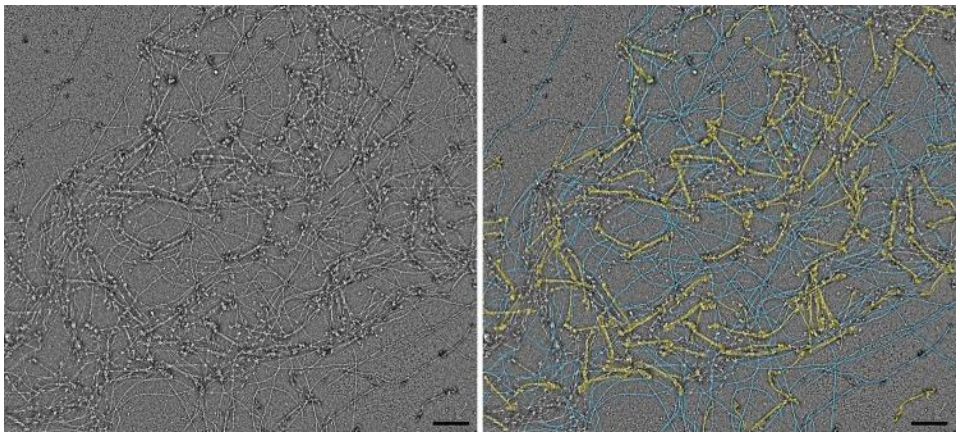

FIG 1.11 Imaging an Actomyosin Network *(A) Electron microscopy image of a network of interacting actin and Non-Muscle Myosin II proteins. (B) Same image with false color highlighting actin (blue) and myosin (yellow). The alternating nature of fibers and motors needed for our chain approach can be seen. Taken by Billington et al 2013.*

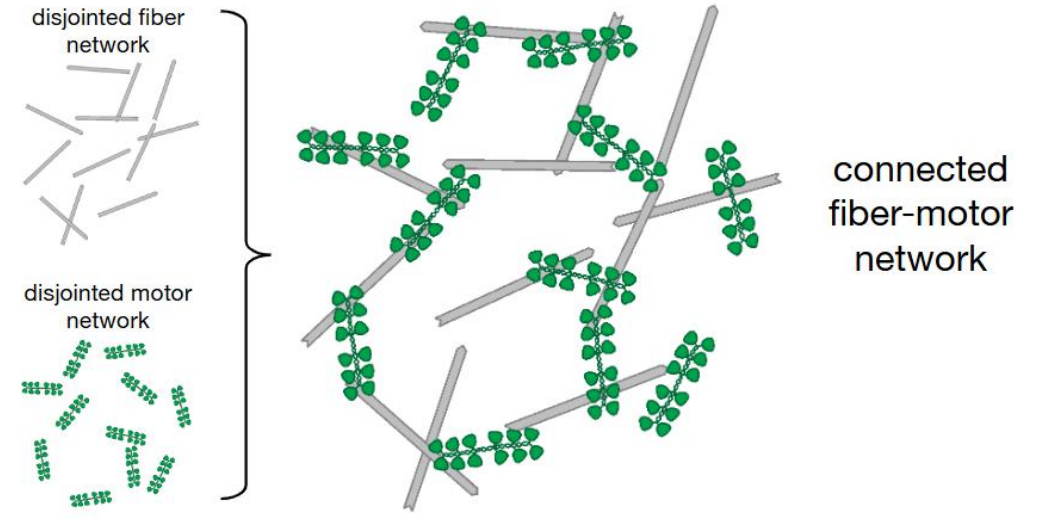

FIG 1.12: Fiber Motor Dual Network *A schematic view of our fundamental approach to connectivity. Neither fiber nor motor are sufficient to propagate force across the network. Connectivity can only be achieved when sufficient amounts of each are present. Forces can only be propagated by following chains of alternating fiber and motor.*

We will also examine variables that are not often considered due to experimental limitations. No previous work we found treated fiber density as fundamental to the measurement of connectivity as the motor or crosslinker density. While there is reason to believe that the resulting dependency on connectivity could be different, we should not treat fibers and motors differently in terms of input. We will also consider objects of differing lengths and length distributions, which are two variables that we found to have a great effect on contraction outcomes. We will use biologically available parameters, when possible, but we will also vary parameters to unrealistic levels to test the robustness of our results. We will examine how our simplified network can be adapted to more biological realistic setups, such as networks with crosslinkers or fiber turnover. We will demonstrate that our focus on local interactions leading to a definition of connectivity grant insight into the contractile behavior of networks and that our approach is applicable to a diverse set of cytoskeletal systems.

Chapter 2 A Theory of Crossing, Connections and Contraction

In Chapter 1, we discussed how forces are generated locally between the direct interactions between fibers and motors and previous attempts at explaining how those local interactions lead to global restructuring and contraction of the whole network. Whether through experiments or simulations, many researchers have identified the concept of network connectivity as a vital aspect. However, connectivity is rarely formally defined, and most approaches miss the fundamental way fibers themselves contribute to network connectivity. No work has proposed a full theory about how connectivity leads to contraction. In this chapter, we will start by examining a direct fiber-motor intersection and expanding towards a full definition of network connectivity to predict when a network will contract globally, locally or not at all.

We will work with the simplest possible network, consisting solely of fibers and motors. As noted in Chapter 1, experimental setups of such a purified system have been shown to be contractile (Linsmeier et al 2016). Many researchers focus on the connectivity provided by crosslinkers without considering the ability of motors themselves to provide a crosslinking behavior. Therefore, if connectivity is a fundamental aspect of contraction, then a simple fiber-motor network should exhibit contractile activity. Work such as Belmonte et al 2017 have considered this simplified network. They assumed motors to be point-like instead of extended, making it a poor model for most myosin type motors, which are typically of comparable size to actin fibers.

To exclude effects created through organized structures like a sarcomere, we will consider collection of fibers and motors with random orientations, uniformly spread throughout a space without hard boundaries. We will assume that a geometric intersection between fiber and motor will lead to a physically active connection.

In order for the local force generation mechanism of polarity sorting to drive network wide contraction, the fibers must be connected to each other. If a given fiber is being pulled by a motor toward the center of the space, it will also pull any motors to which it is attached. Those motors in turn will pull other fibers to which they are bound, even if they are not generating their own forces. Through these fiber-motor connections, forces are propagated across the network, causing global contraction. We thus propose that the expected number and distribution of crossings between fibers and motors is a determining factor in whether a given randomly generated collection of objects will contract.

2.1 Number of Fiber Motor Crossings

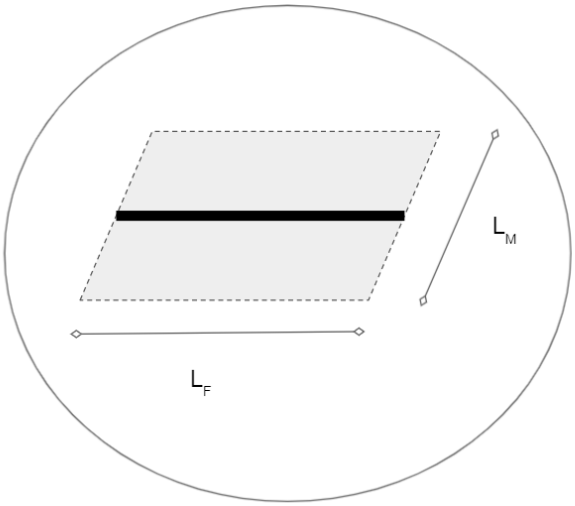

FIG 2.1: Crossing Schematic *One fiber sitting in space of area S at a horizontal orientation. If the center of a motor object at an angle θ from the horizontal axis is placed inside the gray parallelogram, then the motor will intersect the fiber. The comparison of the areas of the full space and parallelogram gives the probability of intersection.*

To determine how the initial density of system components affects contraction, we must define a metric of connectivity. Since polarity sorting is fundamentally caused by the interaction between fibers and motors, we simply count the geometric intersections of one fiber and one motor. Given the typically high count of motors heads in myosin minifilaments, we will assume that every geometrical crossing will be converted to a physical bound. As shown in *Eq 2.1*, the total number of fiber-motor crossings X is a function of fiber count F, motor count M, their respective average lengths L_F and L_M and the system area S.

$$X = FM\frac{2L_F L_M}{\pi S} \tag{2.1}$$

This formula is derived in the following manner. Randomly place one fiber and one motor in a space of area S at random orientations, where θ is the difference in angle between them. We can assume $L_F, L_M \ll S$ and ignore any edge effects from the boundary of the space S. The fiber and motor will intersect if and only if the center of the motor lies inside the parallelogram of side lengths L_F, L_M and angle θ as shown in **FIG 2.1**. Therefore, the probability of intersection is given by *Eq 2.2.*

$$(2.2) \qquad p_\theta = \frac{Area\ of\ Parallelogram}{Area\ of\ Space} = \frac{L_F L_M \sin\theta}{S}$$

To get the total probability of intersection we can average over all relative angles between the two objects, which are uniformly distributed from 0 to π.

$$(2.3) \qquad p = \langle p_\theta \rangle_\theta = \frac{1}{\pi}\int_0^\pi \frac{L_F L_M \sin\theta}{S}\, d\theta = \frac{2L_F L_M}{\pi S}$$

Since each fiber and motor is placed randomly and independently of each other, the total number of expected crossings should be proportional to both the number of fibers F and motors M. Therefore, the total number of crossings is given by the formula for X in *Eq 2.1*. The logic of adding individual pairs does not change if either the fiber or motors have non uniform lengths because the formula is linear in L_F, L_M so the use of average lengths is justified. Of particular interest is a system composed of exponentially or Gaussian distributed fiber lengths as these are the fiber distributions that we expect to see either *in vivo* or *in vitro* experiments with reconstituted systems, respectively.

This formula can be confirmed through the computer generation of disordered networks and directly counting the number of geometric intersections. **FIG 2.2** shows the comparison of this actual count and the expected count predicted by *Eq 2.1* for numerous initial configurations with randomly chosen numbers of fibers and motors. The correlation between prediction and measurement is near exact.

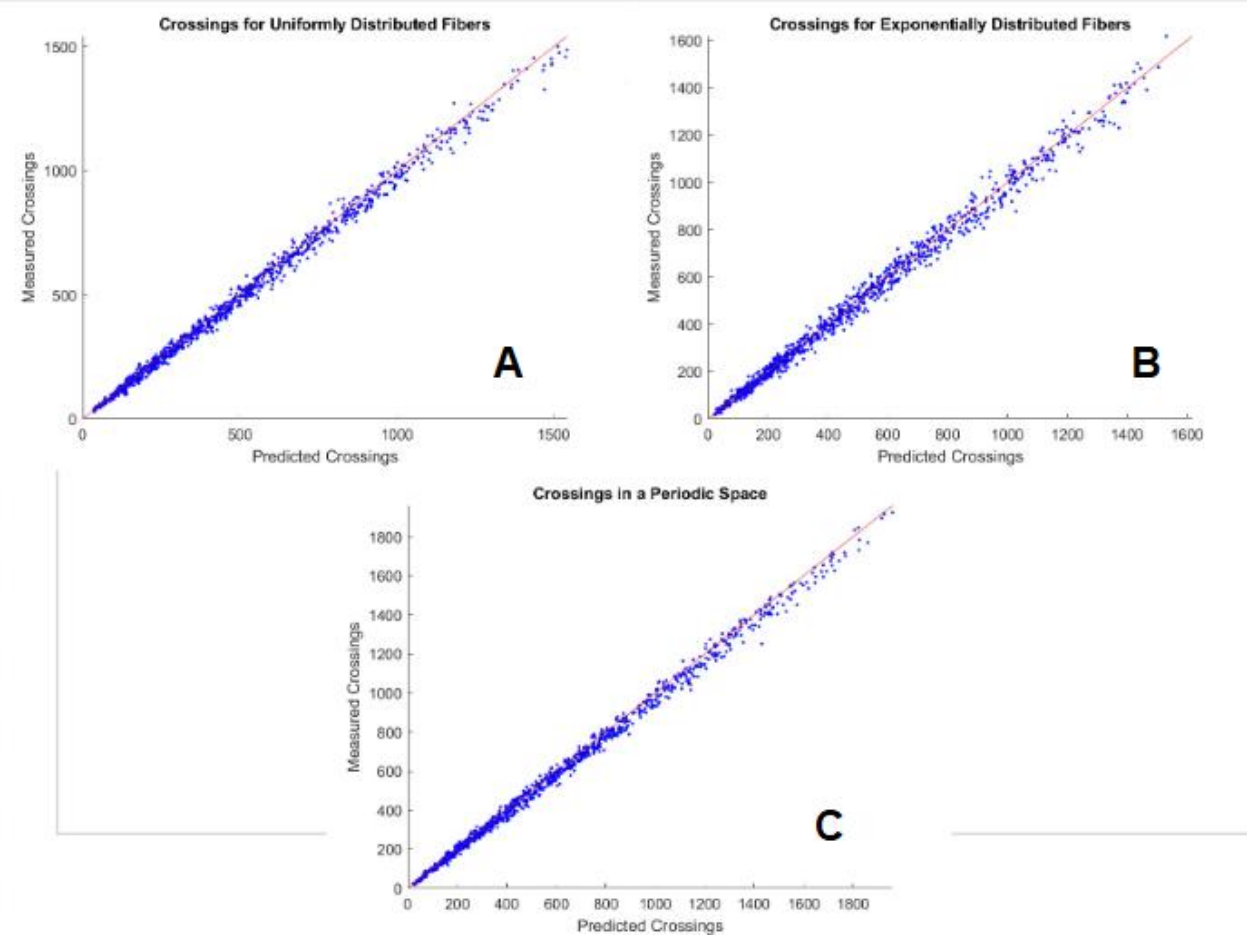

FIG 2.2: Crossing Count Predictions *Comparison of the measured number of fiber motor crossings with the number predicted by Eq 2.1 for a randomly chosen number of fiber and motors. (A) Objects in a circular space with open boundaries, with uniformly distributed fibers. (B) Objects in a circular space with open boundaries, with exponentially distributed fibers. The average length was used to make predictions. (C) Objects in a rectangle space with periodic boundary conditions. The x=y line is overlaid and in all cases the correlation between predictions and measurements is extremely strong.*

We checked that results do not meaningfully change for different lengths of objects or system sizes or if the distribution of lengths is nonuniform. While we do not show every possible configuration here, **FIG 2.2B** shows that when fiber lengths are exponentially distributed around a specified average that average can be used to make accurate predictions.

To show the impact of connectivity on contraction we consider not just the number of crossings X but the density of crossings per system component, crossings per fiber $X/_F$ and crossings per motor $X/_M$. We will present results in a phase space of these two values, allowing the same predictions to be used for any fiber length, motor length or space geometry. Following *Eq 2.*1, it is simple to derive formulas for these two values, as shown in *Eq 2.4.* Importantly, the crossings per fiber depend only on the motor count not the fiber count, and vice versa for the crossing per motor.

$$(2.4a) \qquad X/_F = M\frac{2L_F L_M}{\pi S}$$

$$(2.4b) \qquad X/_M = F\frac{2L_F L_M}{\pi S}$$

We also note that while we count geometric crossings, there is not necessarily an active motor head available to physically bind the fiber and motor together. However, by modeling a motor in a realistic way with many motor heads distributed along its length, we increase the likelihood of realizing a geometric crossing into a physical one, ensuring a more reliable connection between theory, model and simulation.

2.2 Distribution of Crossings

Our probabilistic approach to counting the number of fiber-motor intersections will serve as the basis to predict the distribution of crossings and the connectivity of the network. For a given fiber, it either intersects or does not each of the M motors independently. Therefore, the total number of crossings on that fiber follows the binomial distribution. *Eq 2.3* gives the probability of successful intersection, so it follows that *Eq 2.5* gives the probability of a fiber with exactly x crossings. Notice that geometrically the role of fibers and motors is symmetric, so these formulas are easily modified to predict motor connections as well.

$$(2.5) \quad p_F(x \mid M, L_F) = \binom{M}{x} p(L_F)^x \left(1 - p(L_F)\right)^{M-x}$$

$$= \binom{M}{x} \left(\frac{2L_F L_M}{\pi S}\right)^x \left(1 - \frac{2L_F L_M}{\pi S}\right)^{M-x}$$

If the fiber lengths are not uniformly distributed, then just as we did for the total crossing count, we should average over all fiber lengths. In living cells, actin fiber lengths are commonly distributed exponentially. Our simulations can only model a finite number of finite length fibers, so in order to best model an exponential distribution we truncate the interval of possible lengths to be between some L_{min} and L_{max}. In such a case, the probability of a fiber having x intersections with M motors is given by *Eq 2.6*.

$$(2.6) \quad p_F(x|M, L_F) = \frac{1}{A} \int_{L_{min}}^{L_{max}} \binom{M}{x} \left(\frac{2L_F L_M}{\pi S}\right)^x \left(1 - \frac{2L_F L_M}{\pi S}\right)^{M-x} e^{-L_F} \, dL_F$$

A is a normalization factor obtained by integrating over all possible lengths, as shown in *Eq 2.7*.

$$(2.7) \qquad A = \int_{L_{min}}^{L_{max}} e^{-L_F}\, dL_F$$

While an analytic solution to this integral exists in theory, it would involve a polynomial with a degree of hundreds without a convenient structure of coefficients. Therefore, we will leave the probability in this form and compute integral values numerically. The same logic applies to any possible distribution of fiber lengths. Numerical exploration reveals that both versions of the equation depend only on the crossing densities $X/_F$ and $X/_M$, not the individual values independently.

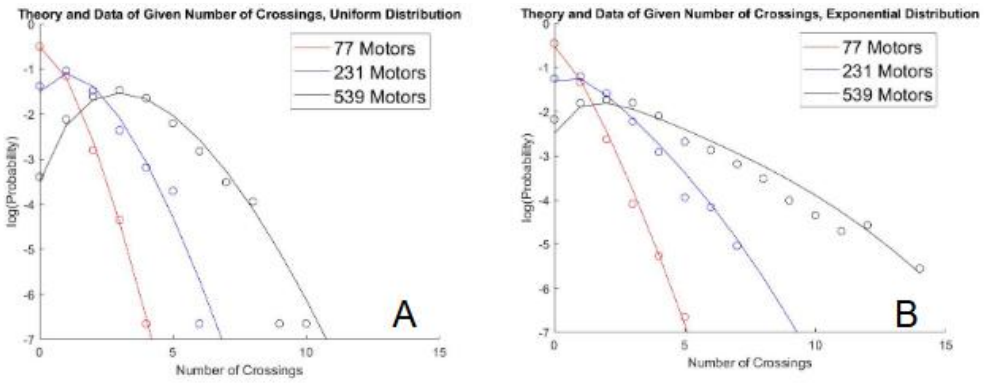

FIG 2.3 Predicting Crossings per Fiber *Three highlighted distributions for (A) uniform and (B) exponential length distributions, shown on a semi log plot for visual clarity. Dots indicate simulated crossing counts averaged over 20 trials. The solid lines show the predicted binomial-like distribution derived in Eq 2.5 and Eq 2.6. Our predictions fit very well and show two important behaviors. Unsurprisingly, more motors mean fibers tend to accumulate more crossings. Exponentially distributed systems have higher probabilities at the extremes since probability of intersection is proportional to fiber length.*

Again, we can use computer generated random collections of fiber and motors to count intersections and create a histogram of the number of fibers with a given number of crossings. **FIG 2.3** compares the measured crossing distribution for uniform and exponential length distributions with the values predicted by *Eq 2.5* and *Eq 2.6,* respectively. Three arbitrary motor counts are shown. Here we highlight that the exponentially distributed fibers favor both high and low extremes of crossing probability. This is because longer fibers tend to accumulate more crossings, while shorter fibers accumulate fewer but are more numerous.

The difference in distribution of crossings between uniform and exponentially distributed fibers suggests that contraction should be easier in exponential systems. While the very short fibers are more likely to be left behind, the longer fibers are more likely to be connected to each other. Since most of the system's mass is in the longer fibers, their contraction is more important to the overall conclusion of whether a network contracted or not. This behavior will be demonstrated in Chapter 5.

2.3 Minimal Configuration for Local Contraction

Finally, we reintroduce physical behavior to our geometry approach. We can take these distribution probabilities and attempt to predict the potential contractility of a network given an initial count of uniformly distributed fibers and motors. In order for a motor to generate local contraction through the polarity sorting mechanism, said motor must be connected to at least two fibers. A configuration of a motor connected to at least two fibers is the "*minimal configuration*," (**FIG 2.4**) and we hypothesize a system can only contract if this configuration is sufficiently likely to occur in a network. We hypothesize that sufficient in this case means that a given fiber

should be more likely than not to be in a *"minimal configuration,"* i.e., the probability of a fiber being in a "*minimal configuration*" must be above 0.5.

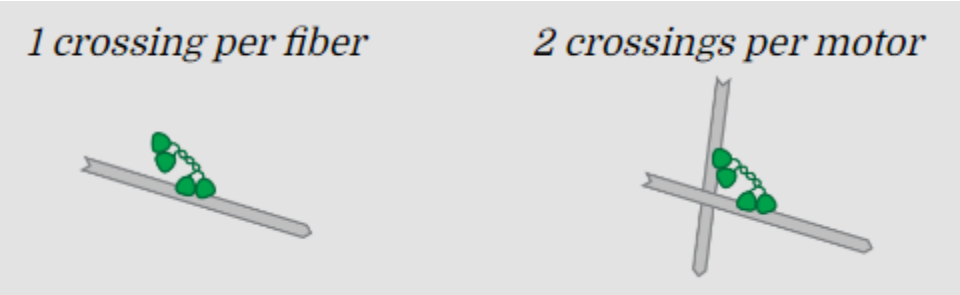

FIG 2.4: Schematic of Minimal Local Configuration *A schematic view of the minimal configuration for some amount of contraction. We hypothesize local configuration dictates global behavior.*

To predict this "*minimal configuration*" probability, we need the probability of a given fiber to intersect at least one motor that intersects at least two fibers. *Eq 2.8* gives the expected number of motors that intersect at least two fibers M^*.

$$M^* = M\, p_M(x \geq 2 \mid F, L_F) = M(1 - (p_M(0 \mid F, L_F) + p_M(1 \mid F, L_F)) \tag{2.8}$$

We can then find the probability C_{local} a given fiber is connected to at least one of these motors.

$$C_{local} = p_F(x \geq 1 \mid M^*, L_F) = 1 - p_F(0 \mid M^*, L_F) \tag{2.9}$$

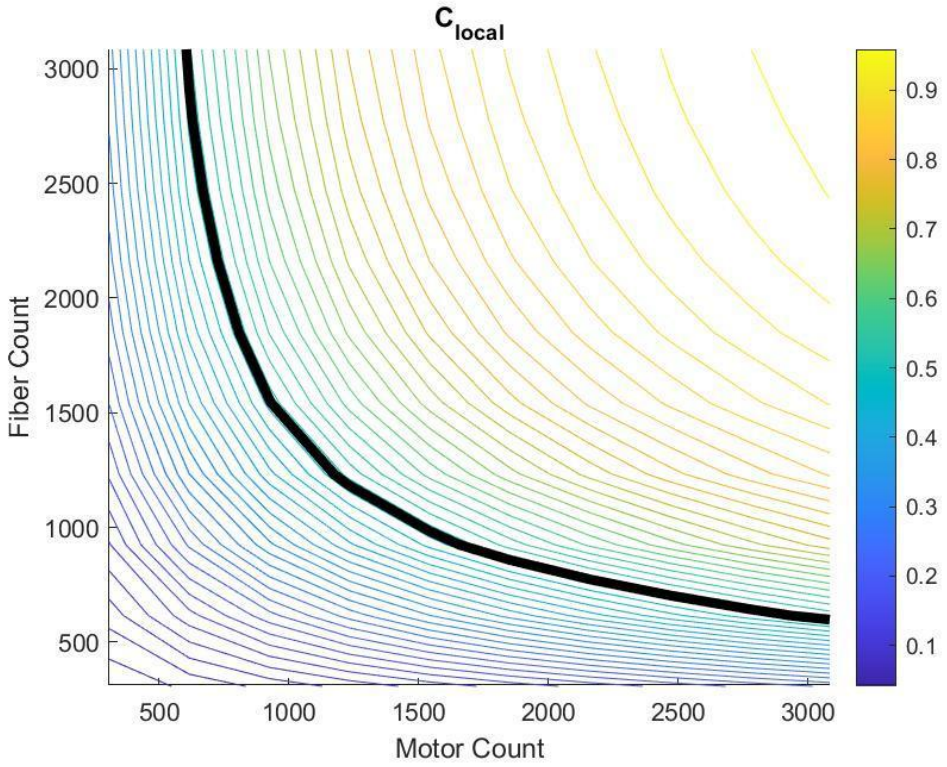

FIG 2.5: Contours of Local Probability *A contour map of the calculated probability C_{local} as a function of the number of crossings per fiber $X/_F$ and crossings per motor $X/_M$ with the contour at .5 highlighted.*

The value of C_{local} as a function of connectivity can be seen in **FIG 2.5**. We predict that a system can only show any contractile behavior at all if C_{local} is greater than 0.5. However, this should tell us only about a minimum condition for contraction to be allowed. If each fiber was actually connected to only one motor, then there would be no way for forces to be propagated across the network. Fibers would tend to be clustered with other fibers on the same motor but not influence the rest of the network. **FIG 2.6** is a snapshot of the final frame of a CytoSim simulation displaying such behavior. White objects are fibers and green objects are motors. A full description of CytoSim simulations can be found in Chapter 3.

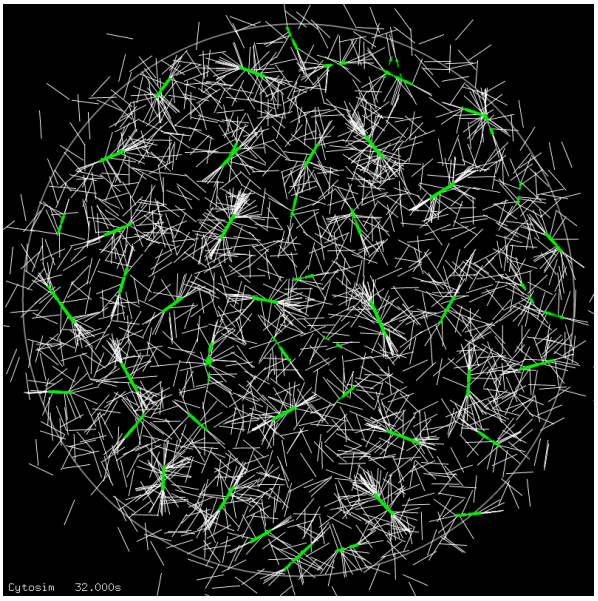

FIG 2.6: Low Connectivity System *A poorly connected system. Fibers (white) can align and bundle with nearby fibers due to motor activity (green), but no network wide contraction takes place.*

2.4 Minimal Configuration for Global Contraction

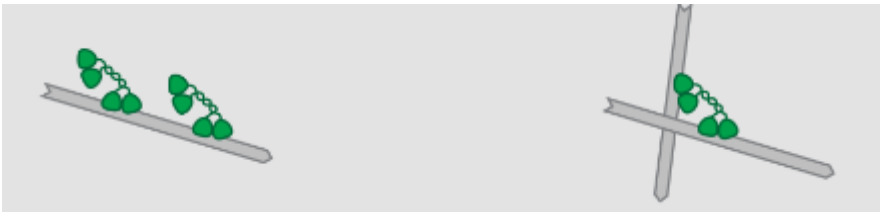

FIG 2.7 Schematic of Minimal Global Configuration *A schematic view of the "reliable configuration," which we hypothesize should lead to global contraction of almost all fibers in the system.*

To find a condition that ensures reliable connectivity, we can take the same approach used to find C_{local} and make the restriction stricter. In order for work done by a motor to be propagated to other parts of the network, the fibers on that motor must be connected to other motors which are also connected to other fibers, which we call the *"reliable configuration"*

(**FIG 2.7**). We predict that a system will contract globally if the probability of a given fiber to intersect at least two motors that intersect at least two fibers, C_{global} is greater than 0.5.

(2.10) $C_{global} = p_F(x \geq 2 \mid M^*, L_F)$

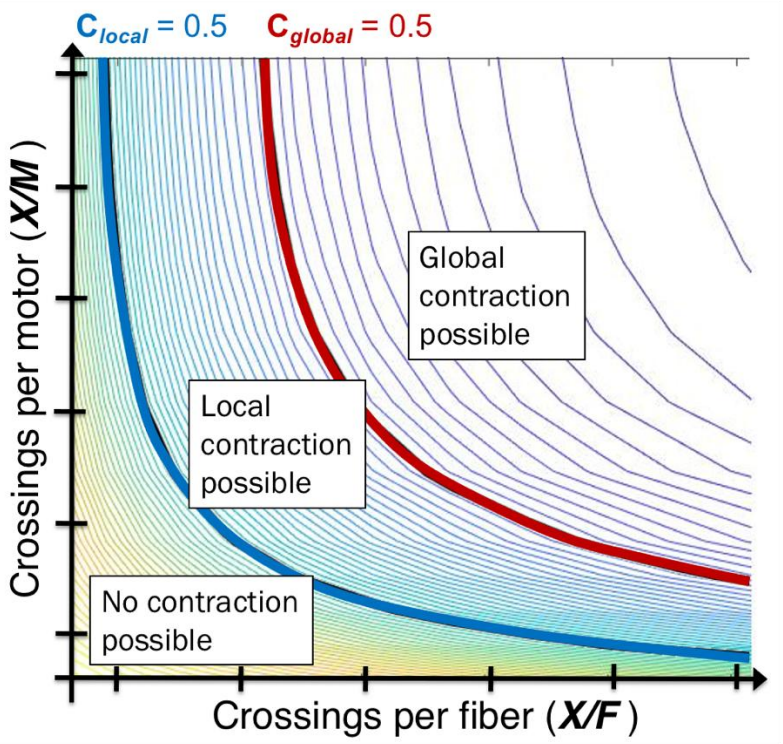

FIG 2.8 Predicted Phase Space *A contour map of the calculated probabilities as a function of the number of crossings per fiber* $^X/_F$ *and crossings per motor* $^X/_M$ *with the contours of* $C_{local} = .5$ *and* $C_{global} = .5$. *Our phase space is split into three distinct regions. We predict that contractile behavior can be predicted by which region the initial fiber and motor counts correspond to. If either the fibers or motors are too low density, then there will be* ***No Contraction*** *in the system. If both are sufficiently high density, then almost all fibers will contract together into one centralized aster. We will call this* ***Global Contraction****. Finally, if the system is in the intermediate zone, then contraction is possible but not fully guaranteed. Fibers can influence their nearby neighbors and form a small aster. Typically, the final state of the system is a collection of separate small asters, therefore the system is considered to have undergone* ***Local Contraction.***

FIG 2.8 shows the values of C_{global} as a function of connectivity. We predict that the space will be divided into three distinct regions of connectivity. Low connectivity systems should generate no noticeable contraction in the system. High connectivity systems should result in global contraction of the system. Medium connectivity systems should result in intermediate behavior where fibers only interact with their direct neighbors and form multiple small asters in process called local contraction.

The above assumes all fibers have the same length. We can broaden our approach to any fiber length distribution. Since our probabilities rely on fiber and motor count, which are discrete, we first need to approximate continuous distributions with a finite set of lengths $\{L_j\}$ with a corresponding set of probabilities $\{q(L_j)\}$. The number of fibers of each length is thus F rounded down so they can be used in a binomial coefficient.

As before we need to find the number of motors attached to at least two fibers. We will make a simplifying assumption here that this can be calculated using the average fiber length $\langle L_F \rangle$, as shown in *Eq 2.11*.

$$M^* = Mp_M(x \geq 2 \mid F_{total}, \langle L_F \rangle) \tag{2.11}$$

Then for each set of fibers we predict the number of fibers of that length connected to at least one of these motors. We then take a weighted sum over each length and find C_{local} and C_{global} as before. As we will show in the results section, a weight of $\left(\frac{L_j}{\langle L_F \rangle}\right)^2$ is appropriate. This captures the fact that longer fibers are more likely to cross many motors, thus contributing more to network connectivity. *Eq 2.12* and *Eq 2.13* give contraction probabilities.

$$C_{local} = \sum_j \left(\frac{L_j}{\langle L_F \rangle}\right)^2 q(L_j)\, p_F(x \geq 1 \mid M^*, L_j) \tag{2.12}$$

$$C_{global} = \sum_j \left(\frac{L_j}{\langle L_F \rangle}\right)^2 q(L_j)\, p_F(x \geq 1 \mid M^*, L_j) \tag{2.13}$$

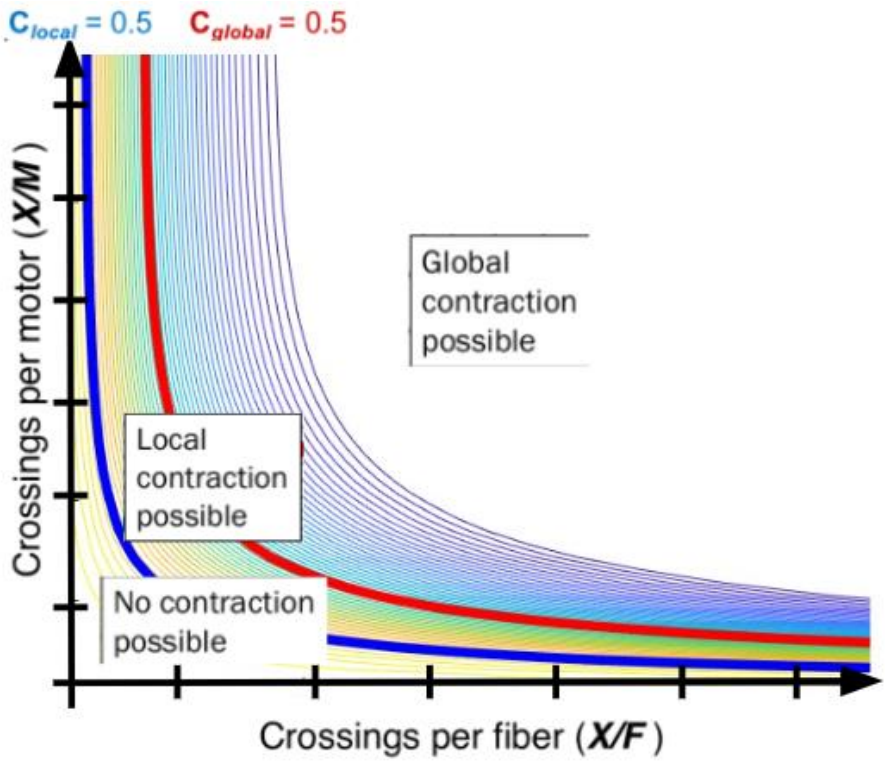

FIG 2.9 Predicted Phase Space with Exponential Fibers *A contour map of the calculated probabilities as a function of the number of crossings per fiber* $^X/_F$ *and crossings per motor* $^X/_M$ *with exponentially distributed fibers. The contours of* $C_{local} = .5$ *and* $C_{global} = .5$ *are highlighted. There is a noticeable shift left and a narrowing of the local contraction zone. However, the space is divided into the same three zones.*

FIG 2.9 shows that the changes in the probabilities are small but notable. This shift comes from the asymmetry between lengthening and shortening fibers. Long fibers easily

accumulate large numbers of crossings as previously shown in **FIG 2.3**. Therefore, the presence of longer fibers leads to more connectivity, and thus fewer components are necessary to drive contraction behaviors.

2.5 Open vs Closed Spaces

These probabilities were developed in a circular space with open boundaries, but we believe these regions will also offer insight into periodic space. The math remains the same, but the interpretation must change. An open space has a clear preferred direction for system contraction, namely inwards towards the space's center. This is no longer the case when the boundaries are periodic. When the system is somewhat connected, fibers can only influence their neighbors and therefore are unaffected by the properties of boundaries either way. When the system is highly connected, every fiber can pull on every other fiber, meaning each should be pulled equally in every direction. This means no system-wide contraction will take place, and instead tension will build up across the network. While not the focus of this work, maintaining internal tension in a cell has many applications such as intracell signal transmission and endocytosis (Wu et al 2017, De Belly et al 2021, Dharan et al 2025).

Therefore, we predict that for initial conditions of a periodic space, those in the No Contraction zone will look the same locally as the open space, those in the Global Contraction zone will no longer contract, and those in the Local Contraction zone will continue to contract into many small asters.

Chapter 3 Modelling in CytoSim

In order to test the predictions made in Chapter 2, we will utilize computer simulations. We must have the ability to finely control the number of each component in the system. Since our theory is probabilistic, we need to be able to generate a large number of tests with the same input parameters and we need to vary those parameters over many different values in a large range. This would be difficult and time-consuming to do using experimental setups. This chapter discusses the methodology of using the cytoskeleton simulation software CytoSim to simulate behaviors of a cytoskeletal network. We discuss the underlying design of CytoSim, how we model biological proteins and list the parameters that define our simulations.

3.1 Dynamics in CytoSim

We simulate the contraction of cytoskeletal networks using the Open-Source engine CytoSim, which is capable of simulating the thermal environment of the cell, individual protein objects, as well as the forces generated by the interaction of biological fibers and binding proteins. The mathematical justification for the model can be found in Nedelec and Foethke 2007. The position of each individual object is tracked. Larger, more complicated objects like a fiber may be divided into smaller segments, which allows for elastic bending on the fiber. In this case, each separate segment is tracked independently.

Two important features arise through the interaction of objects with the fluid environment of the cytoplasm. The combination of relatively small proteins with a viscous environment means inertia is not relevant to the dynamics. The Reynold's Number measures the ratio of inertial to viscous forces. As described by Stokes 1851 and Reynold 1883, the Reynold's Number R can be defined for sphere moving in a fluid using *Eq 3.1* where a is the protein's radius, v is the speed of the object and $\boldsymbol{\nu}$ is the fluid's kinematic viscosity.

$$(3.1) \qquad R = \frac{av}{\boldsymbol{\nu}}$$

The relevant values and consequences when this idea is applied to cells are summarized in Purcell 1976. The kinematic viscosity of the cytoplasm is known to be approximately $10^{-2}\,\frac{cm^2}{s}$. A typical protein or structure is less than a micron across and can move at a max speed on a scale of $10\,\frac{\mu m}{s}$, leading to a Reynold's number on the order of $\sim 10^{-4}$. This means in the absence of an outside force, a moving object will come to a stop in less than 0.1 Angstrom and 0.1 microsecond. Since the length and time scales of cytoskeletal proteins and processes are much larger than that (for example, the average diffusion step of a 1 μm fiber is about 24 nm (Palmer et al 1999)), the effects of inertia can safely be ignored.

Brownian motion describes the random motion of small particles in a viscous fluid. The particle is constantly colliding with the atoms of the fluid, meaning it is impossible to track every interaction the particle experiences and thus predict its trajectory. A stochastic process is used instead, where in every time step a random direction and length are chosen for each object to move. The value of the step is calculated slightly differently depending on the type of object. A

diffusion constant D is calculated using Einstein's relation, where μ_p is the object's mobility which is object dependent, k_B is Boltzmann's constant and T is the fluid temperature.

$$D = \mu_p k_B T \tag{3.2}$$

For each time step of size τ, we generate a uniform random number θ between 0 and 1 and define the movement representing Brownian motion in *Eq 3.3.*

$$B(t) = \sqrt{2D\tau}\theta \tag{3.3}$$

Over many steps, the movement from the initial condition will be normally distributed with mean 0 and variance $2D\tau$. This process is known as a random walk. This motion, when combined with forces and geometric constraints, creates the motion of every individual simulated object in the system.

The equation of motion is derived in the following way, starting with Newton's Second Law. The total force is the sum of viscous drag, Brownian motion and elastic forces.

$$\begin{aligned} m\ddot{x} &= F(x,t) \\ &= -\xi\dot{x} + B(t) + f(x,t) \end{aligned} \tag{3.4}$$

x is the position vector, with a dimension of the product between the number of objects N and spatial dimensions d. ξ is a drag coefficient. f is the sum of all forces acting on the object, which have two potential sources. Two objects may be bound to one other. This bond is

modelled by a Hookean spring. Segments of larger objects are additionally subject to bending elasticity using the standard formula developed in Landau and Lifshitz 1986. These interactions create a large but sparse Nd by Nd dimensional matrix A_t, where each nonzero entry represents a stiffness coefficient for a corresponding interaction. As detailed later in this chapter, these coefficients are specified by the user during the definition of the fiber (rigidity parameter) or binding object (stiffness parameter). The matrix is sparse since practically each object will only interact with a small number of other objects in the simulation. Ultimately, A_t is constructed such that $f(x,t) = A_t x_t$.

Since inertia forces are small compared to viscous forces, we can ignore the acceleration term entirely and rearrange *Eq 3.4* into a linear first order ODE.

$$\xi \dot{x} = B(t) + f(x,t) = B_t + A_t x_t \tag{3.5}$$

This equation is solved numerically through implicit differentiation, meaning we attempt to solve for future position using the force at the future position.

$$\xi \frac{x_{t+\tau} - x_t}{\tau} = B_t + A_t x_{t+\tau} \tag{3.6}$$

Rearranging this gives us an equation in a form well studied in linear algebra, $Ax = y$.

$$\left(1 + \frac{\tau}{\xi} A_t\right) x_{t+\tau} = x_t + \frac{\tau}{\xi} B_t \tag{3.7}$$

Since A_t is large but sparse, instead of trying to invert it, it is faster to solve through an iterative algorithm called the Biconjugate gradient stabilized method, which is described in Van der Vorst 1992.

This equation is coupled with a set of constraints. If a point is part of a larger object like a fiber, then distances between certain other points must be conserved. Consider a set of distances between points a_i and a_j of $|a_i - a_j| = \lambda_{ij}$. The set of all possible positions meeting these constraints defines a subspace of the Nd dimensional space called a constraint manifold (where as in *Eq 3.4, N* is the number of objects and d is the spatial dimension). The tangent space at the current value of x is calculated and then the possible solutions to *Eq 3.7* are required to be in the tangent space. The outcome is then projected onto the manifold, allowing for all constraints to be preserved (**FIG 3.1**).

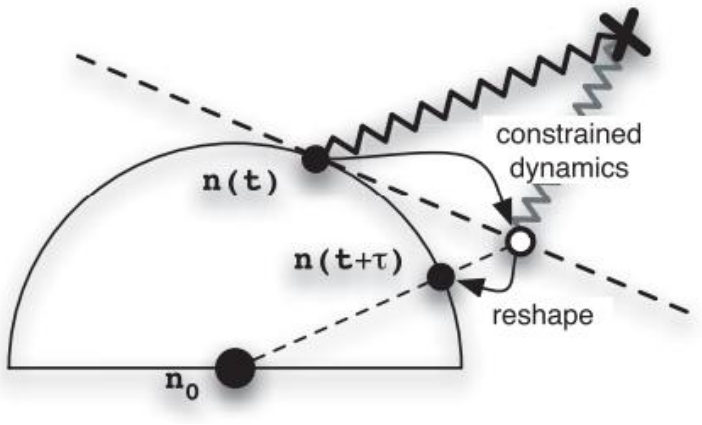

FIG 3.1: Position Update with Constraints *A diagram of the integration process for a particle n_1 constrained to remain a fixed distance from point n_0. The constraint defines a circle the point is constrained to. Numerical integration is performed in the direction tangent to the current position and then projected down onto the constraint circle. Taken from Nedelec and Foethke 2007.*

3.2 Using CytoSim

Simulations are executed through the use of a config file specifying all desired biological objects and physical behaviors. (An annotated example of a config file is found in the Appendix.) We must specify a space with background parameters mimicking a cell or an *in vitro* experimentally setup, create classes of objects to model protein behavior, specify the desired number of each class for a given simulation, and finally set the number of steps to simulate. In some circumstances, parameters can be changed during the simulation after a specified amount of time has passed. For example, motors are typically initialized with a maximum walking speed of zero. Since motors cannot be generated already attached to fibers, this allows them time to find and bind to fibers before the walking behavior disrupts the initial random geometry that is fundamental to our theory. After sufficient time to allow binding and unbinding events to equilibrate, the maximum motor speed is then changed to a nonzero value and the physical dynamics we wish to model begin.

It is possible to format a config file so that it may be quickly replicated with small changes to specified parameters, most commonly object counts. This allows us to quickly write, execute and analyze potentially thousands of simulations at once. These simulation sets are performed remotely in parallel through the use of the NC State High Performance Cluster. Depending on the complexity of the simulation, sets can be completed in as little as a few hours up to a few days. Given this speed, we did not overly focus on maximizing computational efficiency. Other members of the Belmonte group examined how different design choices, especially for motors, impacted efficiency. However, since variation in compute time was at most 10%, biological and physical considerations were of primary importance.

CytoSim tracks the position and condition of every individual object in every frame. In order to minimize the complexity of the output, the number of frames saved is set at the end of the config file. In many cases only the initial and final state are important so as few as two frames are saved per simulation. Even when dynamics are of interest, typically no more than one out of every ten steps is required to analyze the system's behavior.

Data is extracted using a combination of CytoSim's report functionality and a set of Python scripts created in our group. As detailed in Chapter 4, we primarily extract the position data of fiber objects. Simulation sets are scraped in the cluster and collated into a small number of spreadsheets, each of which is small enough to be quickly downloaded from the HPC server. Local analysis is done using MATLAB.

As discussed in Chapter 1, we classify all relevant objects into one of three component categories essential to understanding polarity sorting. First are the fibers that define the network. Second are the myosin motor bundles that generate force. Lastly there are the crosslinking proteins that can provide extra connectivity between fibers. Finally, we must define a space for the objects to move in.

Since the construction of many important biological structures, such as the cytokinetic ring, happens in the cell cortex, components exist in a flat two-dimensional space mimicking the inner membrane of the cell. Fibers have a typical length of around 1 micron, while even small cells such as amoebas and fission yeast have circumferences of tens of microns (Mylnikov et al 2015, Sveiczer et al 1996), while the cortex itself has a typical thickness of only 190 nanometers (Clark et al 2013). Therefore, fibers operate in a space that is effectively flat. Furthermore, actin filaments are approximately $10\ nm$ thick and microtubules are approximately $25\ nm$ thick (Mofrad 2009), they can freely slide over one another in the cortex. This can be modelled in a

flat two-dimensional space by turning off steric interactions between objects, allowing objects to pass freely through each other.

3.3 Fibers

The 'fiber' class is a fundamental tool in CytoSim's design, paralleling the biological fibers' role as the fundamental physical object making up the network. As seen in (**FIG 3.2**), fibers are modelled as a series of rigid one-dimensional rods connected by flexible hinges, with an adjustable overall rigidity. Normally this is set at 22 $pN\mu m^2$ to match the rigid nature of microtubules but is occasionally changed to 0.075 $pN\mu m^2$ to model flexible actin fibers (Gittes et al. 1993). As long as there are no crosslinkers present, we do not expect this rigidity to affect contraction, since contraction will be driven solely by the fiber rigidity-independent polarity sorting mechanism as discussed in Chapter 1.

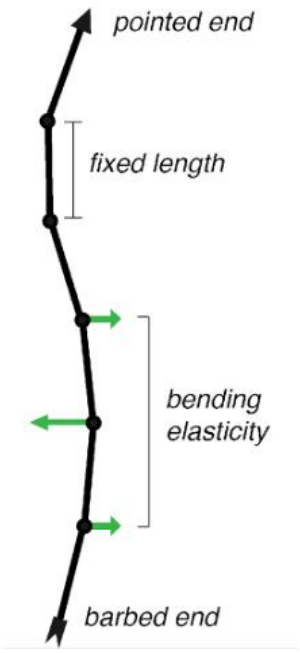

FIG 3.2: Fiber Schematic *A diagram of how CytoSim models fibers. A series of rigid segments connected by flexible hinges form a geometrically polarized fiber.*

Fibers, and each segment, are geometrically polarized with a barbed end at the front and a pointed end at the rear. Motors can bind to the fiber at any position. As discussed in Chapter 1, we choose to focus only on motors that walk towards the barbed end.

Initially fiber segments l_s are 0.1 μm long. However, one segment can be as short as necessary to form a fiber with any total

length. By default, the length of a fiber will not change throughout the simulation. The location and dynamics of each segment are tracked individually, meaning that segment length has a large effect on overall computational cost. Microtubule-like fibers have a high enough rigidity as to be effectively straight at all times. Therefore, we set the segment length for these fibers equal to the full fiber length to minimize computation time.

In contrast, actin-like fibers are flexible enough that thermal fluctuations are sufficient to cause observable bending. The *'equilibrate'* command is used to generate fibers with an initially bent configuration according to the persistence length parameter (l_p). Persistence length measures the correlation of the orientation between differing segments of the fiber. When generating fibers, the angular difference $\delta\theta$ between adjacent segments is pulled from the normal distribution found in *Eq 3.8.* The average persistence length of actin has been measured to be $10\mu m$ (Wisanpitayakorn et al 2017).

$$P(\delta\theta) = \sqrt{\frac{l_p\, l_s}{2\pi}}\, e^{-l_p\, \delta\theta^2/2} \tag{3.8}$$

Fibers by default have a uniform length distribution, that is, all fibers have the same length. We use a default average length of 1 μm to mimic a common fiber length in an actomyosin network (Burlacu et al 1992). Since a uniform length distribution is mathematically simple and experimentally relevant, it is a reasonable default. However, we will show that our results are ultimately independent of the specific length distribution.

In vivo, actin fibers are commonly exponentially distributed, as measured in experiments such as Piekenbrock and Sackmann 1992. CytoSim has the ability to automatically generate a set

of fibers with lengths exponentially distributed around a specified average. However, to avoid computational problems with too large or too small fibers, we must truncate the distribution by setting minimum and maximum lengths. We must therefore modify our probability distribution to that shown in *Eq 3.9*.

$$P(fiber\ length = x) = \lambda e^{-\lambda x} / \int_{L_{min}}^{L_{max}} \lambda e^{-\lambda x}\, dx \tag{3.9}$$

This means the simulated fibers will have an output average different from λ. It is possible to calculate the output average as a function of input average and minimum and maximum lengths. However, this function is not invertible. Therefore, to find an appropriate input average that corresponds to the desired output average, numerical simulations are used to estimate the output average for a given input. After the simulation, it is straightforward to extract the length of each fiber and confirm the system has the desired length distribution.

By default, fibers do not grow over time. After analyzing static fibers, we can add dynamics to determine if such effects matter to the polarity sorting mechanism. Given the complexity of actin fiber dynamics *in vivo*, for which a complete model is still lacking, and many parameters and non-linear effects are still unknown, we decided to create a simple model based on the much better described microtubule dynamics. In our model, dynamic fibers have ends with a growth state and a shrink state where they grow and shrink with pre-defined speeds matching the maximum known growth rates of actin *in vitro* (Carlier et al 2017). The dynamic behavior of barbed and pointed end differs, with all growth happening on the barbed end and depolymerization occurring on both (Narita et al 2011). We also tested extremes by modeling fibers with rates ten times as fast. Each end switches from growth to shrink states at a fixed

catastrophe-like rate and reverts to a growth state at a fixed rescue rate. We prevented fibers from disappearing by defining a minimum length of 0.03 μm where they dwell until a stochastic rescue event happens.

When testing growing fibers, we begin with fibers of a uniform length. Because we choose the rates in such a way to preserve the average length of the fibers, as they grow and shrink, the distribution of lengths becomes Gaussian. The width of the distribution widens over time but tends to stabilize after about two minutes of growth, with an average length identical to the initial length and an average measured standard deviation of .39 μm. With Cytosim, we cannot directly initialize fibers with a Gaussian length distribution as we can with exponential, so growth dynamics is used to test the effects on contraction of both the dynamics and a Gaussian length distribution.

We will generally assume that motors and crosslinkers can bind and move to any location on the fiber and that more than one object can bind to the same fiber location. As discussed in Chapter 1, actin fibers are made up of a series of G-actin monomers roughly 6 nm in diameter. In some cases, it may be appropriate to take this discrete nature into account and split the fiber up into sites separated by 6 nm. In any given simulation frame, at most one object can bind to each lattice site. Motor heads can only directly move to an empty adjacent site. This leads to competition between motors and crosslinkers, which can affect network dynamics. The implications of this binding site competition are discussed in Chapter 6.

Table 3.1: Simulation Parameters for Fibers

Parameter	**Symbol**	**Typical Value**	**Reference**
Rigidity (rigid)	μ_{rigid}	22 $pN\mu m^2$	Gittes et al. 1993
Rigidity (flexible)	$\mu_{flexible}$	0.075 $pN\mu m^2$	Gittes et al. 1993
Persistence Length (flexible)	l_p	10 μm	Wisanpitayakorn et al 2017
Segmentation Length (flexible)	l_f	0.1 μm	
Initial Fiber Length (average)	L_F	.5-3 μm	Burlacu et al 1992
Minimum Fiber Length	L_{min}	.1 μm	
Maximum Fiber Length	L_{max}	5 μm	
Barbed Growing Speed (realistic, extreme)	$v_{g,+}$	0.08, 0.80 $\frac{\mu m}{s}$	Carlier et al 2017
Pointed Growing Speed (realistic, extreme)	$v_{g,-}$	0	Carlier et al 2017

Table 3.1 (continued)

Barbed Shrinking Speed (realistic, extreme)	$v_{s,+}$	0.056, 0.56 $\frac{\mu m}{s}$	Carlier et al 2017
Pointed Shrinking Speed (realistic, extreme)	$v_{s,-}$	.014, 0.14 $\frac{\mu m}{s}$	Carlier et al 2017
Barbed Catastrophe Rate	$r_{c,+}$	4 Hz	Carlier et al 2017
Pointed Catastrophe Rate	$r_{c,-}$	8 Hz	Carlier et al 2017
Barbed Rescue Rate	$r_{r,+}$	3.4 Hz	Carlier et al 2017
Barbed Rescue Rate	$v_{r,-}$	2 Hz	Carlier et al 2017

3.4 Motors

As discussed in Chapter 1, we choose Non-Muscle Myosin II motor bundles as our representative motor. These motors consist of a long, thin, rigid backbone connecting a large number of binding heads (**FIG 3.3**).

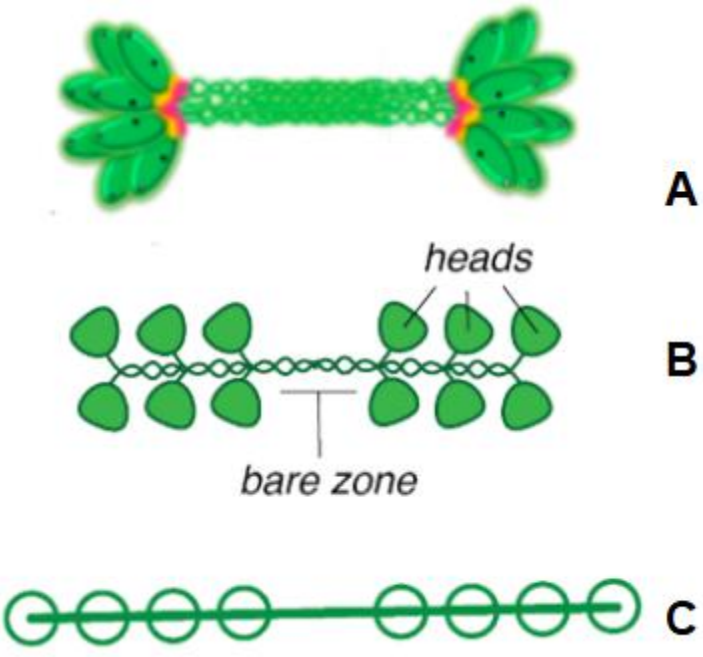

FIG 3.3: Motor Schematic *Images of increasing abstraction of a Non-Muscle Myosin II bundle. The motor consists of individual heads that attach to and walk along fibers. Our model is shown in (C) where 12 motor heads are equally spaced on each end of a straight, rigid backbone, with a large bare zone in the middle third. (A) Adapted from Brito, C., & Sousa, S. (2020).*

The backbone of the motor is a 0.8 μm long rigid solid. In CytoSim, the '*solid'* class are geometric shapes (in this case a 1D 'cylinder') which lack any of the bending behavior of fibers. *Solids* are computationally efficient and can easily be distinguished from fiber objects when extracting information from completed simulations. When the *solid* is generated, motor heads are explicitly attached at specified locations along the backbone, ensuring every motor is identical and that motor heads will never detach or stretch away from the backbone during the simulation.

Binding heads are *'single'* objects, called such since they are made up of a single 'filament grabbing' object (or *'hand'* in CytoSim syntax), as opposed to *'couple'* objects, which are formed by two *'hands'* and a Hookean constraint that connects them. *Hand* objects contain all the binding behavior of the head and walking behavior of the motors, while all location

information, including the attachment to the backbone, is tracked through the *single* class. The *hand* object also contains the binding stiffness needed to construct the interaction force described in section 3.2. We choose a high stiffness of $100\ \frac{pN}{\mu m}$ so that the physical connection between fiber and motor is effectively rigid. This allows for efficient transmission of forces between fibers and motos.

There are 12 binding heads on each end of the backbone, equally spaced 0.022 μm apart, starting from the ends of the *solid*. Therefore, one motor has a total of 24 binding domains covering approximately two-thirds of the backbone's length. This coverage ensures reliable physical connections between the simulated fibers and motors. Each head can bind to any actin fiber within a range of 0.01 μm at a rate of 10 *Hz*. Unbinding follows a slip-bound unbinding process (Cortes et al 2020). While bound, heads unbind at a rate u_{m_0} of 0.3 *Hz* (Guo et al 2006) modified by the total force f exerted on the head as calculated by Cytosim. As shown in *Eq 3.10*, the force exerted on the head is modified by a specified unbinding force f_u, which can be set to infinity to remove the force dependence.

$$u_m = u_{m_0} e^{-\frac{f}{f_u}} \tag{3.10}$$

While bound to an actin fiber, motor heads walk towards the barbed end of the fiber. The background environment is assumed to have an abundance of the ATP required to fuel walking. The walk is modelled as continuous with a specified maximum speed v_0, which is then suppressed by the amount of drag force f on the motor and any other fibers it may be bound to according to *Eq 3.11*.

$$v = v_0(1 - \frac{f}{f_0}) \quad (3.11)$$

Motor movement will cease if total drag reaches a specified stall force value f_0, typically around 4 pN (Walcott et al 2012). Binding heads follow normal unbinding rules when reaching the end of fibers as opposed to immediately falling off. As discussed in the introduction, this end-dwelling property is necessary for polarity sorting. When attached to a dynamic fiber, if the barbed end of a fiber attempts to grow or shrink while a motor head is attached to the end, the motor head will remain attached.

While we focus on reproducing Non-Muscle Myosin II, it is easy to adapt this design process for motors with different geometry or walking behavior. It may be that the backbone of the motor should be flexible, in which case it is possible to use the '*fiber'* class instead of the '*solid'* class to model the motor backbone. In such a scenario, the use of a *'binding key'* identifier is used to tell hands which instance of '*fiber'* class they are allowed to attach to. This ensures motors do not mistakenly bind to each other instead of the objects modelling actual fibers. This technique is not used for motors in this work, but it is important for crosslinker design, discussed in the next section.

Table 3.2: Simulation Parameters for Non-Muscle Myosin II motors

Parameter	**Symbol**	**Typical Value**	**Reference**
Backbone Length	L_M	0.8 μm	
Number of Binding Heads	n	24	

Table 3.2 (continued)

Binding Range	d_m	0.01 μm	Guo et al 2006
Binding Rate	b_m	10 Hz	Guo et al 2006
Unbinding Rate	u_m	0.03 Hz	Guo et al 2006
Binding Stiffness	k	100 $\frac{pN}{\mu m}$	
Unbinding Force Modifier	f_u	infinite	
Maximum Motor Speed	v_o	2 m/s	
Stall Force	f_0	4 pN	Walcott et al 2012

3.5 Crosslinkers

Like motors, crosslinkers can be modelled in multiple ways (**FIG 3.4**), but generally fall into one of two categories. Extremely short range (effectively point like) crosslinkers like Plastin are modelled using the *'couple'* class. Intermediate and long range crosslinkers, like Alpha-Actinin and βH-Spectrin respectively, are modelled with the *'fiber'* class.

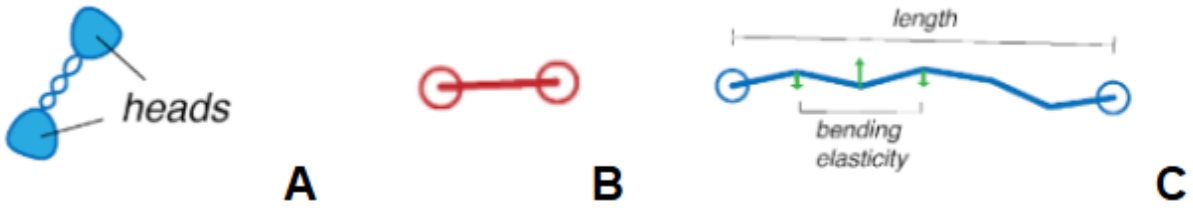

FIG 3.4: Crosslinker Schematics *Crosslinker design models. (A) All crosslinkers consist of two binding heads with a connector. The connector can be a short spring like in (B) or a longer flexible fiber object like in (C).*

Point-like crosslinkers are implemented with the CytoSim class *'couple.'* As with the *single*, the *couple* is named after the fact that it connects two *'hand'* objects. In a *couple*, two hands are connected by a 0.012 μm long spring with a spring constant of 250 $\frac{pN}{\mu m}$ (Matsudaira et al 1983). Location of the crosslinker is tracked through the *couple* class, though we never had a need to do so explicitly.

Each *hand* can bind any fiber within 0.01 μm at a binding rate of 10 *Hz*. To maximize computational consistency, crosslinkers remain bound once attached to a pair of fibers. While attached to dynamic fibers, binding heads have a chance to rescue a shrinking fiber. If the fiber attempts to shrink past the location with a bound head, it will be forced into the growth state with a 10% probability, otherwise the binding head will unbind and allow the fiber to continue shrinking.

While we typically ignore the details of how our modelled objects physically bridge two objects, we must take that into account when dealing with such short, small proteins like plastin. The crosslinker *hands* can only attach to the fiber at a particular angle due to the local structure of the crosslinker. The crosslinker's small size means its two binding sites do not have the freedom to rotate with respect to each other. So once one *hand* has bound to a fiber, the other

hand will only be able to bind to fibers with a similar orientation. Both *hands* will be able to be simultaneously bound between a pair of fibers with at most a 10 degree difference in orientation.

Table 3.3: Simulation Parameters for Short Crosslinkers

Parameter	**Symbol**	**Typical Value**	**Reference**
Backbone Resting Length	l_p	0.012 μm	Matsudaira et al. 1983
Spring Stiffness	k_p	250 $\frac{pN}{\mu m}$	Matsudaira et al. 1983
Binding Range	d_{link}	0.01 μm	
Binding Rate	b_{link}	10 Hz	
Unbinding Rate	u_{link}	0 Hz	
Rescue Probability	r_{link}	0.1	
Maximum Orientation Difference	$\delta\theta$	10^o	

Long crosslinkers are modelled by connecting two *hands*, not with a short spring, but with a full *fiber* object backbone (**FIG 3.5**). Implementation of these long crosslinkers involves an additional step in the CytoSim config file. The crosslinker binding sites must be implemented with a *couple* object, where one *hand* binds to fibers representing the actin or microtubule filaments, and the other *hand* attached the couple to the fiber object representing the crosslinker backbone. The first *hands* have the same binding rates and ranges as the short crosslinkers but now the *'binding key'* identifier is added to ensure it only binds to *'fiber'* objects that model

biological fibers, not crosslinker backbone fibers. The second *hands* are created with a distinct binding key that allows it to bind only to the *fiber* object that forms the backbone of the long crosslinker. This second *hand* is not meant to model an actually existing object, since in reality the hand and backbone are a part of the same protein.

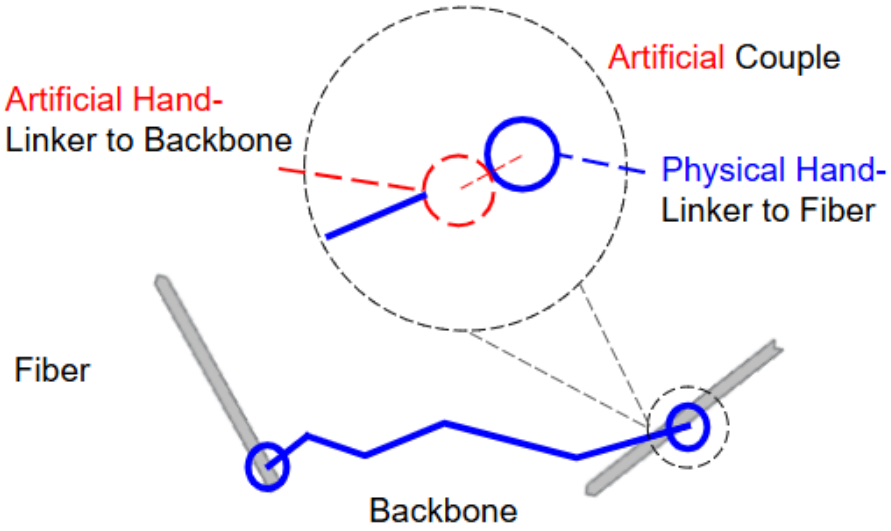

FIG 3.5: Detailed Long Crosslinker Schematic *The schematic for a long crosslinker connecting two fibers. The binding domain of the crosslinker is a 'couple' object that contains one 'hand' that models the physically existing protein domain that binds the crosslinkers to a fiber (shown in solid blue circle in the inset). The other 'hand' is purely for computational purposes and attaches the binding domain to the end of the backbone 'fiber' object (shown as a dotted blue circle in the inset).*

Ultimately, we have an extended object that allows a crosslinker to connect to fibers that are at a far distance apart, with no orientation restriction. The length of the long crosslinker backbone varies based on the protein being modelled. For example, the Alpha-Actinin backbone is .036 μm long (Meyer et al 1990) while the βH-Spectrin is .2 μm long (Derbala et al 2018). The rigidity of βH-Spectrin is extremely low at $7.5*10^{-5}$ $pN\mu m^2$ (100 times lower than actin fibers), thus requiring small segmentation size of .05 μm.

Table 3.4: Simulation Parameters for Long Crosslinkers

Parameter	**Symbol**	**Typical Value**	**Reference**
Backbone Length (Alpha-Actinin)	l_{AA}	0.036 μm	Meyer et al 1990
Backbone Length (βH-Spectrin)	l_s	0.2 μm	Derbala et al 2018
Backbone Rigidity	μ_{link}	7.5*10-5 $pN\mu m^2$	
Binding Range	d_{link}	0.01 μm	
Binding Rate	b_{link}	10 Hz	
Unbinding Rate	u_{link}	0 Hz	
Rescue Probability	r_{link}	0.1	

For both the motor and crosslinker heads, it is important that the binding range is small. While making it harder to find a fiber to bind to, a short range prevents unphysical contraction due to snapping of objects together that are far apart. The physics of the spring attached to the head does not activate until the hand successfully binds to a fiber. If the binding occurs far from the location of the *hand*, the spring force may be large enough to move the attached fiber by itself, despite not being attached to another object in the network. The binding activity should allow for the transmission of forces between objects, not generate movement on its own. As long as the binding range is small, this unwanted force will be kept at insignificant levels.

3.6 Simulation Space

In order to study polarity sorting in an isolated way and allow our results to be experimentally recreated as simply as possible, we initialized components in a 2D space. Depending on the application, this space may be circular, cylindrical or toroidal. Our most important space is a simple circular space with a radius between 5 and 10 μm. 2D is used instead of full 3D space. As mentioned earlier, it is reasonable to model the cortex as 2D since the thickness of the objects is at least one order of magnitude smaller than their lengths or the size of the environment. Simulations in 2D are significantly more efficient than trying to model even a thin 3D space.

The environmental temperature and medium viscosity of the space match that commonly found in *C. elegans* embryonic cells (Daniels et al 2006). While we must assign some value for these parameters, they do not affect connectivity or local motor activity. Therefore, we expect results to be independent of the particular choice.

Here is also where we specify the timestep between simulation frames. We find that .002 *sec* is a good compromise between simulation accuracy and runtime.

We do not explicitly model the membrane itself. While other work done by the Belmonte group explores the forces generated on a fiber network created by its interaction with membranes and anchors, this is not necessary for the geometric understanding we pursue in this work.
For most simulations, the centers of all objects are uniformly, randomly placed inside a circular radius. This radius is used only to define initial positions, and there is no physical boundary around the space. Objects may diffuse outside with no loss in physical behavior or ability to interact with other objects. The choice for space size is a tradeoff between computation time and

ensuring contraction effects are not a result of small sample noise or of a too constricted space. Since the space is unbounded and radially symmetric, this configuration gives a preferred direction for contraction radially inward. For applications studying the constriction of a cytokinetic ring, we use the same circular space, but objects are initialized tangent and near to the boundary instead of randomly placed inside, which still gives a preferred constriction direction radially inward.

We also make use of rectangular spaces. In order to model an infinite space, we periodically identify both pairs of opposite sides of the rectangular space. This creates a toroidal space with no preferred contraction direction at all. When comparing contraction behavior between multiple space designs, size values are chosen so that system area is approximately the same.

Once we have defined a space and all the classes of objects described above, we are ready to specify the number of each object that should be initialized into the space. Our theory will focus on examining how the system behaves over a large range of object counts.

Table 3.5: Simulation Parameters for Cell Environment

Parameter	**Symbol**	**Typical Values and Range**	**Reference**
Viscosity	ν	.18 $\frac{pNs}{\mu m^2}$	Daniels et al 2006
Temperature	kT	0.0042 $pN\mu m$	Daniels et al 2006
Timestep	dt	.002 s	
Circular Space Radius	R_0	5-10 μm	

Table 3.5 (continued)

Fiber Count	F	150-3000	
Motor Count	M	150-3000	
Crosslinker Count	Cl	0-30,000	

Chapter 4 Measuring Contraction

To test the theory described in Chapter 2, we need a way to measure the change in network size and shape over time. Since it is usually clear from visual inspection whether a network has reorganized itself, our metrics aim to capture that intuition. The exact details we need to measure will change depending on the situation and geometry though. The contraction behavior of a network randomly distributed over a borderless disk is clearly different from that of a network randomly distributed over a rectangle with periodic boundary conditions.

This chapter will discuss three metrics. The first, Radius of Gyration $\boldsymbol{R}$, is a common metric used generally to measure the size of a cytoskeletal network. The second and third metrics, $\boldsymbol{\Gamma}$, and $\boldsymbol{M}$ (which will be discussed in chapter 6) , were designed by us with the explicit attempt to capture the behavior of a particular network geometry.

4.1 Radius of Gyration *R*

The most common method of measuring contraction of simulated cytoskeletal networks is by looking at the *Radius of Gyration*, which measures the deviation of a set of fiber positions from their center of mass. This metric can be easily calculated and interpreted for a single image and over time, works over a diverse set of system geometries and is of obvious appeal to physicists since it is analogous to the Moment of Inertia for a system with a uniform mass

distribution. Here we give a definition based on the exact knowledge of fiber location data, but this approach is easy to adjust to experimental images collected using the light intensity profile of GFP or other common tagging proteins.

As discussed in Chapter 3, our simulation model fibers as a series of rigid line segments connected by flexible hinges. The position of the center of every one of these segments is recorded on each frame of the simulation. The position of the segment j of the fiber i is recorded as r_{ij}. Therefore, in a simulation with F fibers and N segments per fiber, the location of the center of mass r_{CM} is calculated in *Eq 4.1*.

$$r_{CM} = \frac{1}{FN}\sum_{i=1}^{F}\sum_{j=1}^{N} r_{ij} \tag{4.1}$$

And then the *Radius of Gyration R* is calculated in *Eq 4.2*.

$$R = \frac{1}{FN}\sum_{i=1}^{F}\sum_{j=1}^{N} \left|r_{ij} - r_{CM}\right|^2 \tag{4.2}$$

Whether this metric is appropriate depends on the context. This is an excellent metric when studying the constriction of cytokinetic rings. When fibers are arranged in a ring, the *Radius of Gyration* is exactly equal to the average radius of the ring at any given step in the process.

However, for any more complicated geometry and contraction behavior, the metric loses much of its descriptive value. In our open disk environment, many different fiber configurations

could all have the same *Radius of Gyration* but obviously different contractile behaviors. This is seen in **FIG 4.1**. It is important for us to be able to quickly distinguish between a system like **FIG 4.1A** with one large central aster (an example of global contraction), and **FIG 4.1C** with many small distinct asters (an example of local contraction).

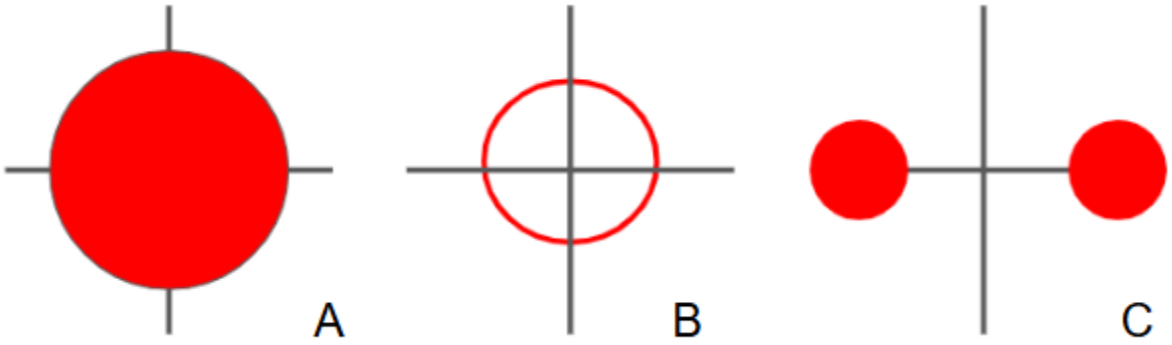

Figure 4.1: Measuring Radius of Gyration *Consider the following three configurations. (A) A uniform disk of radius* r_1 *with Radius of Gyration* $R_1 = \frac{r_1}{\sqrt{2}}$*, (B) a ring of radius* r_2 *and* $R_2 = r_2$*, and (C) two disks of radius* r_3 *each with a center a distance* d *from the origin and therefore* $R_3 = \sqrt{2d^2 + r_3^2}$*. If we choose* $r_1 = 32, r_2 = 3, r_3 = 1, d = 2$ *then the Radius of Gyration of each configuration is equal to 3. This shows that this metric is not reflective of our visual understanding of contraction outside a very particular geometry.*

This measurement also has little meaning in spaces with periodic boundary conditions since it becomes impossible to define a meaningful origin and thus center of mass.

4.2 Contraction Metric Γ

As discussed in our theory, we are most interested in distinguishing between systems that have undergone no meaningful contraction, local contraction and global contraction. These three

states are visually distinct, so we desired to build a metric taking that intuition into account. We wanted this metric to be usable across many types of systems, primarily the open disk environment, as well as a periodic space and any potential experimental setups. This Contraction Metric $\boldsymbol{\Gamma}$ will measure the distribution of fiber locations recorded by CytoSim and analyze them in a novel approach we have developed.

We start by dividing the space into square boxes of equal size. The exact size of each box is not important as long as it is sufficiently larger than the resolution of the object. In simulations, which means larger than the fiber segment size of $0.1\ \mu m$. We will use a box size of $0.5\ \mu m$. We then count the number of fiber points positioned in each box, N_{kl}. We then define a deviation σ as the standard deviation of $\{N_{kl}\}$.

As the system contracts, we expect that σ increases as the system changes from an initially uniform distribution of fibers to a heterogenous one. However, interpreting this output directly may be difficult as the initial value will not be zero even for a perfectly randomly distributed system, due to the inherent limitations of finite simulation. Therefore, in order to better understand the relationships between different simulations and system configurations, it is better to look not at the final deviation but an overall percent change from first to final frame, $\frac{\Delta\sigma}{\sigma_i}$.

A further subtly is that the maximum possible value of σ will depend on the fiber length. Longer fibers will be spread out over more boxes, even when a system has fully contracted to a single aster. Therefore, by scaling the metric by the average length of fiber, we can compare between simulations where the distribution of the fiber lengths is the same, but the average length varies (**FIG 4.2**).

Overall, we will measure the contraction of a system using the Contraction Metric **Γ** given by *Eq 4.3*.

$$\Gamma = \langle L_F \rangle \frac{\Delta\sigma}{\sigma_i} \tag{4.3}$$

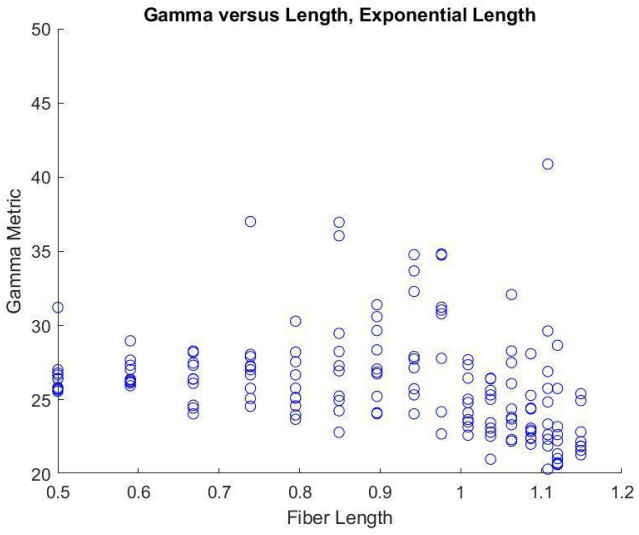

FIG 4.2 Length Correction*: Contraction Metric* ***Γ*** *values versus average fiber length for 1000 simulations with exponentially distributed fiber lengths. While the spread is wide between different individual simulations, after proper scaling, there is no dependence on fiber length.*

However, even with this scaling, we must be careful comparing results between simulations with different length distributions. There is an asymmetry between making a fiber shorter versus longer. Once a fiber is smaller than the size of a dividing box, it no longer matters if you make it shorter. However, longer lengths will always increase the potential for the fiber to cross multiple boxes. An exponentially distributed set of fiber lengths will have many short fibers mixed with some long ones, but the effects of the long ones will dominate. Therefore **Γ** may be smaller than expected based on a uniform distribution of fibers with the same average

length as the exponential set. From here on, any discussion of **Γ** values will refer to uniform length distributions unless explicitly stated otherwise.

With those considerations in mind, this metric has many advantages over the *Radius of Gyration*. This metric does a good job of distinguishing between networks that don't contract at all (every box has the same small number of fibers so **Γ** is small), contract into multiple small asters (many intermediate count boxes so **Γ** is intermediate) or fully contract into a central aster (a few boxes containing a large number of fibers with many nearly empty ones so **Γ** is very large). Since it does not rely on any particular point in space, it can be used in periodic spaces as well as our standard open disk. It is also easy to replace box count with fluorescence intensity in experimental images.

By looking at a large collection of snapshots, we can distinguish the three separate types of contraction we predicted in Chapter 2. **FIG 4.3** shows that anytime the measured **Γ** value is less than 1, the system did not contract.

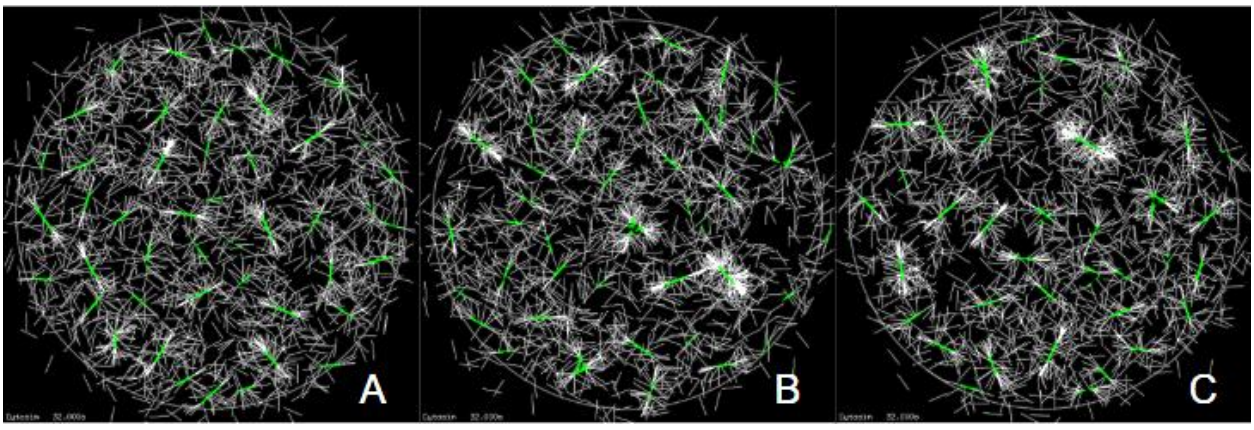

FIG 4.3: No Contraction Simulations *Three typical No Contraction simulations with* ***Γ*** *= 0.22, 0.65, 0.82, respectively. There are some local bursts visible where many fibers connected to a few motors are pulled together, but forces are not able to propagate beyond very short ranges. No asters are visible.*

As soon as **Γ** exceeds one, definable structure becomes visible (**FIG 4.4**). The system is well connected enough that fibers from different areas of the space are pulled together in an aster. For Γ values slightly above 1, only one clear aster is visible, but as **Γ** increases, local asters become more numerous and more distinctive. However, as **Γ** continues to increase towards 40, the asters begin merge and to move towards the center.

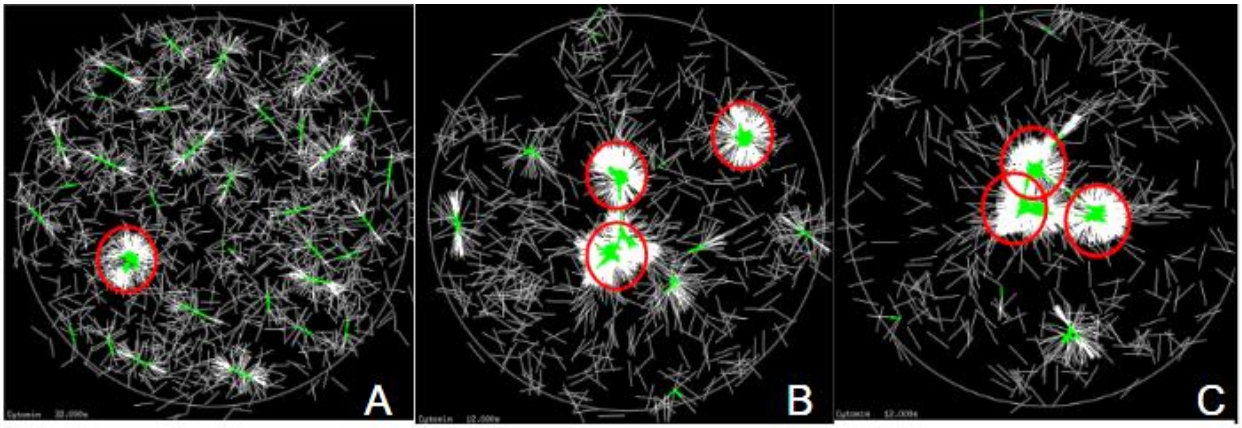

FIG 4.4: Local Contraction Simulations *Three typical Local Contraction simulations with* ***Γ****=1.05, 18, 28, respectively. There are clear, distinct asters forming, circled in red. They initially grow in number, size and distinction as* ***Γ*** *increases, however eventually they begin to merge at the space center as* ***Γ*** *approaches 40.*

We observed that once **Γ** exceeds 40, all simulations have completely formed a single central aster, completing Global Contraction (**FIG 4.5**). The metric can continue to increase beyond 40 depending on system size and simple numerical variation. Variations above this value do not reveal any meaningful behavior about the system, so any simulation producing an **Γ** value above it will be considered as globally contracted and we will crop **Γ** values higher than 40 in the legends of our parameter maps. The threshold value itself holds no special meaning, and as we will show in the next section, changes depending on the fiber distribution. Therefore, we must be

careful to consider **Γ** qualitatively and in the appropriate context. For example, it can be used directly to compare simulations of differing numbers of uniformly distributed fibers but not a simulation with F uniformly distributed fibers to one with F exponentially distributed fibers.

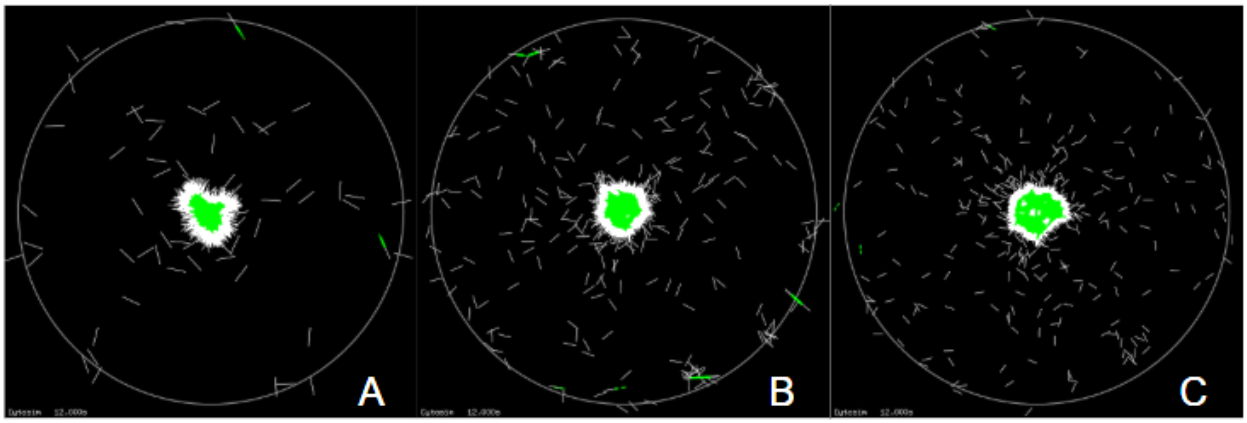

FIG 4.5: Global Contraction Simulations *Three typical Global Contraction simulations with* $\boldsymbol{\Gamma} = 40, 49, 60$ *respectively. There is clearly one central aster containing almost every fiber and motor in the system.* **Γ** *can increase beyond 40, but there are no longer any meaningful physical or visual differences.*

These three ranges and behaviors are clearly distinguishable when varying the fiber count while holding the motor count steady, as shown in **FIG 4.6**. As long as the motor density is high enough to ensure connectivity is possible, then **Γ** increases with fiber count. The metric slowly ramps up towards 1 as the density gets high enough to ensure the minimal configuration is likely. Once hitting this threshold, contraction becomes possible and **Γ** rapidly increases, until global contraction is achieved. Once exceeding the global threshold of 40, the metric increases much more slowly.

By repeating this sweep over fiber counts for many different motor values, we create a full phase space. We are now ready to test our predictions for contractility based on the

connectivity. The transition from $\boldsymbol{\Gamma} < 1$ No Contraction to $\boldsymbol{\Gamma} > 1$ Local Contraction should correspond to the location of the $C_{local} = 0.5$ contour, and the $\boldsymbol{\Gamma} < 40$ Local Contraction to $\boldsymbol{\Gamma} > 40$ Global Contraction transition should correspond to the location of the $C_{global} = 0.5$ contour. Results found using our $\boldsymbol{\Gamma}$ metric can be found in Chapter 5.

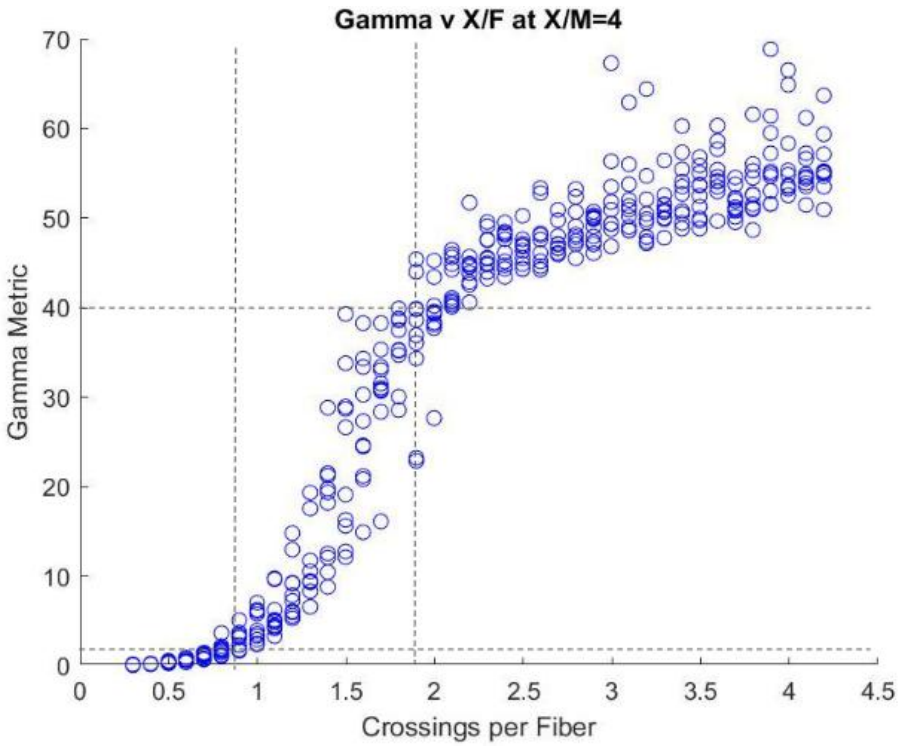

FIG 4.6: Fiber Dependence of $\boldsymbol{\Gamma}$ *The Contraction Metric $\boldsymbol{\Gamma}$ as a function of Crossings per Fiber X/F for a fixed density of 4 Crossings per Motor. $\boldsymbol{\Gamma}$ increases slowly toward 1 in the No Contraction region, increases rapidly in the Local Contraction region, before leveling off around 40 once Global Contraction has been achieved. Vertical lines indicate the value of the predicted 0.5 contours at $X/M = 4$. The intersection of the $\boldsymbol{\Gamma}$=1 and $\boldsymbol{\Gamma}$ =40 lines, contour value lines and the $\boldsymbol{\Gamma}$ curve itself indicate that our predictions and measurements about contraction are compatible.*

These three categories of behavior are present for any fiber length distribution. The value of the global contraction threshold changes based on the distribution (40 for uniform, 20 for

exponential), while the local contraction threshold remains at 1**. FIG 4.7** and **FIG 4.8** were produced using exponentially distributed fibers and show the same fundamental behavior as the uniform length simulations (**FIG 4.9**). We therefore expect that any behavioral pattern present for the simplest situation (uniform length) should remain present for more complicated setups.

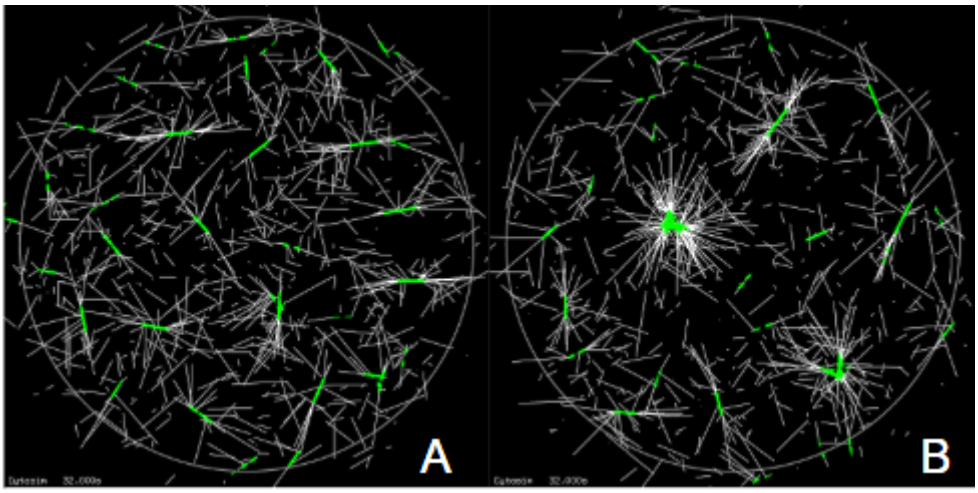

FIG 4.7: Local Contraction Transition for Exponentially Distributed Fibers *Typical simulations with exponentially distributed fiber lengths, with* $\boldsymbol{\Gamma}$ *=.47 and 1.38, respectively. As before, local asters are only seen in simulations with* $\boldsymbol{\Gamma}$ *>1.*

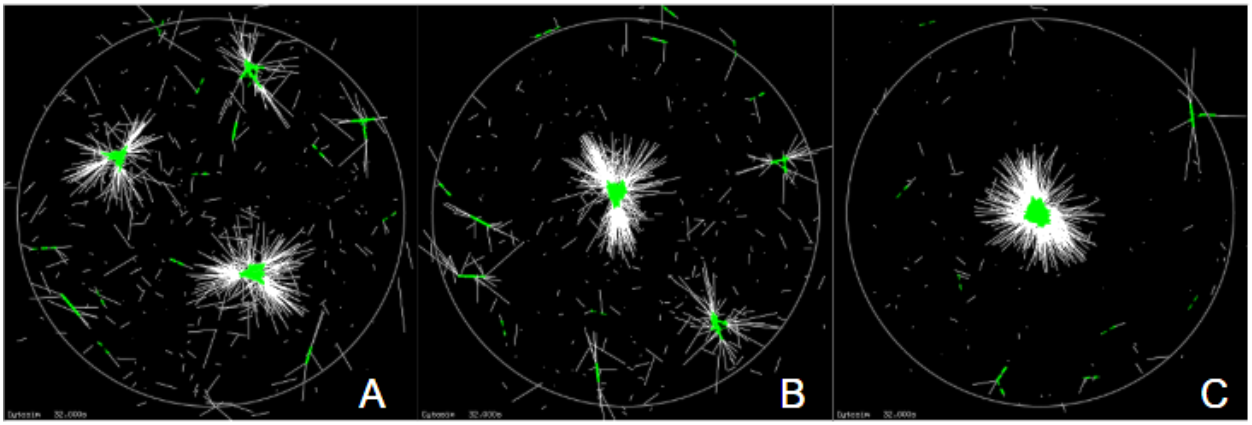

FIG 4.8: Local-Global Contraction Transition for Exponentially Distributed Fibers *Typical simulations with exponentially distributed fiber lengths, with* $\boldsymbol{\Gamma}$ *=8, 16, 21, respectively. The global contraction threshold is 20 for exponentially distributed fibers. As* $\boldsymbol{\Gamma}$ *increases, we see the formation of well-formed local asters that eventually merge into one central aster once* $\boldsymbol{\Gamma}$ *exceeds the global threshold. The aster is noticeably larger and asymmetric compared to the uniform length asters.*

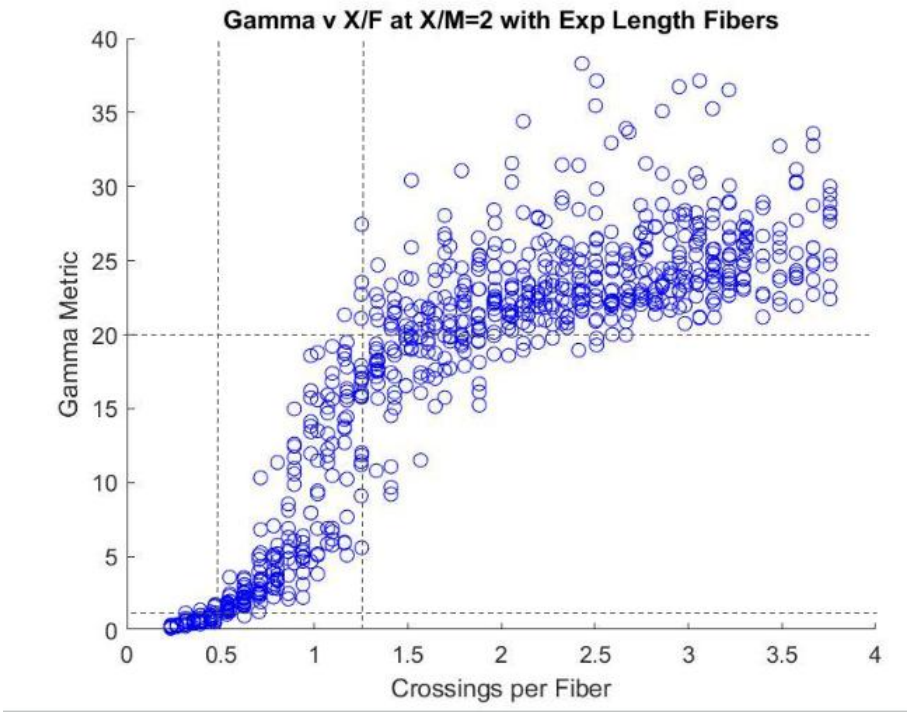

FIG 4.9: Exponential Length Fiber Dependence of Γ *The Contraction Metric* ***Γ*** *as a function of Crossings per Fiber* $X/_F$ *for a fixed density of 2 Crossings per Motor with exponentially distributed fiber lengths.* ***Γ*** *increases slowly toward 1 in the No Contraction region, increases rapidly in the Local Contraction region, before leveling off around 20 once Global Contraction has been achieved. While the variation of the* ***Γ*** *value is higher than for uniform fibers, the basic shape remains. This is unsurprising given there is more input randomness than before. Like in* ***FIG 4.****6, the threshold and contour lines intersect near areas of behavioral transition in the* ***Γ*** *curve.*

That the global threshold differs for different length distributions means we must be careful assigning a concrete interpretation of the value of **Γ** directly. We view this metric as being able to distinguish trends and turning points through comparison of simulations done in a consistent context. While we believe this value can be used in a wide variety of contexts, a calibration must be done in each new context for any particular **Γ** value to be of use.

Chapter 5 Results

In this Chapter, we present our results combining theoretical predictions described in Chapter 2, CytoSim Simulations described in Chapter 3, and the **Γ** Metric measurements described in Chapter 4. Our connectivity metrics show that out theory does an excellent job of predicting when a system will not contract, will contract locally or contract globally. With proper modifications to the theory, this method works for all tested variations of fiber parameters. We also show that connectivity is fundamentally to contraction by introducing crosslinkers and changing the space to have periodic boundaries. These configurations introduce new connectivity which can both help and harm the contraction behavior in predictable ways.

5.1 Results in an Open Space

5.1.1 Standard Parameter Choice

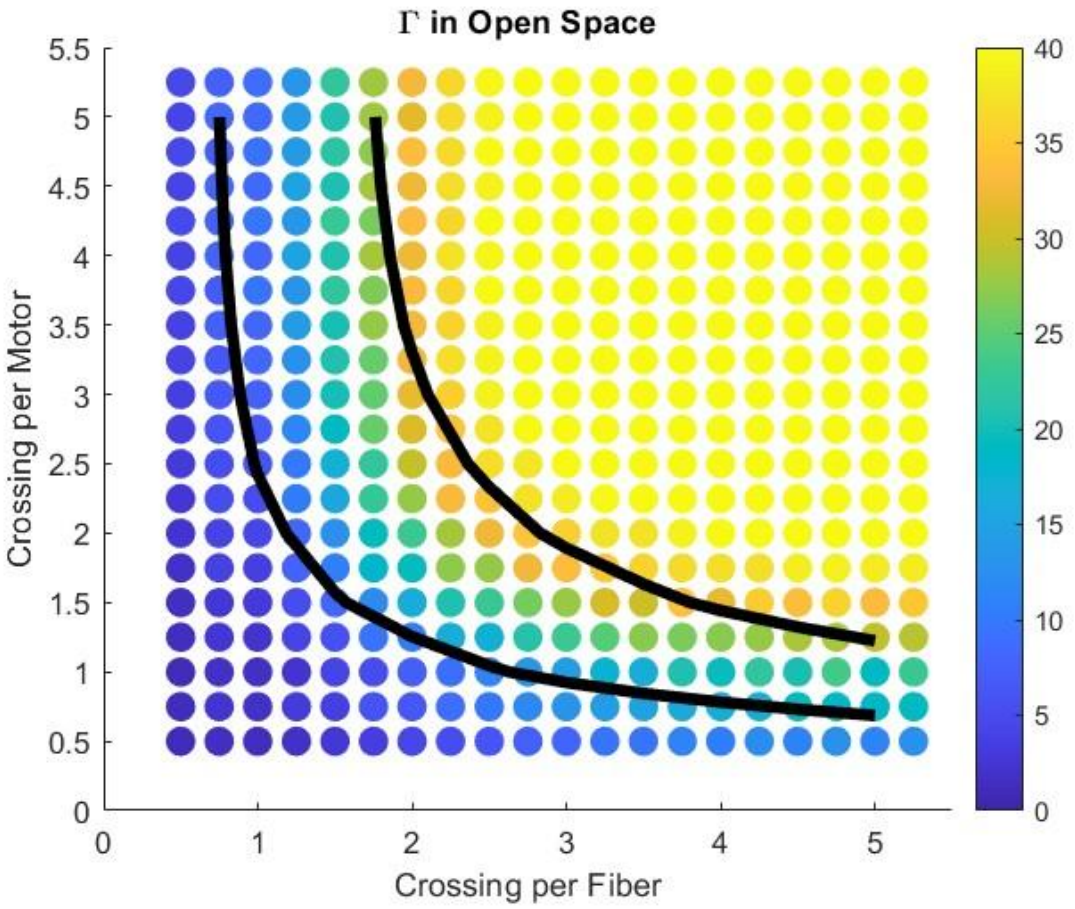

FIG 5.1: Standard Parameters Phase Space *The Contraction Metric* **Γ** *as a function of Crossings per Fiber* $^{X}/_{F}$ *and Crossings per Motor* $^{X}/_{M}$*. Black curves represent the theory contours and correctly separate the regions into a blue No Contraction region, a blue to orange Local Contraction region, and a yellow Global Contraction region. Each point is an average of ten simulations.*

FIG 5.1 shows the full phase measurements of **Γ** when varying both the Crossings per Fiber $^{X}/_{F}$ and Crossings per Motor $^{X}/_{M}$ counts. The contour lines do not act as perfect dividers

but do create guarantees. Any configuration that lands above the $C_{local} = 0.5$ contour has some level of local contraction. Any configuration that lands above the $C_{global} = 0.5$ contour is guaranteed to globally contract.

To ensure the universality of our results, we tested several major variations to the nature of the fibers, including fiber length distribution, fiber rigidity and fiber dynamics. We have already shown that the predicted crossing formula *Eq 2.1* depends only on average length and number of fibers, thus no variation in any other fiber properties should fundamentally affect the connectivity of the network. When analyzing the minimal configuration necessary for polarity sorting contraction, we needed two fibers, but since the fiber-motor interaction is localized to the motor head binding region, none of the specific fiber properties should have an impact on the contraction mechanism. Therefore, if the local fiber polarity sorting mechanism and the global connectivity requirements are indeed sufficient to predict the contractility of a given configuration, variations in most fiber parameters should not fundamentally change contractile behavior.

5.1.2 Variation in Fiber Rigidity

The simplest variation is fiber rigidity. So far, we have tested simulations of microtubule-like fibers, which are very rigid ($22\ pN\mu m^2$). This has the advantage of being computationally efficient since the fiber can be made of only one segment. However, in real systems non-muscle myosin II only interacts with actin, not microtubules. We expect that since neither the network connectivity nor the contraction mechanism geometry depends explicitly on fiber flexibility, decreasing the rigidity to be more like the highly flexible actin should not alter the results.

To generate realistic actin networks, we generate bent fibers using the *'equilibrate'* command as discussed in Chapter 3. Our theory for the number of crossings assumed the fiber was straight. However, since the persistence length is much longer than the total fiber length and the bending direction is symmetric, we do not expect fibers to divergence significantly from the straight configurations.

As **FIG 5.2** shows, fiber flexibility is indeed unimportant to contractile behavior. Going forward, all simulations will be done with rigid fibers for efficiency. The importance of geometry over the exact details of the components suggests that simulations designed to test polarity sorting of microtubules using a more realistic microtubule-binding motor design should not meaningfully change the results.

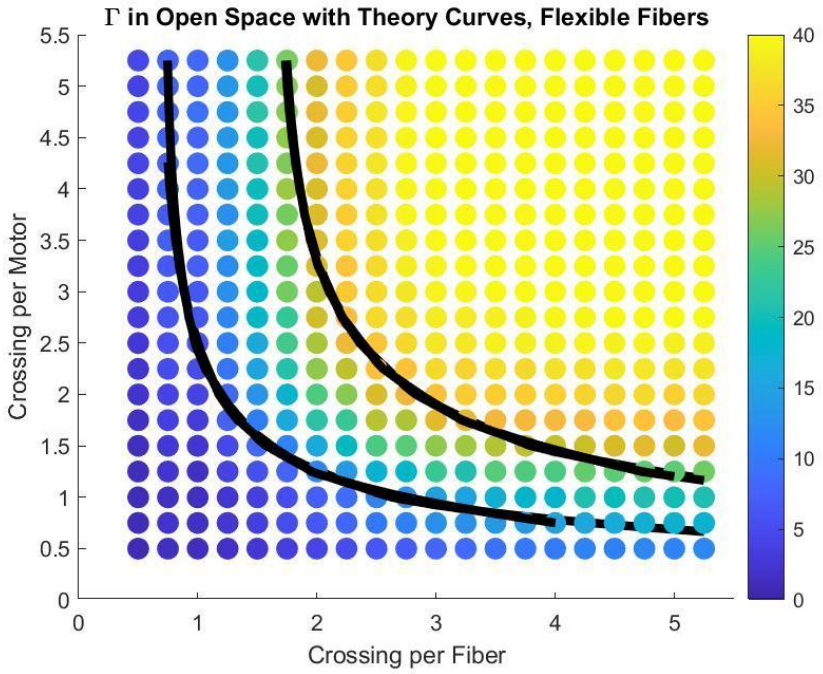

FIG 5.2: Flexible Fiber Phase Space *The Contraction Metric* $\boldsymbol{\Gamma}$ *as a function of Crossing per Fiber* $X/_F$ *and Crossing per Motor* $X/_M$ *with uniformly distributed flexible fibers. Since neither the connectivity nor the contraction mechanism depends on fiber flexibility, the results unsurprisingly have not changed.*

5.1.3 Variation in Fiber Length Distribution

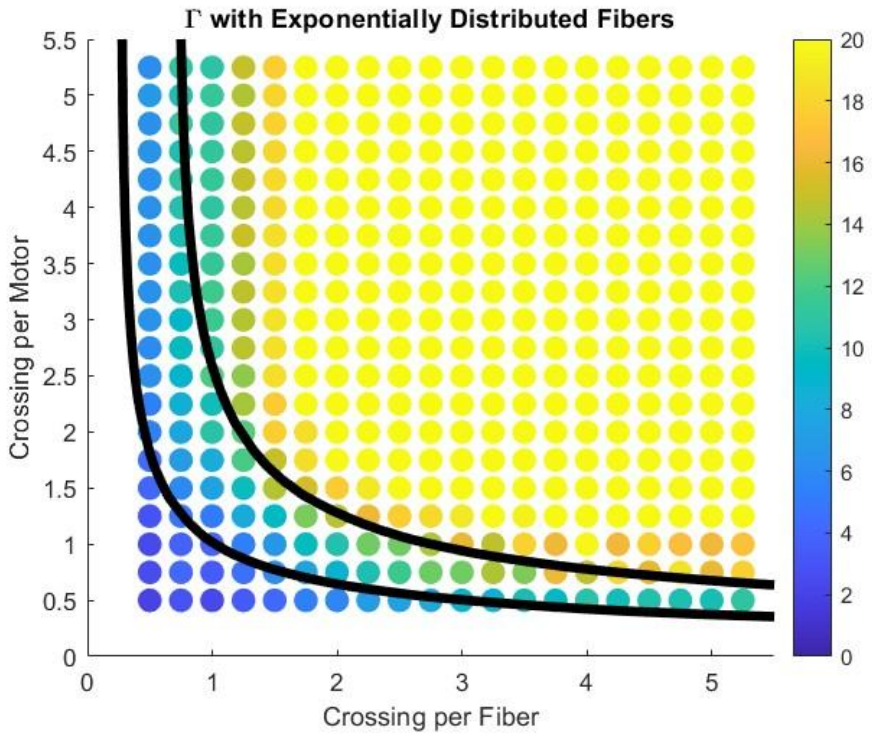

FIG 5.3: Exponential Length Phase Space *The Contraction Metric* ***Γ*** *as a function of Crossing per Fiber* $^{X}/_{F}$ *and Crossing per Motor* $^{X}/_{M}$ *with an exponential length distribution. Due to the presence of longer fibers, the maximum value indicating global contraction needs to be reduced. However, the adjusted theory contours still separate the space into regions of differing contractile behavior.*

An exponential length distribution for the fibers is a more reasonable model of fibers *in vivo*. Experimental measurements (Piekenbrock et al 1992) have shown actin has this distribution which is the expected result from a polycondensation process where long polymers are assembled from monomers (Oosawa 1970, Schallar 2025). However, since our basic measure of connectivity relies on average length, it is reasonable to think that the length distribution should not fundamentally alter the ability of the system to contract. As discussed in Chapter 2 and 4 respectively, the exact contours and the upper limit of **Γ** need to be adjusted due to the

asymmetry between short and long fibers. This leads to a similar but shifted separation of the phased based on predicted contractile behavior. As **FIG 5.3** shows, the simulation results do confirm our theory predictions for exponential length distribution. Global contraction reliably occurs at lower fiber and motor densities than the uniform length distribution due to the fact more mass is contained in long fibers and fewer longer fibers are needed to ensure connectivity. This also means that the local contraction region is thinner than in the uniform fibers case.

An alternative distribution of lengths is a Gaussian one. However, as discussed in Chapter 3, CytoSim does not allow us to initialize fibers in a Gaussian distribution directly. Instead, we create dynamic fibers capable of growing and shrinking stochastically, which in the absence of motors, grow from a uniform to Gaussian length distribution. In order to separate the effects of the Gaussian fiber distribution and the dynamics itself, we first allow the dynamic fibers to grow for two minutes before turning off the dynamics. We then added motors and allowed the system to contract as before. **FIG 5.4** shows that, like the exponential distribution, once we adjust for the asymmetry between long and short fibers, our conclusions remain unchanged.

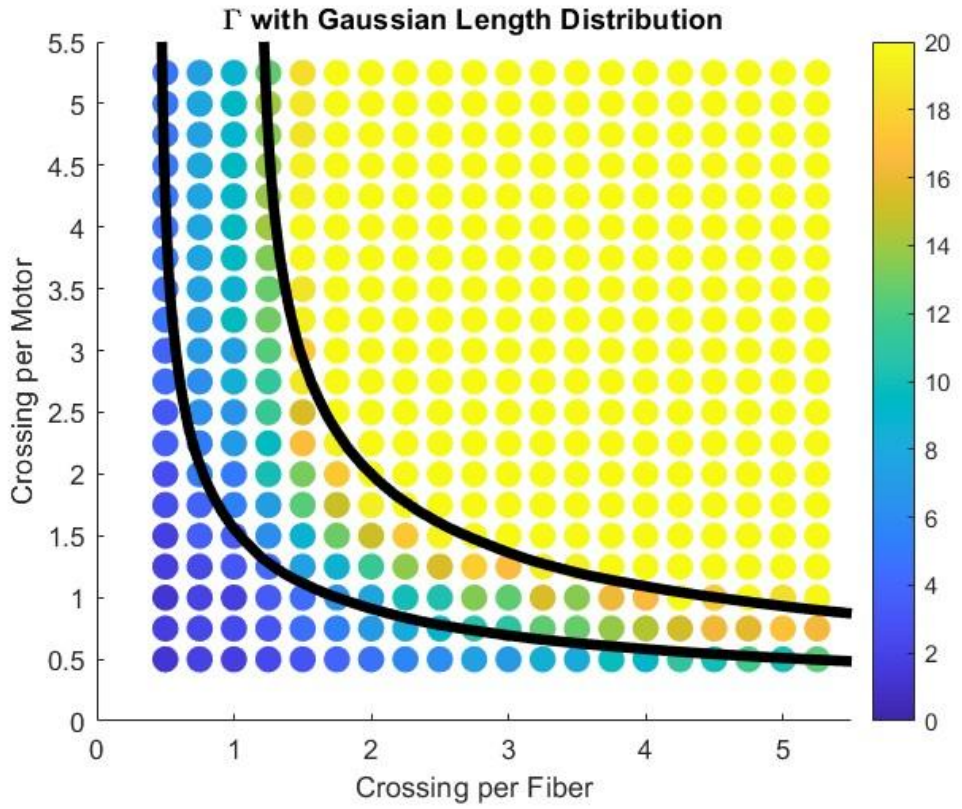

FIG 5.4: Gaussian Length Phase Space *The Contraction Metric* ***Γ*** *as a function of Crossing per Fiber* $^{X}/_{F}$ *and Crossing per Motor* $^{X}/_{F}$ *with a Gaussian length distribution. Due to the presence of longer fibers, the maximum value indicating global contraction needs to be reduced. However, the adjusted theory contours still separate the space into regions of differing contractile behavior.*

5.1.5 Variation of Fiber Dynamics

Next, we check whether the dynamical behavior of the fibers could affect overall network contractility. This time, we grow the fibers and leave the dynamics on while adding motors. As discussed in Chapter 3, we define standard growth as the fastest growing actin currently measured experimentally. Unlike the pure Gaussian test, we leave on motor dynamics when motors are added to the system.

FIG 5.5 shows the network contraction for fibers that grow and shrink at standard and ten times standard rate. For reasonable growth rates, the results are predictably similar to the Gaussian phase space. Here, the timescale for a fiber to appreciably change size is much longer than the timescale of contraction, and therefore the dynamics are unimportant. Just like with non-uniform length distributions, global contraction does occur at slightly lower fiber densities due to the asymmetry between longer than average and shorter than average fibers. For an unrealistically large growth rate, the behavior changes but in a manner consistent with our model of connectivity driven contraction. Here the average length of fiber noticeably increases early in the simulation since the fibers are equally likely to start in the relatively fast-growing state and the slower shrinking state. This increases the connectivity and allows diffuse configurations normally in the non-contractile region to contract. While the unrealistically fast growth shows there are limits to our simulation, the fact it takes such an extreme to show overall behavioral differences increases confidence in our model.

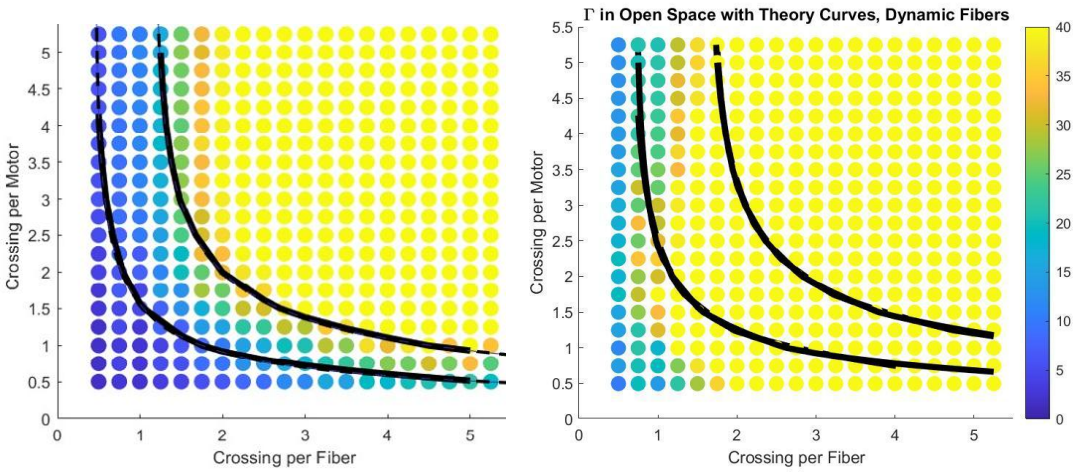

FIG 5.5: Dynamic Growth Phase Space *The Contraction Metric* ***Γ*** *as a function of Crossing per Fiber* $X/_F$ *and Crossing per Motor* $X/_M$ *with dynamic fibers. At reasonable growth rates, the overall contractile behavior does not change, and our theory curves still make good guarantors of contraction. However, if the fibers grow unreasonably fast, the fibers grow and connect the entire system once a minimum motor density is achieved.*

Another approach to fiber dynamics is fiber turnover. To model extremely fast polymerization and depolymerization, instead of tracking the growth of individual fiber ends, an entire fiber is removed and replaced at a random location in the space. While we were not able to construct a reliable metric to measure systems without a steady end state, our contractile regions provide insight into the behavior of turnover systems. Every set number of frames, a set number of fibers are removed from the system and an equal number of new fibers are placed randomly in the system. This disorganizes a network, and while not a truly random system our theory assumes, the relative level of connectivity is preserved. Therefore, we can hypothesize that the type of contraction is preserved as well.

A poorly connected network remains poorly connected regardless of the turnover rate. As **FIG 5.6** shows, a low connectivity network that never contracts without turnover does not become contractile with the addition of turnover.

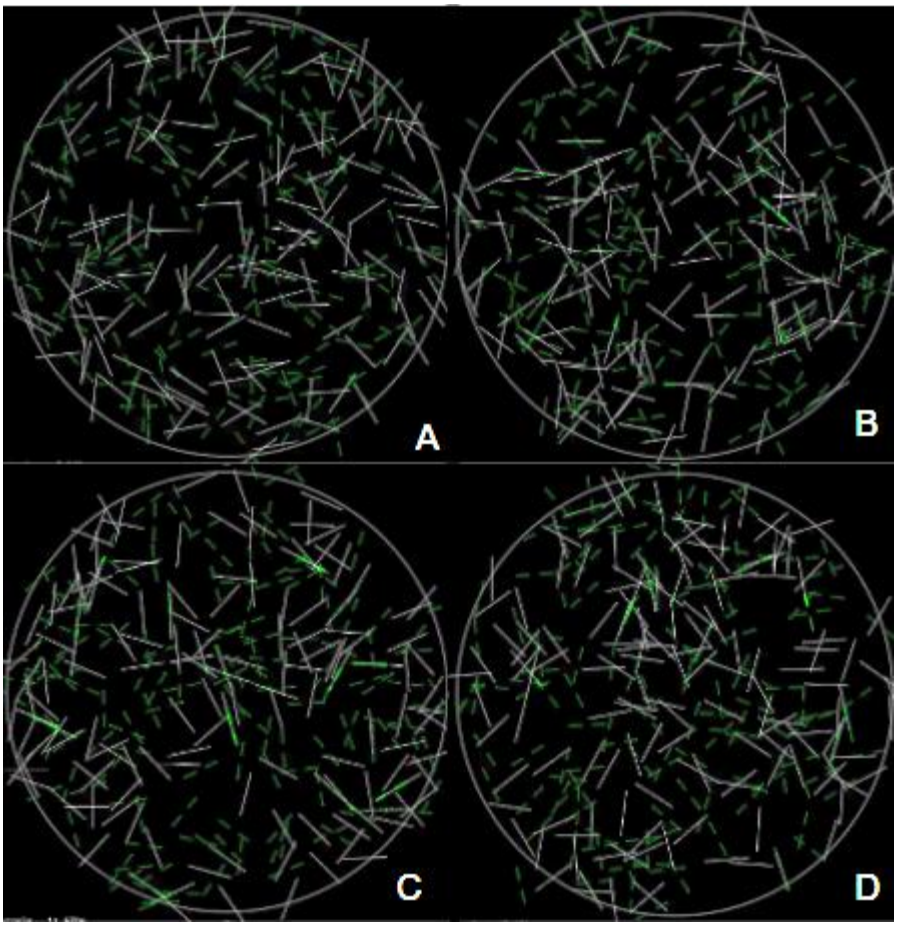

FIG 5.6: No Contraction with Turnover *Snapshots taken at (A) 0, (B) 5, (C) 10, and (D) 15 seconds of a low connectivity system with turnover. The system never contracts.*

If a network shows local contraction without turnover, then a turnover system will show pulsatile contraction behavior. This cytoskeletal behavior has been observed in many biological systems, such as during the gastrulation of *Drosophila* (Martin et al 2009). Small asters will form somewhere in the space, but since the network is only locally connected, the asters will slowly disappear over time. When removed from the aster, fibers are most likely to return in an area that is not connected to that aster. Over time fibers will be moved from within an aster back to disorganized areas, until the disorganized area is full enough to initiate the formation of new asters. This process can be seen in **FIG 5.7**

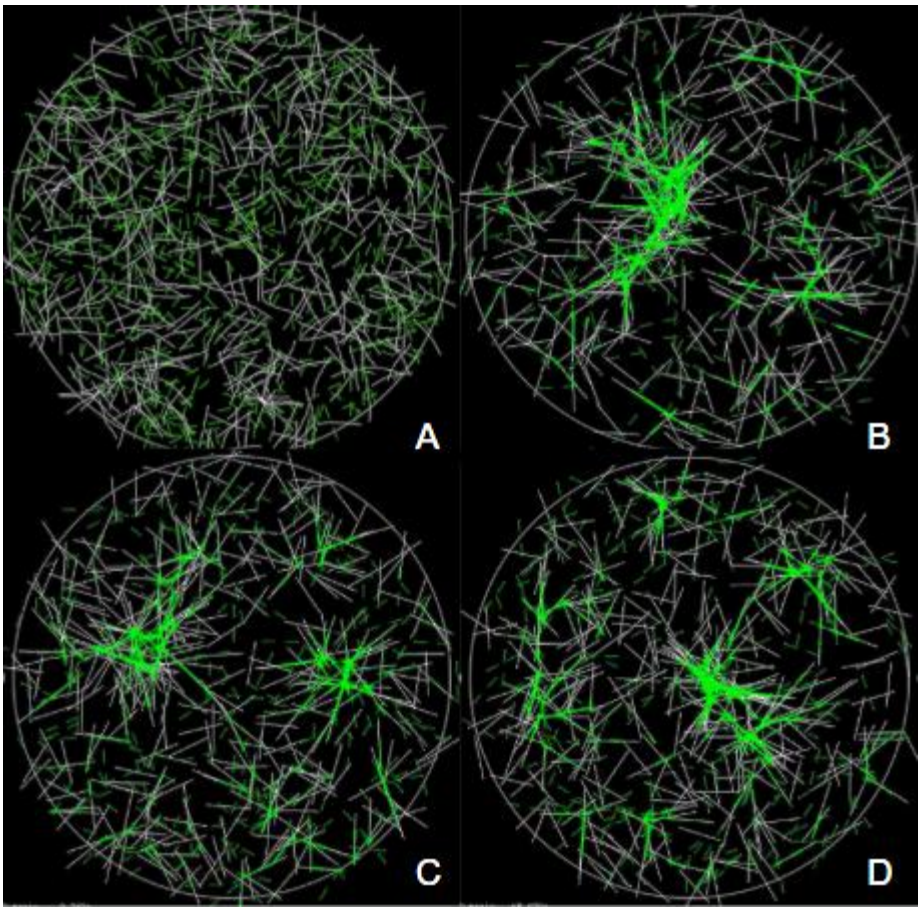

FIG 5.7: Local Contraction with Turnover *Snapshots taken at (A) 0, (B) 5, (C) 10, and (D) 15 seconds of a locally connected system with turnover. A small aster has formed in the left side of the cell in (B) but has shrunk in (C) and mostly collapsed by (D). A connected area can be seen on the right in (B) and fully form a separate aster by (D).*

Finally, a highly connected network will stay connected as fibers turnover. No matter where new fibers are generated, they will still be connected to the rest of the network. An initial large, central aster will form, and as new fibers are added around it, they will form asters that are connected to the central aster and will be pulled towards it through the motor activity, as can be seen in **FIG 5.8**. Such steady state influx has been observed in starfish oocytes (Bun et al 18).

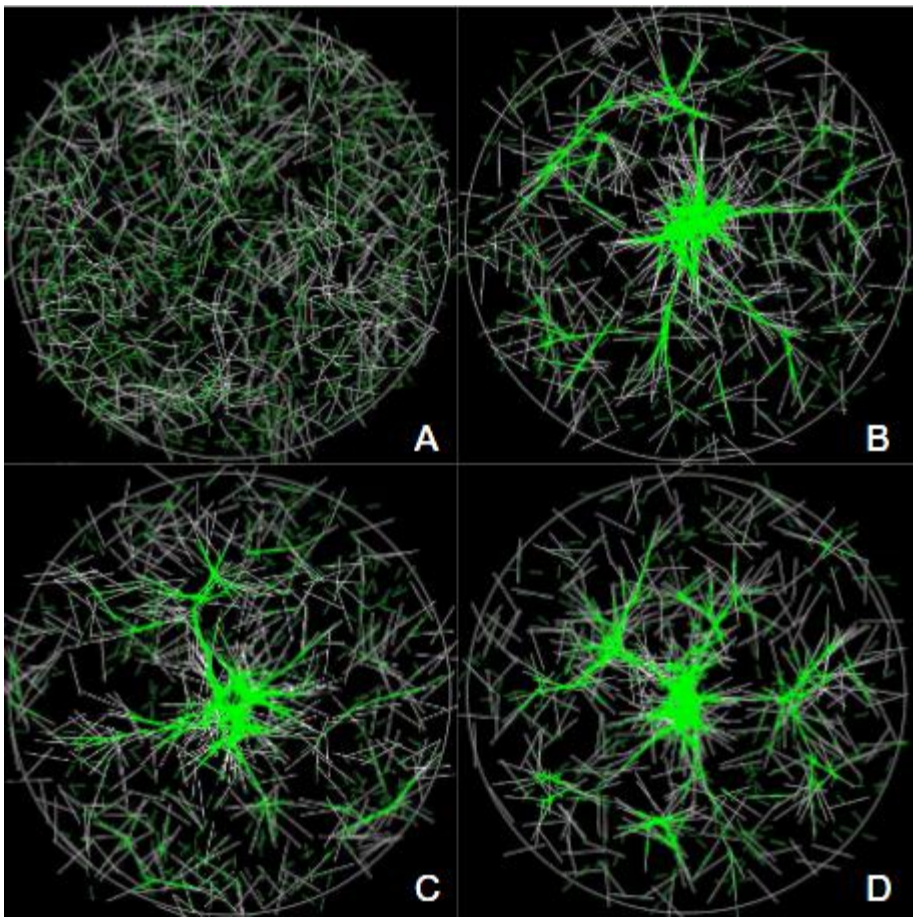

FIG 5.8: Global Contraction with Turnover *Snapshots taken at (A) 0, (B) 5, (C) 10, and (D) 15 seconds of a locally connected system with turnover. A large aster has been formed by (B) and remains present throughout the simulation. Tendrils connecting the edges of the network and local asters to the central aster will grow and fluctuate over time. Almost all fibers slowly move towards the center until being turned over.*

From these results we conclude that our connectivity maps, while derived for static fiber networks that better represent *in vitro* system of reconstituted cytoskeletal systems, is also able to predict the *in vivo* behavior of highly dynamic cytoskeletal networks as seen in different developmental processes.

5.2 Addition of Crosslinkers

Another way of proving the importance of connectivity is to introduce new types of bonds to the system that, on a local mechanical level, cannot contribute to polarity sorting driven contractions. Crosslinking proteins can bridge pairs of fibers and motors, but do not consume energy or generate forces directly. For rigid fibers, this means that the addition of crosslinker connections should harm the contraction of the network by preventing the free reorganization of the fibers by motors. (As discussed in Chapter 1, crosslinkers in the presence of flexible fibers can drive contraction through fiber buckling, the implications of which are discussed later in this section.) However, introducing crosslinkers also increases the quantity of fiber-to-fiber connections in the network, and for non-contractile and transition regions, inactive connections may be better than no connections at all. However, if too many of these inactive connections are present, the system will become locked in place and unable to contract.

By introducing crosslinkers, we add a third dimension to our phase space defined by number of crosslinkers Cl. We are not capable of examining every detail of this higher dimensional phase space, so instead we will simply consider the absolute number of crosslinkers to be the interesting variable and will focus on a select set of particular $X/_F \ vs \ Cl$ and $X/_M \ vs \ Cl$ planes.

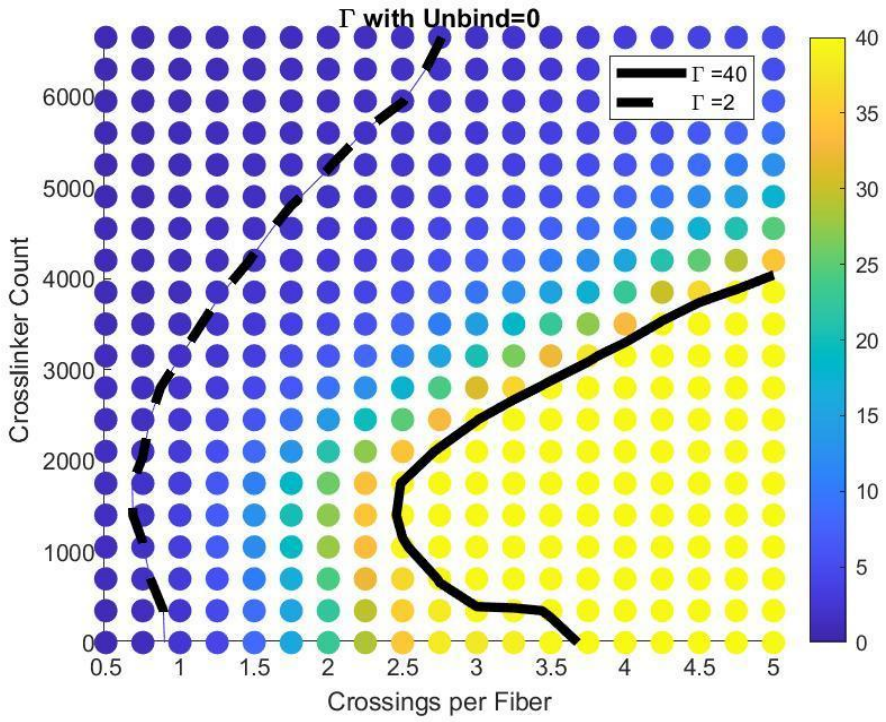

FIG 5.9: Crosslinker Phase Space *The Contraction Metric* ***Γ*** *as a function of Crossing per Fiber* $X/_F$ *and Crosslinker count Cl at* $X/_F$ *=1.75. A small number of crosslinkers add connectivity to the system. Even though crosslinkers create no new contraction mechanism, increasing connectivity itself makes contraction possible when it was not without crosslinkers and more effective when it already was possible. Eventually though the crosslinkers create too much rigid connectivity and the motors, no matter how many, cannot generate enough force to reconfigure and contract the network.*

FIG 5.9 shows that by adding a small number of cross linkers, low $X/_F$ configurations solidly in the local contraction region become globally contractile. Increasing the connectivity of the system increases the contraction potential despite not adding a new contraction mechanism. Fibers that were only bound to one motor and thus not contributing much to the network's contraction now may be indirectly bound to multiple motors through a chain of intermediate fibers and crosslinkers. While not as reliable, a motor-fiber-crosslinker-fiber-motor chain drives the same global contraction behavior the motor-fiber-motor chain did. The forces generated by

one motor walking and sorting across the network are propagated through crosslinker connections and across the network. However, as **FIG 5.10(C)** makes clear, introducing too many inactive crossings locks the system in its current configuration and stops contraction. **FIG 5.10(B)** shows there is an optimal balance between the quantity and quality of connectivity to drive contraction in complex networks. The full effect on contractile behavior due to crosslinker count can be seen in **FIG 5.11**.

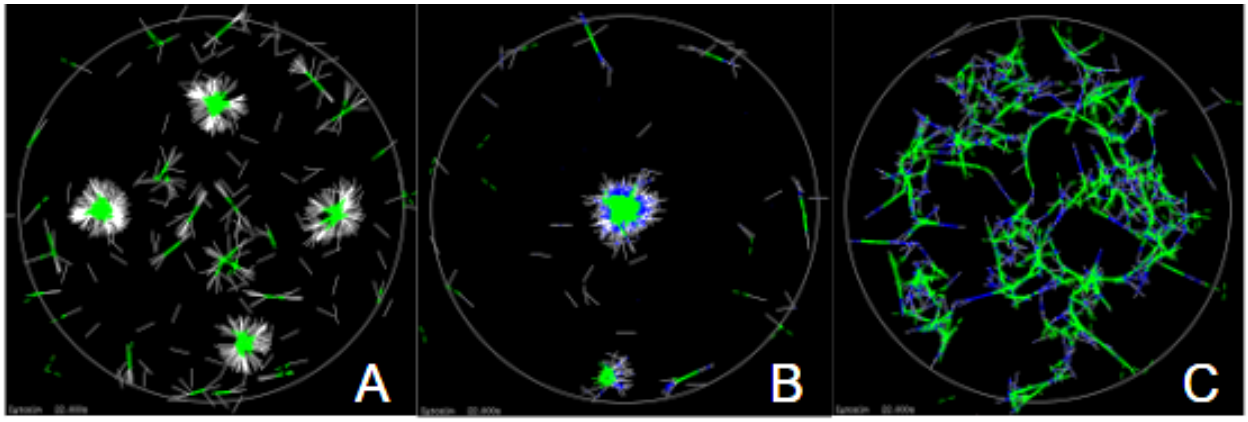

FIG 5.10: Crosslinker Simulations *Snapshots of the final states for three different crosslinker counts (A) Left: 0 crosslinkers. Without crosslinkers, the system is slightly connected and contracts into several local isolated asters. (B) Middle: 1050 crosslinkers. By adding just enough connectivity, forces perpetuate across the network, allowing for everything to contract into one central cluster. (C) Right: 6650 crosslinkers. The high number crosslinkers have locked the initial condition in place with enough rigidity to prevent all contraction.*

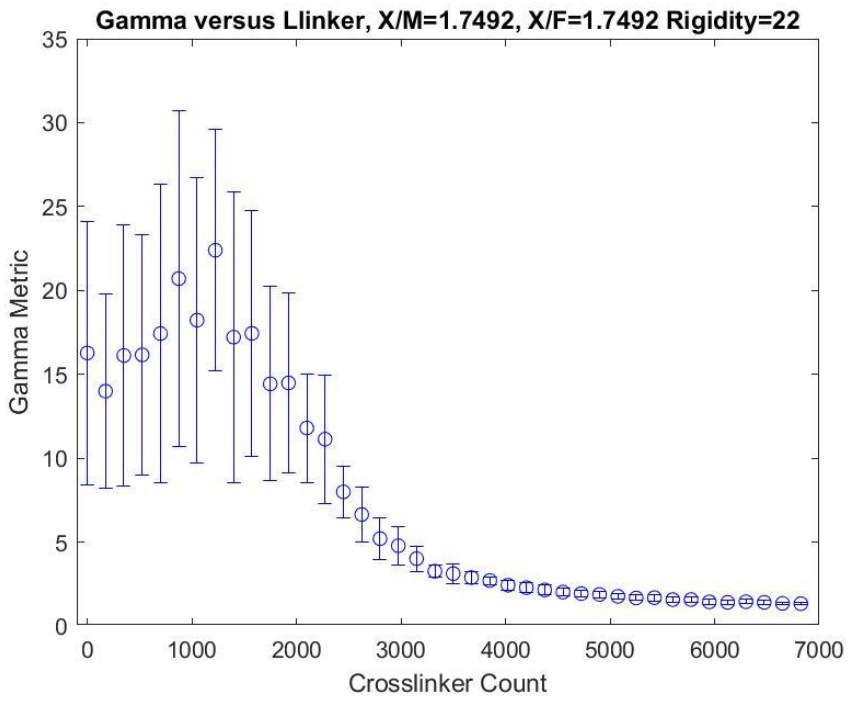

FIG 5.11: Crosslinker Dependence of Γ *The average with error bars over many trials of Contraction Metric* ***Γ*** *as a function of Crosslinker count at* $^{X}/_{F}$ *=* $^{X}/_{M}$ *=1.75. As before, a small number of crosslinkers increases the amount of contraction until an optimal level is reached. Further adding crosslinkers begins to lock the system in place until there is the guarantee of no contraction.*

To confirm connectivity is the necessary explanation for this new contraction, we can compare the system when the fibers are flexible. In the presence of crosslinkers, flexible fibers can contract through the buckling mechanism. When the fiber buckling contraction mechanism is possible, the network contraction increases much more dramatically and falls much slower with the addition of crosslinkers, as seen in **FIG 5.12**. Since the introduction of a new contraction mechanism creates large changes, the small changes observed with flexible fibers suggest that a new mechanism is not responsible for the results. We do know that crosslinkers increase connectivity, and therefore it is reasonable to conclude that this higher connectivity is driving the slight increase in contractility.

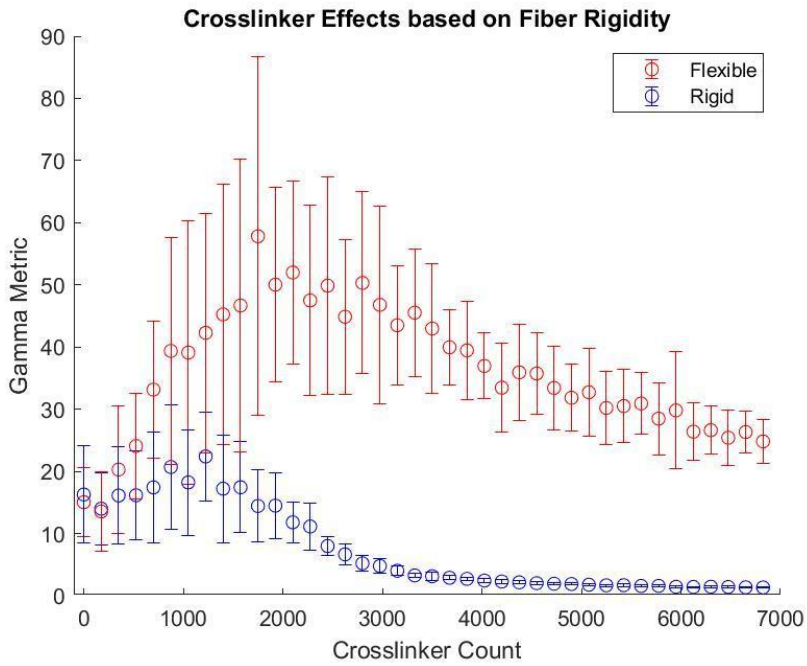

FIG 5.12: Crosslinker Dependence of Γ with Flexible Fibers *The average with error bars over many trials of Contraction Metric* ***Γ*** *as a function of Crosslinker count at* $^{X}/_{F} = {}^{X}/_{M} = 1.75$ *for rigid (blue) and flexible (red) fibers. Crosslinkers help contract both systems through increases in connectivity. Due to the ability to drive contraction through the buckling of flexible fibers, the presence of crosslinkers is far more impactful for flexible fibers.*

5.3 Results in a Periodic space

One simulation difference that does meaningfully change the interpretation and conclusions is attempting contraction in a periodic space. This geometry better reflects conditions where the cytoskeleton network spans over a very large space or the cortex of a cell, where the membrane wraps itself along both directions. The biggest difference being that high connectivity no longer leads to global contraction. Instead, a well-connected network in a periodic space will not contract at all. A given fiber will be connected to its neighbors in all directions and thus feel forces pulling it equally in all directions. Without an asymmetry caused

by the edge of the network, there is no preferred sorting or contraction directions, and no global network restructuring can take place. We thus expect a different contractility output, where contraction is only possible within the local connectivity region of the parameter space. (While not exhibiting contractile behavior, high and low connectivity networks will have differing ability to generate internal tension. This may be a fruitful direction for future exploration and will be briefly discussed in Chapter 7.)

Our metrics for both connectivity and contraction work the same in a periodic space. **FIG 2.2** already showed that we can use the same approach to correctly predict the number of crossings in a periodic space. The $\boldsymbol{\Gamma}$ value correctly represents our visual intuition, just as it does in the open circle space. $\boldsymbol{\Gamma} < 1$ still indicates no contraction, but as **FIG 5.13** shows, this now occurs at both high and low connectivity. $\boldsymbol{\Gamma} > 1$ still indicates local contraction leading to the formation of many small but distinct asters (**FIG 5.14**). Since connectivity is low enough, fibers can only interact with nearby neighbors. They cannot feel the influence of fibers far away and so cannot tell the difference between open versus periodic boundaries.

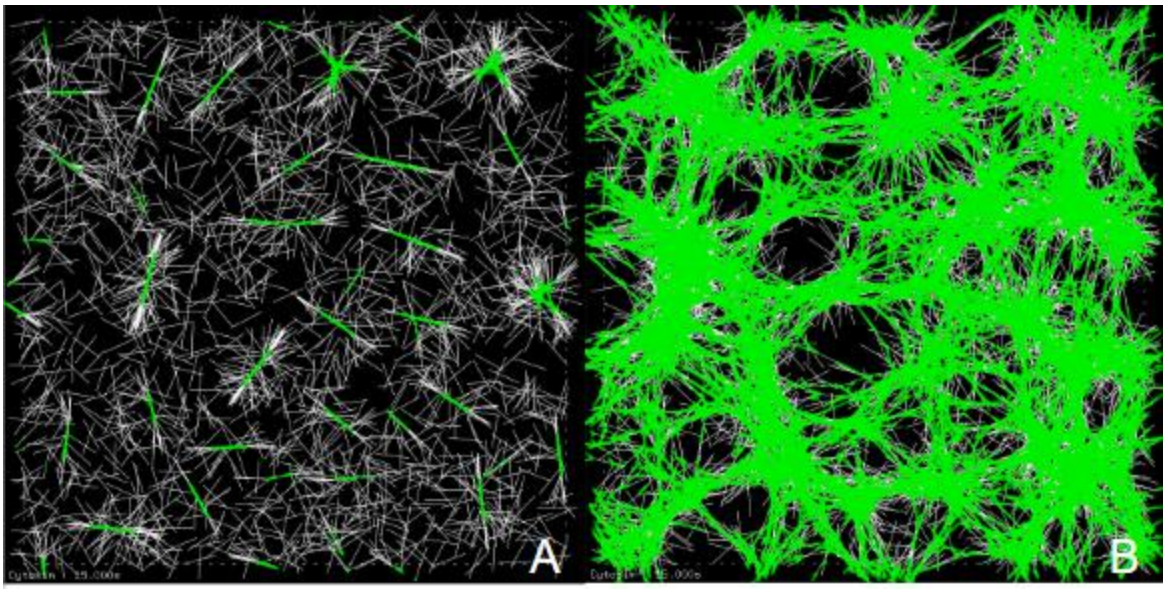

FIG 5.13: Periodic Boundary No Contraction Simulations *Two typical No Contraction simulations in a periodic space. A very low connectivity simulation has* $\boldsymbol{\Gamma} = 0.5$ *and a very high connectivity simulation has* $\boldsymbol{\Gamma} = 0.435$*. The presence of periodic boundary conditions means high connectivity no longer leads to global contraction.*

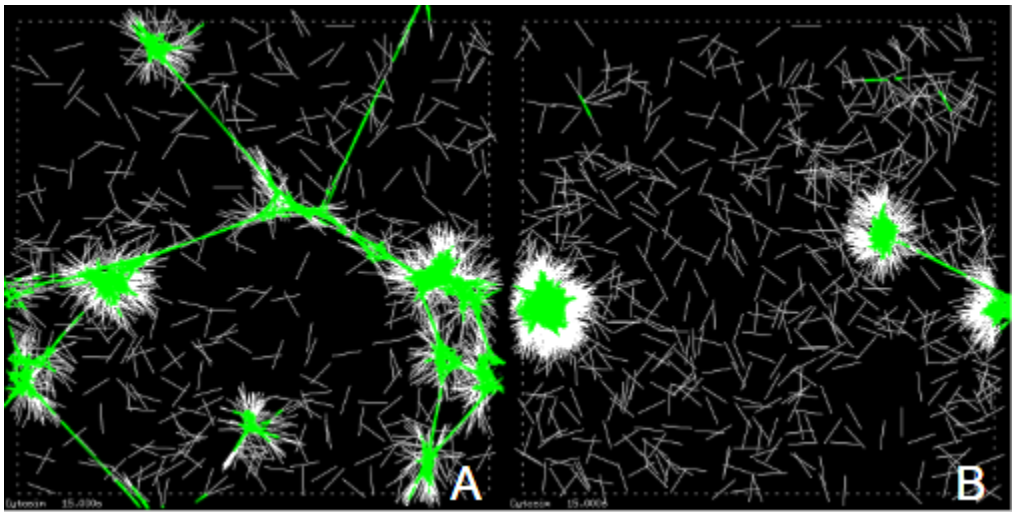

FIG 5.14: Periodic Boundary Local Contraction Simulations *Two typical Local Contraction simulations with* $\boldsymbol{\Gamma} = 4, 14$ *respectively. Like in the open space,* $1 < \boldsymbol{\Gamma}$ *indicates local contraction, characterized by many small but distinct asters spread across the space.*

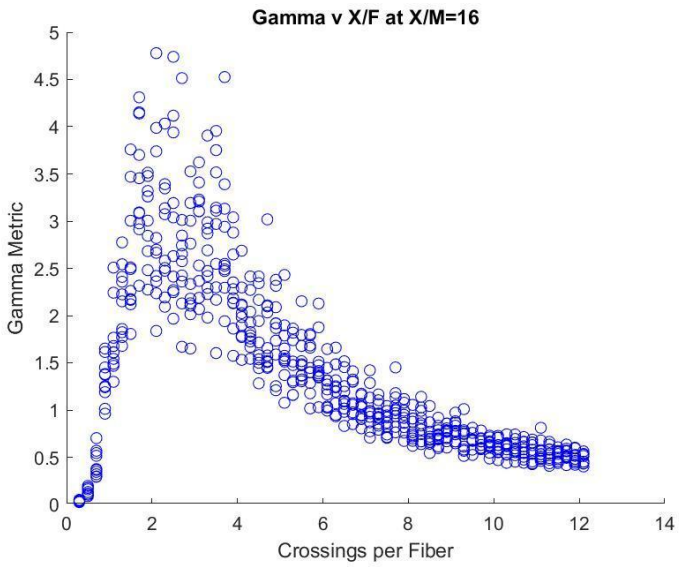

FIG: 5.15 Γ in a Periodic Space *The Contraction Metric* ***Γ*** *as a function of Crossings per Fiber* $X/_F$ *for a fixed density of 16 Crossings per Motor* $X/_M$ *in a periodic space.* ***Γ*** *increases slowly toward 1 in the No Contraction region, increases rapidly in the Local Contraction region, before beginning to decrease as the system becomes connected enough for the boundary conditions to be relevant to the local behavior of fibers. Eventually the metric goes back below one, indicating the system is so connected it has locked into the initial configuration*.

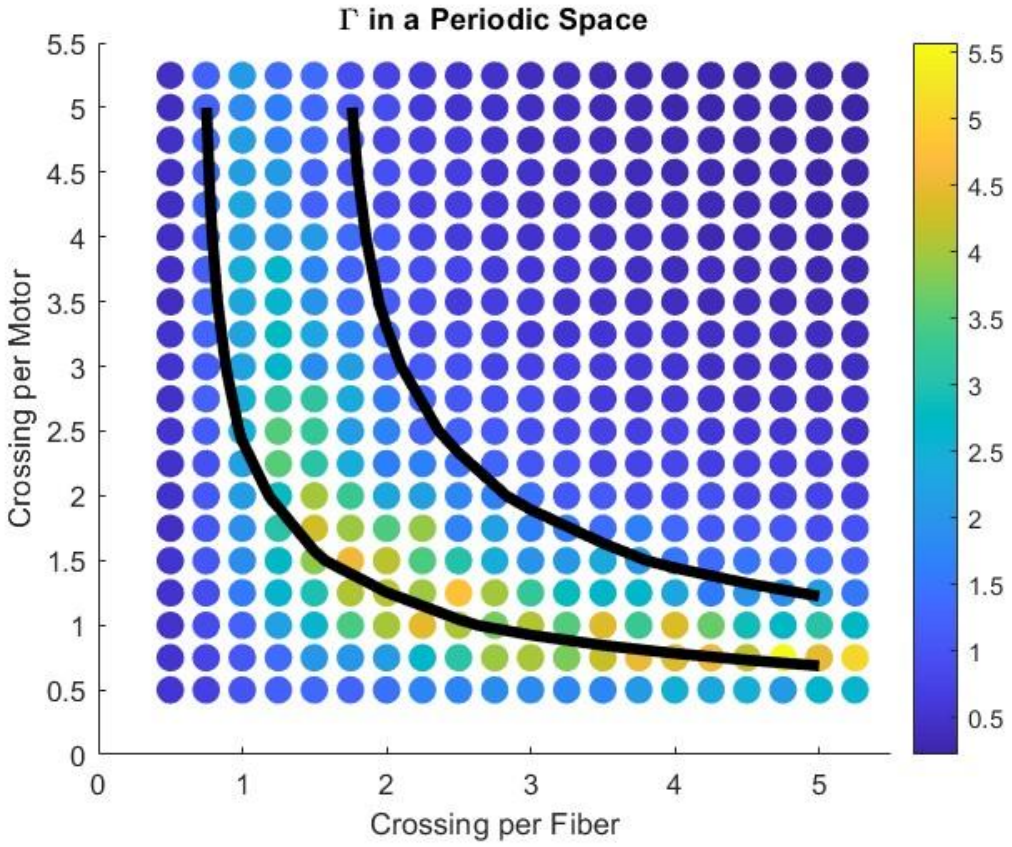

FIG 5.16 Periodic Space Phase Space *The Contraction Metric* ***Γ*** *as a function of Crossing per Fiber* $X/_F$ *and Crossing per Motor* $X/_M$ *in a Periodic Space. Unsurprisingly, since Global Contraction is no longer possible, the upper contour no longer acts as a meaningful divider of behavior. Instead, local contraction can only be seen along the lower contour.*

Both a horizontal cut (**FIG 5.15**) and the full phase (**FIG 5.16**) space match the understanding that global contraction is no longer possible. While the theory contours still tell us about the probability of local configurations, they no longer necessarily translate to global behavior, acting as neither guarantees nor dividers of the space into regions of contractile behavior. However, the fact that local contraction can only occur along the local contour confirms that our connectivity approach can still tell us about contraction in periodic space.

While it is important to adjust interpretations based on the context, our connectivity approach defined by fiber-motor interactions and expansion of local thinking into global predictions, allows us to predict the contractile behavior in a diverse set of cellular component configurations and behaviors.

Chapter 6 Connectivity in the Cytokinetic Ring

In this chapter we will extend our discussion of connectivity into a new geometry modelling the formation of the cytokinetic ring. The research group led by Ana Carvalho performed experiments designed to study the role of crosslinkers in the formation and maintenance over time of a cytokinetic ring. They proposed that their measurements of the rate of successful ring formation could be recreated *in silico*. Ring failure occurs when the ring is not well connected enough to resist the tension needed to drive constriction and cell division. We provided support by simulating ring formation, identifying parameters that recreate success rates, and tested variations not easily accessible in experiments. Doing so requires slight modification of our approach to measuring contractile behavior to more accurately reflect a new geometry.

6.1 Cytokinesis

Cytokinesis is the final stage of cell division, where a dividing cell is physically separated into two distinct daughter cells. Earlier phases sperate chromosomes into two regions, which defines an equator around the cell membrane between the regions. Actin fibers from across the cell membrane are driven by myosin activity towards this equator and form the cytokinetic ring. If formed properly, further motor activity will generate tension in the ring. As tension grows, the

ring begins to constrict towards the ring's center point, deforming the cell membrane along with it.

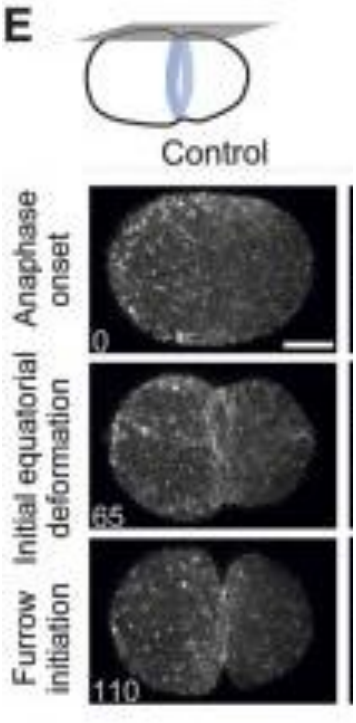

FIG 6.1: Cytokinesis *Cross section of a cell undergoing cytokinesis, with myosin motors tracked used GFP. Starting from the onset of anaphase (separation of the chromosomes), actin and myosin spread across the cortex migrate to the equator and form the cytokinetic ring. As the ring constricts, it deforms the membrane with it, ultimately cleaving the cell. Taken from Sobral et al 2021.*

As seen in the experimental images of **FIG 6.1**, ultimately, this constriction pinches the cell into the two daughter cells. In collaboration with the Carvalho group, we applied our idea of connectivity to study under what conditions this important biological structure can form and remain stable over sufficiently long periods of time.

6.2 Cylindrical Geometry

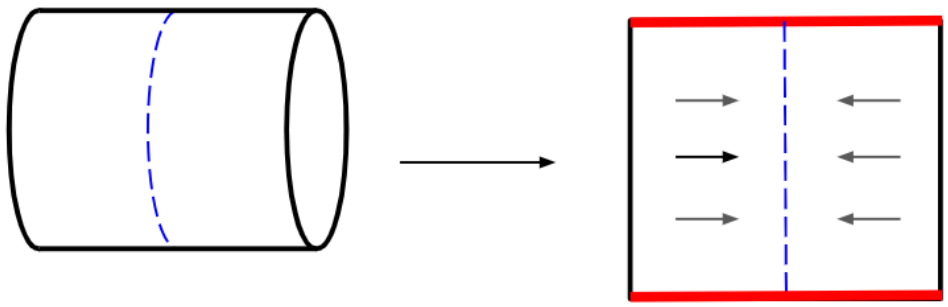

FIG 6.2 Cylindrical Space *We model a cylindrical space by creating a rectangular space and periodically identifying the two opposite red edges. This creates a preferred contraction direction towards the blue dotted line as indicated by the arrows.*

To study the construction of the cytokinetic ring from a disordered network, we need to restrict network components to the surface of an open cylinder (**FIG 6.2**). We create a rectangular space and periodically identify one pair of sides while leaving the other open. This creates a cylindrical space that mimics the construction of a cytokinetic ring when viewed from a side projection instead of a cross section. This arrangement creates a preferred contraction direction inward towards the line halfway between the nonperiodic sides. The position of the contracted fibers relative to this center line will be used to measure the successful formation of the cytokinetic ring.

6.2: Ring Contraction Metric $\boldsymbol{M}$

While we believe $\boldsymbol{\Gamma}$ is widely useful across a large variety of contexts, unique geometries call for a more unique metric to best illuminate cell behavior. In the cylindrical geometry, contraction occurs only in one direction. The $\boldsymbol{\Gamma}$ metric is less appropriate here since it treats all directions symmetrically. Instead, a metric designed to efficiently measure these ring construction systems should take this asymmetry into account. By modifying the same basic box counting approach used to construct $\boldsymbol{\Gamma}$ in a circular space, we create a metric designed for easily determining whether a simulation in a cylindrical space ends in the construction of a ring. We call this metric $\boldsymbol{M}$.

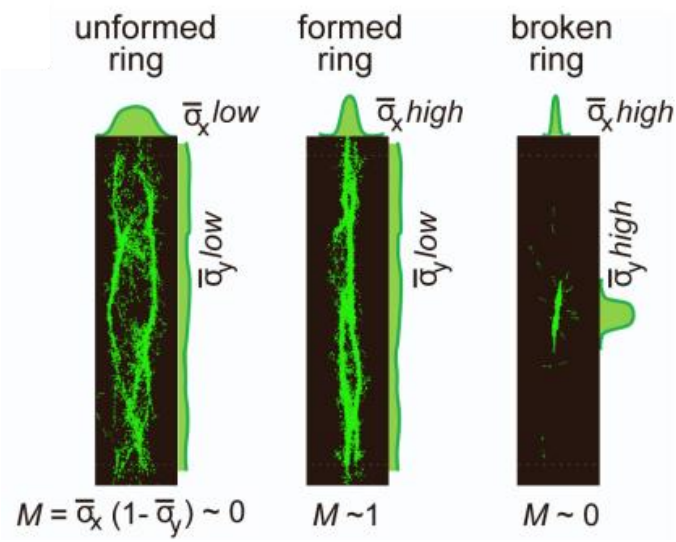

FIG 6.3: Ring Metric *Three typical snapshots of simulated cytokinetic ring construction demonstrating the visual intuition motivating the Ring* ***M*** *metric. A) No Ringe. Motors have not bound tightly enough in the center for this to be considered a cohesive ring capable of constriction later in their lifetime.* $\overline{\sigma_x}$ *is small and therefore* $\boldsymbol{M \sim 0}$*. B) A well-formed ring. Concentrated horizontally, evenly spread vertically and therefore* $\overline{\sigma_x} \sim 1$*,* $\overline{\sigma_y} \sim 0$ *and* $\boldsymbol{M} \sim 1$**.** *C) A broken ring. A hole formed in the ring and the space effectively lost its periodic boundary condition. This allows the system to contract in an undesired direction and creates* $\overline{\sigma_y} \sim 1$ *and therefore* $\boldsymbol{M} \sim 0$*.*

Instead of boxes, this time we take our simulation space and divide it up into horizontal and vertical bins, where the space is periodic only in the vertical direction. The details of the division are not important as long as the bin size is sufficiently large, meaning the width must be at least as wide as a well-formed ring. Since the ideal ring has all components making a ring around the halfway point between the ends of the cylinder, the center of the central horizontal bin should coincide with the vertical midline of the space. We then count the number of the motor points with their horizontal coordinate in each bin and take the standard deviation of these counts to define the horizontal deviation σ_x. This value is normalized by dividing it by the largest possible deviation, which could occur when all objects can fit into the same central bin. We record this value as the normalized horizontal deviation $\overline{\sigma_x}$. We repeat the process for the

vertical bins to produce the normalized vertical deviation $\overline{\sigma_y}$. Finally, we combine these two values to create the Ring $\boldsymbol{M}$ metric in the following way.

$$(6.1) \quad M = \overline{\sigma_x}(1 - \overline{\sigma_y})$$

As with **Γ**, this metric is motivated by our visual intuition. A well-formed ring should have all its components concentrated horizontally but spread out evenly across the periodic vertical direction. **FIG 6.3** diagrams possible combinations of $\overline{\sigma_x}$, $\overline{\sigma_y}$, and $\boldsymbol{M}$, which all range from 0 to 1. By visually checking simulated construction events, the threshold for ring formation is $\boldsymbol{M} = 0.5$. This metric can be tracked over time to measure the time it takes to form a ring and whether a ring is stable over the long term.

6.3: Collaboration with the Carvalho Experimental Group

Our novel approach to connectivity and contraction and computer modelling experience has drawn interest from experimental collaborators. Working with the Carvalho Group, our designs have contributed to the understanding of cytokinetic ring formation. In Sobral et al 2021, we examined the role of crosslinker geometry on the migration rate of cytoskeletal fibers from across the cortex into an equatorial ring and the long-term stability of the ring. The short range Plastin and the flexible and extended Spectrin crosslinkers cooperate in maintaining the ring by increasing the connectivity of the network, as can be seen in **FIG 6.4**.

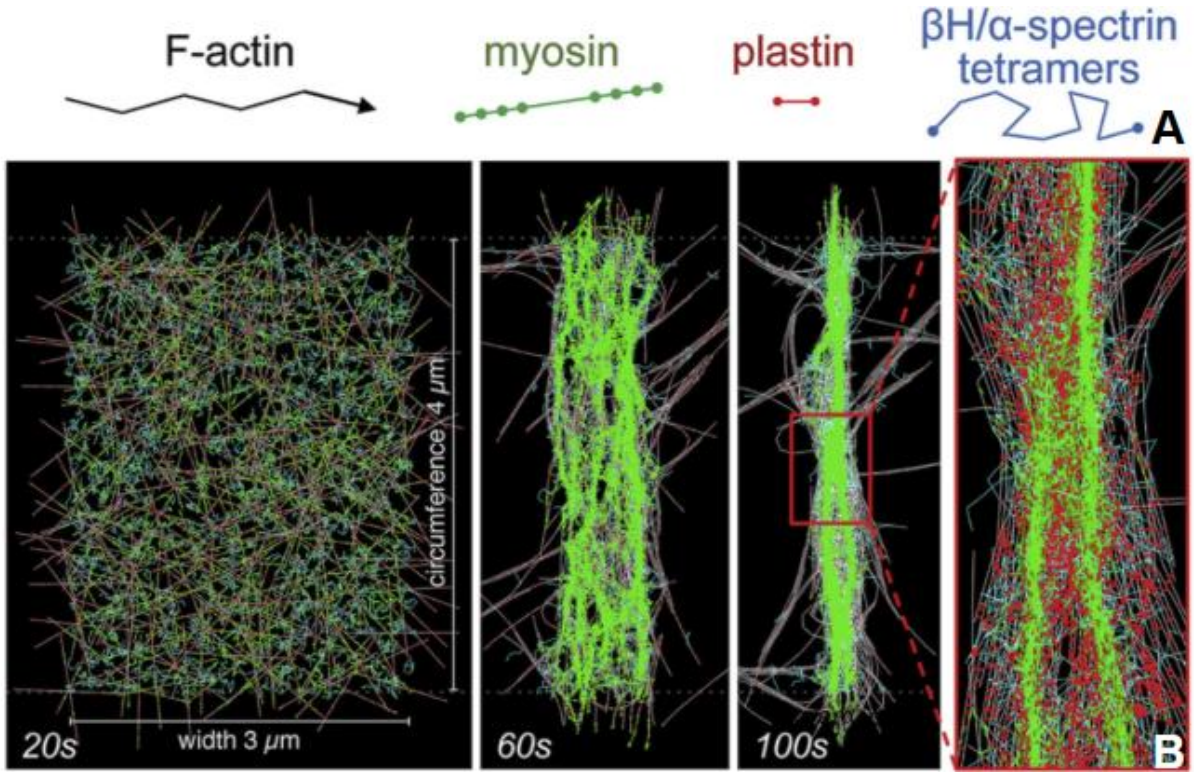

FIG 6.4: Simulating the Cytokinetic Ring *(A) A color coded diagram of the components needed to simulate the construction of a cytokinetic ring. (B) A time evolution of an initially disorganized network that contracts towards a center line until the components form a single thin ring that spans the periodic vertical direction.*

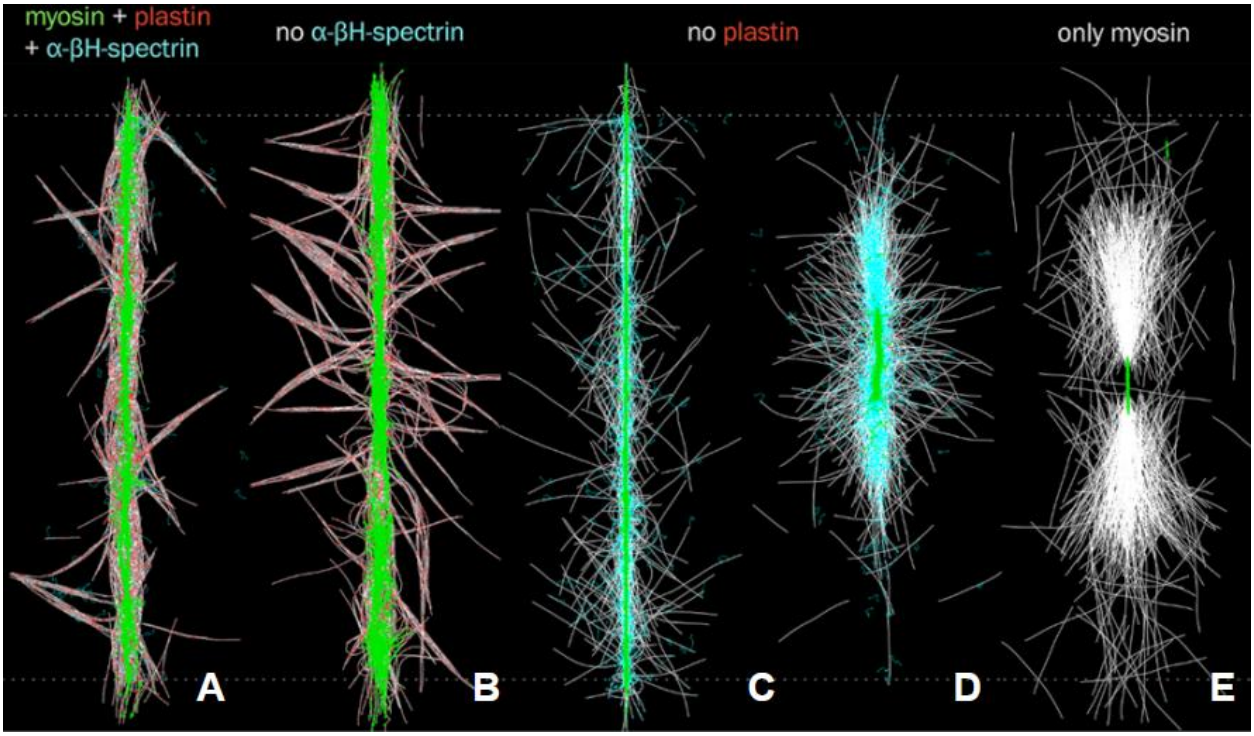

FIG 6.5: Role of Crosslinkers in the Cytokinetic Ring *(A) A ring formed with both crosslinkers present. (B) A ring without spectrin, characterized by many tendrils tightly bound by plastin but not connected to the main ring without the long range spectrin. (C) A successfully formed ring without plastin, but without the tightly packed plastin the ring is slightly fragile. (D) A hole in the ring can form, destroying the periodic nature and allowing the ring to contract towards a point. (E) A ring without either crosslinker. The connectivity provided by the motors is sufficient for a ring to form, but it lacks any long-term stability. Crosslinkers play a crucial role in determining long term connectivity across the space.*

FIG 6.5 shows the role crosslinkers play in creating and maintaining connectivity in a system. Either is sufficient to maintain ring integrity over the long term, but the rings are qualitatively different. Plastin is abundant but short ranged and can only bind fibers of similar orientation, making it capable of forming tight bundles. Without the flexible, long-range spectrin, those bundles tend to drift away from the central ring. Spectrin can hold the ring together, but the

long-range nature and lower relative abundance means this connectivity is less reliable, and in a small number of simulations, a hole formed that was not bridged by the crosslinkers. (Experimental exploration of these ruptures was explored more the in the follow up paper described at the end of this chapter.) Holes in the ring destroy the periodic geometry and the structure now has a preferred direction of contraction away from the hole. The ring collapses into a 1-dimensional analog of an aster. This problem is greatly exacerbated when neither crosslinker is present. Motors provide sufficient connectivity to sort a disordered network but cannot reliably provide any long-term stability once the ring has been constructed. Holes formed in almost all these rings.

The success rate of ring formation was measured first experimentally and reproduced through our simulations (**FIG 6.6**). Using our approach, a ring is successful if $\boldsymbol{M} > 0.5$ after a sufficiently long time. Success rates align with the possible outcomes identified in **FIG 6.5.** The control system with both crosslinkers and the system without spectrin nearly always form successfully, the system without plastin forms approximately 90% of the time, and the motor only system create rings with long term stability in only 10% of simulations.

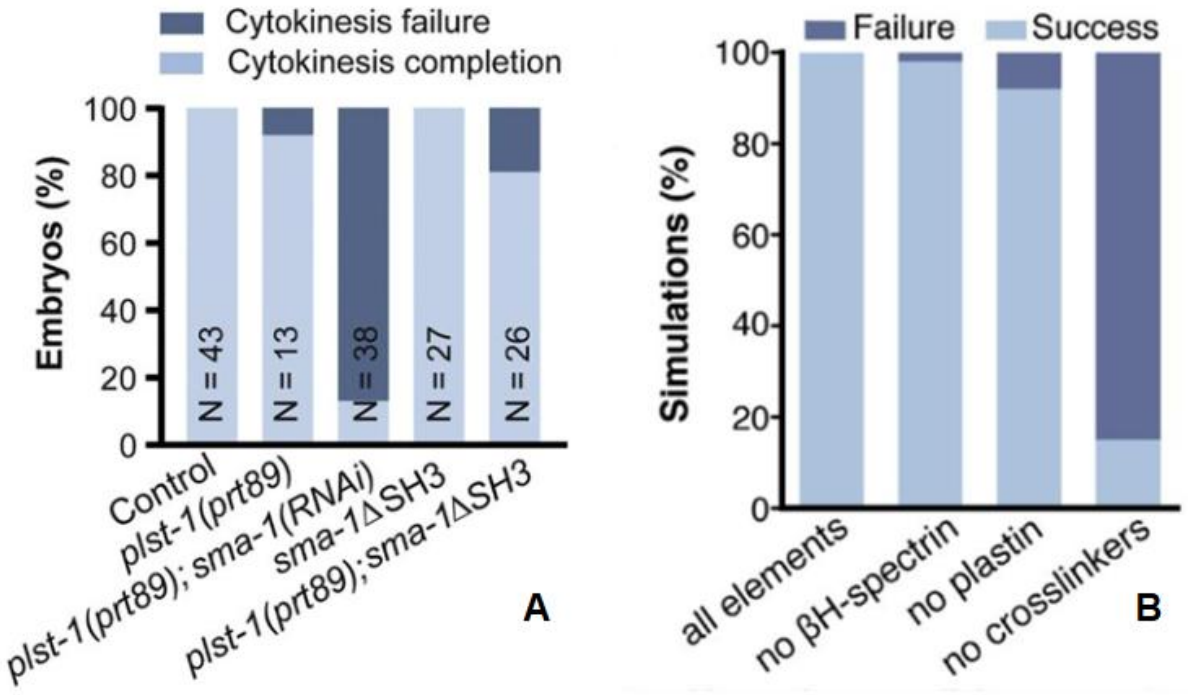

FIG 6.6: Success Rates of Cytokinetic Ring Formation *(A) Experimentally measured success rates, (B) reproduced in simulations. While either crosslinker type is sufficient to form and stabilize rings, at least one type in necessary. Taken from Sobral et al 2021.*

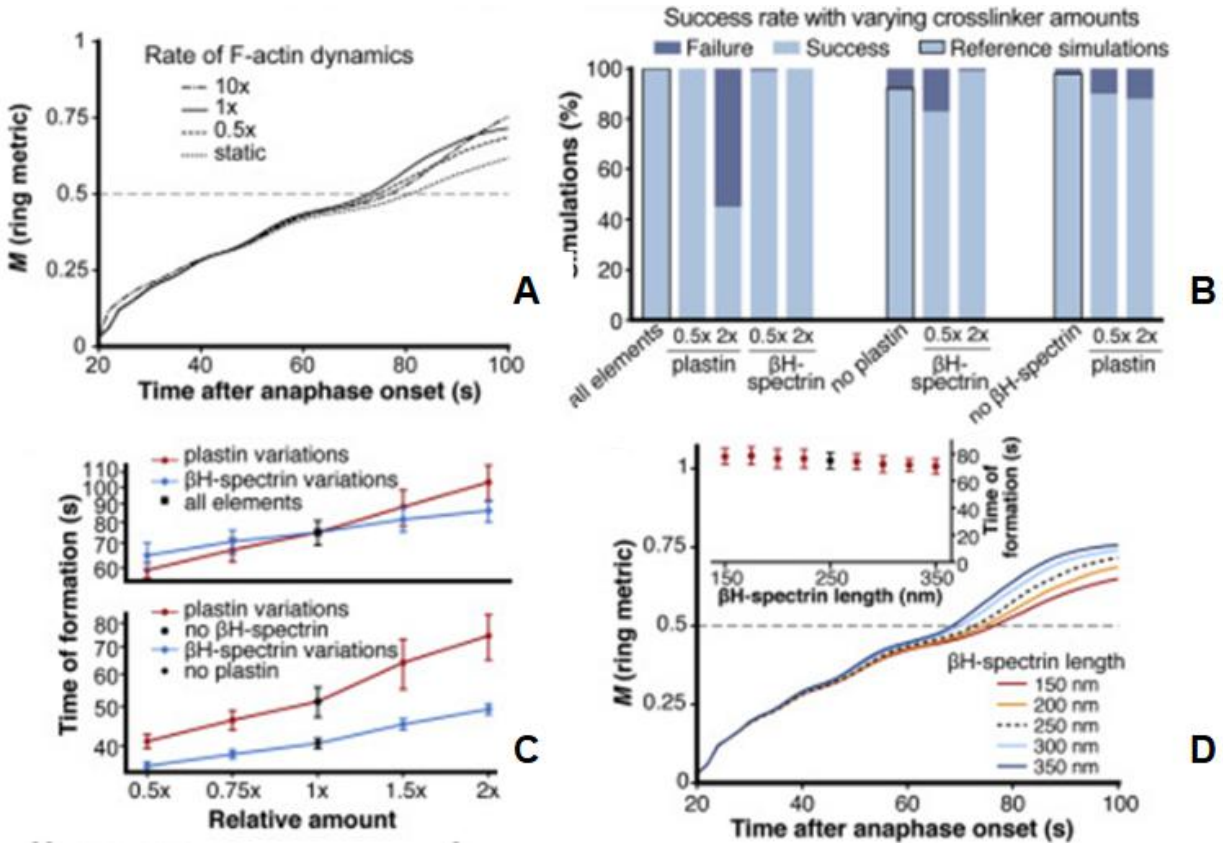

FIG 6.7: Simulation Only Variations of Cytokinetic Ring Formation *(A) Records of the average* ***M*** *over time for multiple levels of fiber dynamics. As with the results for the open space, contraction behavior is independent of dynamics. (B) Success rate due to the variation of relative crosslinker counts. The most significant effect can be seen when the plastin count is doubled while spectrin is also present. Like with the open space, this introduces an extremely high level of connectivity and prevents the disordered network from coalescing into a ring in the first place. (C) Shows the time after anaphase it takes to construct a ring for variations in the crosslinker counts. As expected, the amount of either type of crosslinker is proportional to the time it takes to contract the network. (D) Variations in the length of the spectrin backbone. Even large changes cause only minimal changes in the time evolution or ring formation time (inset). Taken from Sobral et al 2021.*

Using our metric ***M***, we can track both the time evolution of network, as well determine when the ring successfully formed. After reproducing the experimental measurements, we were able to extend results to configurations and variations that are not easily accessible in real cells,

such as changes to length of the spectrin backbone or level of fiber dynamics. A summary of results can be found in **FIG 6.7**

A follow up collaboration examining what role connectivity plays in ring constriction resulted in Silva et al 2022. When actin fibers were removed from rings, the constriction rate significantly slowed and the dependence on spectrin concentration largely disappeared. Attempts to explain this solely using our logic of connectivity failed. The reduction of actin increases the myosin to actin ratio, suggesting that constriction rate should increase. We identified that another mechanism holds primary responsibility. The observed results are only explained when considering connectivity with binding site competition, meaning myosin and spectrin had to compete for places to bind to the actin fiber. If the actin binding sites are already saturated, then the expected increase in motor activity cannot actualize and instead the loss of connectivity to other fibers hinders polarity sorted driven contraction. Likewise, increasing the crosslinker count is irrelevant because no more spectrin can bind to the fiber.

Chapter 7: Conclusion

7.1: Summary

The transformation of local interactions of individual proteins into the global behavior of a cell's cytoskeletal network is an area of ongoing interest, with the introduction of ideas from percolation becoming commonplace in investigations. The purpose of this work was to introduce a novel approach that combines ideas about percolated networks, the role of local motor-fiber interactions and the integration of many fundamental properties of biological fibers and molecular motor proteins.

In Chapter 1, after detailing the recent history of mathematical modelling in understanding the role of connectivity in cytoskeletal contraction, we introduced our novel approach to connectivity. The direct interaction of one motor walking along one fiber while connected to a second fiber is fundamental to the contraction process known as polarity sorting. Therefore, we must model the network not as a collection of abstract connections, but as a series of fiber-motor-fiber chains.

In Chapter 2, we developed our theory about how the geometric connectivity of an initially disordered network is able to predict the long-term contractile behavior of the system. Through the use of simple geometric and probabilistic arguments, we were able to predict the distribution of fiber-motor intersections. By considering our understanding of the local

interaction, we identified two important configurations that must be present in the network to drive polarity sorting contraction. We were able to predict the probability of these important configurations as a function of fiber count, motor count and object length distributions. By assuming the fibers in the system must be at least more likely than not to be in the necessary configurations, we divided up our phase space of fiber-motor densities into three distinct regions. A low connectivity region where no contraction occurs, a mid-connectivity region where the network can restructure itself into small isolated local asters, and a high connectivity region where the whole network is guaranteed to contract into a single spot.

In Chapter 3, we laid out the computational tools we use to model and simulate cytoskeletal networks, the open-source software package CytoSim. Since CytoSim is capable of simulating every individual object in the system, we laid out the design of fibers, motors and crosslinkers, with a particular focus on how objects extend into space and the binding dynamics between them. We also discussed different spatial configurations and their potential effects on the dynamics.

In Chapter 4, we defined metrics that could be used to classify when and how a network has contracted. After seeing that the common measurement of network size leaves out crucial details, we used our visual intuition to design a new contraction metric. By examining the spatial distribution of fibers, we created a metric that can consistently identify the difference between uncontracted, local contracted and globally contracted networks.

In Chapter 5, we presented the results we obtained through computer simulations of network contraction. We showed that the regions identified by our theory are predictive of contractile behavior. Our predictions were accurate despite changes in fiber rigidity, meaning they can be applied to biological networks made up of either actin or microtubules, and fiber

length distribution and dynamics, suggesting applicability to both *in vitro* and *in vivo* experiments. To test whether connectivity was truly fundamental to our approach, we added crosslinkers into a network of rigid fibers which can add connectivity without introducing a new contraction mechanism. We discovered that even for rigid fiber systems, the introduction of a small number of crosslinkers can enhance contractility while a large number will introduce a rigidity that stalls a motor's ability to walk. We also tested the importance of connectivity in periodic spaces. The lack of a preferred contraction direction means that a small amount of connectivity is needed to drive local contraction, but a well-connected network will try to pull all components in all directions simultaneously and therefore not contract.

In Chapter 6, we discussed how our approach to connectivity can be adapted to the study of cytokinetic rings. The cylindrical geometry that drives the construction of these rings requires a modification of our contractility metric. Using this metric, we studied the connectivity provided by two different crosslinker designs and reproduced the successful formation rate of cytokinetic rings gathered in coloration with the experimental Carvalho group.

7.2: Future Research

There are many possible avenues for future research that can use our metrics and theories as a baseline. We believe we have exhausted the examination of the polarity sorting mechanism, but as discussed in Chapter 1, there are many local interactions that can produce global contractile behaviors. Revisiting Table 1.1 we see immediate changes to our modelling choices we can make to emphasize new contraction mechanisms.

Table 7.1: Summary of Local Contraction Mechanisms

Mechanism	Fiber Rigidity	Fiber Dynamics	Motor End Dwelling	Crosslinker Presence	Crosslinker End Tracking
Polarity Sorting	Either	Optional	**Required**	Optional	Optional
Buckling	**Flexible Only**	Optional	Optional	**Required***	Optional
Disassembly	Either	**Required**	None Present	**Required**	**Required**

For example, when introducing crosslinkers in Chapter 5, we were explicit that those simulations must be done using rigid microtubule-like fibers. This was to avoid the introduction of fiber buckling. As we showed in **FIG 5.8**, when the simulations were repeated with flexible actin-like fibers, the contractile behavior greatly increased, and the contribution of increased connectivity was impossible to distinguish from the contribution of buckling. An attempt to isolate those contributions could be made by designing a third set of simulations where end dwelling motor behavior is turned off, preventing any contraction from polarity sorting. A comparison between simulations with end dwelling motors and rigid fibers (Polarity Sorting only), non-end dwelling motors and flexible fibers (Buckling only) and end dwelling motors and flexible fibers (Polarity Sorting and Buckling) could identify potential regions in a fiber-motor-crosslinker phase space where each mechanism dominates, where they frustrate and where they cooperate. Preliminary attempts to do so were carried out, but we have not included any results given both the theoretical and practical challenges of measuring connectivity due to simultaneous motor and crosslinker binding and the resultant search through a full 3D phase space. We could then further complicate the picture through the introduction of disassembly dynamics and crosslinker end tracking.

Another framework to examine the importance of network connectivity is through the measurement of tension applied to individual fibers due to motor activity. It seems reasonable to suspect that network connectivity plays a significant role in both the propagation of tension forces through the network as well as potentially providing structural relief from them. In experiments, the tracking of relaxation following laser ablation is a common method of measuring tension with structures like mitotic spindles (Elting et al 2014) and cytokinetic rings (Moshtohry et al 2022). Similar simulations can be performed within CytoSim. Fibers intersecting a specified plane can be severed, and the motion of the severed ends tracked. Relaxation rates can then be directly translated into the tension present in the system before the cut. Mapping tension into the same fiber-motor phase space used in this work could be used to explain the relationship between network connectivity and tension. Preliminary work investigating the relationship between connectivity, tension, and constriction rates in cytokinetic rings has been performed in collaboration with the Laplante lab at NC State. Modifications to our connectivity theory to incorporate the geometrically 1D nature of a ring have been attempted. However, several complications have arisen that will need to be addressed in future research.

This work has presented a novel fiber-motor connectivity approach examining the crucial relationship between local protein interactions and global network behaviors. Through the combination of theory and computer simulations, we have identified conditions that dictate the contractile behavior of cytoskeletal networks. This approach is appropriate to use a wide range of fiber, motor and crosslinker parameters and cell geometries. By focusing on geometric and mechanical conditions instead of primarily biological ones, we have thoroughly explored the

potential activity driven by the polarity sorting mechanism from a perspective not commonly found in the preexisting literature.

REFERENCES

Alvarado, J., Sheinman, M., Sharma, A., MacKintosh, F. C., & Koenderink, G. H. (2013). Molecular motors robustly drive active gels to a critically connected state. Nature physics, 9(9), 591-597.

Alvarado, J., Sheinman, M., Sharma, A., MacKintosh, F. C., & Koenderink, G. H. (2017). Force percolation of contractile active gels. Soft matter, 13(34), 5624-5644.

Belmonte, J. M., Leptin, M., & Nédélec, F. (2017). A theory that predicts behaviors of disordered cytoskeletal networks. Molecular systems biology, 13(9), 941.

Bendix, P. M., Koenderink, G. H., Cuvelier, D., Dogic, Z., Koeleman, B. N., Brieher, W. M., Field, C. M., Mahadevan, L. & Weitz, D. A. (2008). A quantitative analysis of contractility in active cytoskeletal protein networks. Biophysical journal, 94(8), 3126-3136.

Billington, N., Wang, A., Mao, J., Adelstein, R. S., & Sellers, J. R. (2013). Characterization of three full-length human nonmuscle myosin II paralogs. Journal of Biological Chemistry, 288(46), 33398-33410.

Brito, C., & Sousa, S. (2020). Non-muscle myosin 2A (NM2A): structure, regulation and function. Cells, 9(7), 1590.

Bueno, C., Liman, J., Schafer, N. P., Cheung, M. S., & Wolynes, P. G. (2022). A generalized Flory-Stockmayer kinetic theory of connectivity percolation and rigidity percolation of cytoskeletal networks. PLoS Computational Biology, 18(5), e1010105.

Bun, P., Dmitrieff, S., Belmonte, J. M., Nédélec, F. J., & Lenart, P. (2018). A disassembly-driven mechanism explains F-actin-mediated chromosome transport in starfish oocytes. Elife, 7, e31469.

Burlacu, S., Janmey, P. A., & Borejdo, J. (1992). Distribution of actin filament lengths measured by fluorescence microscopy. American Journal of Physiology-Cell Physiology, 262(3), C569-C577.

Bustamante, C., Chemla, Y. R., Forde, N. R., & Izhaky, D. (2004). Mechanical processes in biochemistry. Annual review of biochemistry, 73(1), 705-748.

Carlier, M. F., & Shekhar, S. (2017). Global treadmilling coordinates actin turnover and controls the size of actin networks. Nature Reviews Molecular Cell Biology, 18(6), 389-401.

Clark, A. G., Dierkes, K., & Paluch, E. K. (2013). Monitoring actin cortex thickness in live cells. Biophysical journal, 105(3), 570-580.

Cortes, D. B., Gordon, M., Nédélec, F., & Maddox, A. S. (2020). Bond type and discretization of nonmuscle myosin II are critical for simulated contractile dynamics. Biophysical journal, 118(11), 2703-2717.

Costa, K. D., Hucker, W. J., & Yin, F. C. P. (2002). Buckling of actin stress fibers: a new wrinkle in the cytoskeletal tapestry. Cell motility and the cytoskeleton, 52(4), 266-274.
Daniels, B. R., Masi, B. C., & Wirtz, D. (2006). Probing single-cell micromechanics in vivo: the microrheology of C. elegans developing embryos. Biophysical journal, 90(12), 4712-4719.

Dharan, R., Barnoy, A., Tsaturyan, A. K., Grossman, A., Goren, S., Yosibash, I., Nachmias, D., Elia, N., Sorkin, R., & Kozlov, M. M. (2025). Intracellular pressure controls the propagation of tension in crumpled cell membranes. Nature Communications, 16(1), 91.

De Belly, H., Stubb, A., Yanagida, A., Labouesse, C., Jones, P. H., Paluch, E. K., & Chalut, K. J. (2021). Membrane tension gates ERK-mediated regulation of pluripotent cell fate. Cell stem cell, 28(2), 273-284.

Derbala, M. H., Guo, A. S., Mohler, P. J., & Smith, S. A. (2018). The role of βII spectrin in cardiac health and disease. Life sciences, 192, 278-285.

Doherty, G. J., & McMahon, H. T. (2008). Mediation, modulation, and consequences of membrane-cytoskeleton interactions. Annu. Rev. Biophys., 37(1), 65-95.

Elting, M. W., Hueschen, C. L., Udy, D. B., & Dumont, S. (2014). Force on spindle microtubule minus ends moves chromosomes. Journal of Cell Biology, 206(2), 245-256.

Ennomani, H., Letort, G., Guérin, C., Martiel, J. L., Cao, W., Nédélec, F., De LA Cruz, E. Théry, M. & Blanchoin, L. (2016). Architecture and connectivity govern actin network contractility. Current Biology, 26(5), 616-626.

Frolov, N., Bijnens, B., Ruiz-Reynés, D., & Gelens, L. (2024). Dynein-driven self-organization of microtubules: An entropy-and network-based analysis. Chaos, Solitons & Fractals, 184, 115053.

Forgacs, G. (1995). On the possible role of cytoskeletal filamentous networks in intracellular signaling: an approach based on percolation. Journal of cell science, 108(6), 2131-2143.

Gardner, M. K., Zanic, M., & Howard, J. (2013). Microtubule catastrophe and rescue. Current opinion in cell biology, 25(1), 14-22.

Gittes, F., Mickey, B., Nettleton, J., & Howard, J. (1993). Flexural rigidity of microtubules and actin filaments measured from thermal fluctuations in shape. The Journal of cell biology, 120(4), 923-934.

Guo, B., & Guilford, W. H. (2006). Mechanics of actomyosin bonds in different nucleotide states are tuned to muscle contraction. Proceedings of the National Academy of Sciences, 103(26), 9844-9849.

Hodge, T., & Cope, M. J. T. (2000). A myosin family tree. Journal of cell science, 113(19), 3353-3354.

Köhler, S., & Bausch, A. R. (2012). Contraction mechanisms in composite active actin networks. PloS one, 7(7), e39869.

Kruse, K., & Jülicher, F. (2000). Actively contracting bundles of polar filaments. Physical review letters, 85(8), 1778.

Kumar, A., Quint, D. A., & Dasbiswas, K. (2023). Range and strength of mechanical interactions of force dipoles in elastic fiber networks. Soft Matter, 19(30), 5805-5823.

Landau, L. D., Pitaevskii, L. P., Kosevich, A. M., & Lifshitz, E. M. (2012). Theory of elasticity: volume 7 (Vol. 7). Elsevier.

Lee, G., Leech, G., Rust, M. J., Das, M., McGorty, R. J., Ross, J. L., & Robertson-Anderson, R. M. (2021). Myosin-driven actin-microtubule networks exhibit self-organized contractile dynamics. Science Advances, 7(6), eabe4334.

Li, J., Biel, T., Lomada, P., Yu, Q., & Kim, T. (2017). Buckling-induced F-actin fragmentation modulates the contraction of active cytoskeletal networks. Soft matter, 13(17), 3213-3220.

Linsmeier, I., Banerjee, S., Oakes, P. W., Jung, W., Kim, T., & Murrell, M. P. (2016). Disordered actomyosin networks are sufficient to produce cooperative and telescopic contractility. Nature communications, 7(1), 12615.

Lwin, P., Sindermann, A., Sutter, L., Jackson, T. W., Bonassar, L., Cohen, I., & Das, M. (2022). Rigidity and fracture of biopolymer double networks. Soft Matter, 18(2), 322-327.

Martin, A. C., Kaschube, M., & Wieschaus, E. F. (2009). Pulsed contractions of an actin–myosin network drive apical constriction. Nature, 457(7228), 495-499.

Matsudaira, P., Mandelkow, E., Renner, W., Hesterberg, L. K., & Weber, K. (1983). Role of fimbrin and villin in determining the interfilament distances of actin bundles. Nature, 301(5897), 209-214.

Meyer, R. K., & Aebi, U. (1990). Bundling of actin filaments by alpha-actinin depends on its molecular length. The Journal of cell biology, 110(6), 2013-2024.

Mofrad, M. R. (2009). Rheology of the cytoskeleton. Annual Review of Fluid Mechanics, 41(1), 433-453.

Moshtohry, M., Bellingham-Johnstun, K., Elting, M. W., & Laplante, C. (2022). Laser ablation reveals the impact of Cdc15p on the stiffness of the contractile ring. Molecular Biology of the Cell, 33(6), br9.

Mylnikov, A. P., Weber, F., Jürgens, K., & Wylezich, C. (2015). Massisteria marina has a sister: Massisteria voersi sp. nov., a rare species isolated from coastal waters of the Baltic Sea. European Journal of Protistology, 51(4), 299-310.

Narita, A., Oda, T., & Maéda, Y. (2011). Structural basis for the slow dynamics of the actin filament pointed end. The EMBO journal, 30(7), 1230–1237.

Nedelec, F., & Foethke, D. (2007). Collective Langevin dynamics of flexible cytoskeletal fibers. New Journal of Physics, 9(11), 427.

Nedrelow, D. S., Bankwala, D., Hyypio, J. D., Lai, V. K., & Barocas, V. H. (2018). Mechanics of a two-fiber model with one nested fiber network, as applied to the collagen-fibrin system. Acta biomaterialia, 72, 306-315.

Odronitz, F., & Kollmar, M. (2007). Drawing the tree of eukaryotic life based on the analysis of 2,269 manually annotated myosins from 328 species. Genome biology, 8, 1-23.

Oosawa, F. (1970). Size distribution of protein polymers. Journal of theoretical biology, 27(1), 69-86.

Palmer, A., Mason, T. G., Xu, J., Kuo, S. C., & Wirtz, D. (1999). Diffusing wave spectroscopy microrheology of actin filament networks. Biophysical journal, 76(2), 1063-1071.

Piekenbrock, T., & Sackmann, E. (1992). Quasielastic light scattering study of thermal excitations of F-actin solutions and of growth kinetics of actin filaments. Biopolymers: Original Research on Biomolecules, 32(11), 1471-1489.
Pollard, T. D., & Borisy, G. G. (2003). Cellular motility driven by assembly and disassembly of actin filaments. Cell, 112(4), 453-465.

Purcell, E. M. (2014). Life at low Reynolds number. In *Physics and our world: reissue of the proceedings of a symposium in honor of Victor F Weisskopf* (pp. 47-67).

Rao, A. N., & Baas, P. W. (2018). Polarity sorting of microtubules in the axon. Trends in neurosciences, 41(2), 77-88.

Reynolds, O. (1883). XXIX. An experimental investigation of the circumstances which determine whether the motion of water shall be direct or sinuous, and of the law of resistance in parallel channels. Philosophical Transactions of the Royal society of London, (174), 935-982.

Ross, J. L., Ali, M. Y., & Warshaw, D. M. (2008). Cargo transport: molecular motors navigate a complex cytoskeleton. Current opinion in cell biology, 20(1), 41-47.

Schallar, C. (2025). *Polymer Chemistry*. LibreTexts.

Silva, A. M., Chan, F. Y., Norman, M. J., Sobral, A. F., Zanin, E., Gassmann, R., Belmonte J.M., & Carvalho, A. X. (2022). β-heavy-spectrin stabilizes the constricting contractile ring during cytokinesis. Journal of Cell Biology, 222(1), e202202024.

Sheinman, M., Broedersz, C. P., & MacKintosh, F. C. (2012). Actively stressed marginal networks. Physical review letters, 109(23), 238101.

Sobral, A. F., Chan, F. Y., Norman, M. J., Osório, D. S., Dias, A. B., Ferreira, V., Barbosa, D. J., Cheerambathur, D., Gassmann, R., Belmonte J.M., & Carvalho, A. X. (2021). Plastin and spectrin cooperate to stabilize the actomyosin cortex during cytokinesis. Current Biology, 31(24), 5415-5428.

Stokes, G. G. (1901). On the effect of the internal friction of fluids on the motion of pendulums. Trans. Cambridge Philos. Soc., 9, 1-141.

Surrey, T., Nédélec, F., Leibler, S., & Karsenti, E. (2001). Physical properties determining self-organization of motors and microtubules. Science, 292(5519), 1167-1171.

Sveiczer, A., Novak, B., & Mitchison, J. M. (1996). The size control of fission yeast revisited. Journal of cell science, 109(12), 2947-2957.
Thoresen, T., Lenz, M., & Gardel, M. L. (2013). Thick filament length and isoform composition determine self-organized contractile units in actomyosin bundles. Biophysical journal, 104(3), 655-665.

Ueda, Y., Matsunaga, D., & Deguchi, S. (2023). Mutual interplay of actin meshwork and stress fibers in cellular adaptive response: Insights from percolation dynamics. bioRxiv, 2023-12.

Van der Vorst, H. A. (1992). Bi-CGSTAB: A fast and smoothly converging variant of Bi-CG for the solution of nonsymmetric linear systems. SIAM Journal on scientific and Statistical Computing, 13(2), 631-644.

Wang, S., & Wolynes, P. G. (2012). Active contractility in actomyosin networks. Proceedings of the National Academy of Sciences, 109(17), 6446-6451.

Wang, W. Y., Thornton, S. J., Chakraborty, B., Barth, A., Singh, N., Omonira, J., Michel, J., Das, M., Sethna, J., & Cohen, I. (2024). Rigidity transitions in anisotropic networks happen in multiple steps. arXiv preprint arXiv:2409.08565.

Walcott, S., Warshaw, D. M., & Debold, E. P. (2012). Mechanical coupling between myosin molecules causes differences between ensemble and single-molecule measurements. Biophysical journal, 103(3), 501-510.

Winder, S. J., & Ayscough, K. R. (2005). Actin-binding proteins. Journal of cell science, 118(4), 651-654.

Wisanpitayakorn, P., Mickolajczyk, K. J., Hancock, W. O., Vidali, L., & Tüzel, E. (2017). Measurement of the persistence length of cytoskeletal filaments using curvature distributions. *Biophysical Journal*, *112*(3), 566a.

Wollrab, V., Belmonte, J. M., Baldauf, L., Leptin, M., Nédeléc, F., & Koenderink, G. H. (2019). Polarity sorting drives remodeling of actin-myosin networks. Journal of cell science, 132(4), jcs219717.

Wu, X. S., Elias, S., Liu, H., Heureaux, J., Wen, P. J., Liu, A. P., Kozlov, M. M., & Wu, L. G. (2017). Membrane tension inhibits rapid and slow endocytosis in secretory cells. Biophysical journal, 113(11), 2406-2414.

Zemel, A., & Mogilner, A. (2008). Expansion and polarity sorting in Microtubule-Dynein bundles. Progress of Theoretical Physics Supplement, 173, 17-25.

Zeng, Y., Yip, A. K., Teo, S. K., & Chiam, K. H. (2012). A three-dimensional random network model of the cytoskeleton and its role in mechanotransduction and nucleus deformation. Biomechanics and modeling in mechanobiology, 11, 49-59.

APPENDIX

```
% This is a configuration file for CytoSim, an Open Source project:
% http://www.github.com/nedelec/cytosim
%
% This config creates an open space with rigid, dynamic fibers, myosin
%    like motors and point like crosslinkers.
%
% Authored by Michael Norman based on work by Julio Belmonte

%%%%%%%%%%%%%%%%%%%%%%%%%%%%%%%%%%%%%%
%Environment
%%%%%%%%%%%%%%%%%%%%%%%%%%%%%%%%%%%%%%


% Define background environments and timestep

set simul contract
{
     time_step = 0.002
     viscosity = 0.18
     kT = .0042
     display = ( style=2; point_size=2; )
}

% Define parameters for and create a circular open 2D space

set space cell
{
     geometry = ( sphere 10 )
}
new space cell

%%%%%%%%%%%%%%%%%%%%%%%%%%%%%%%%%%%%%%
% Motor Definition
%%%%%%%%%%%%%%%%%%%%%%%%%%%%%%%%%%%%%%

% Define motor head walking, binding and unbind behaviors
% max_speed is set to zero to avoid problems in initial frames
%    and will be changed later

set hand plus_motor
{
    binding = 10, 0.01
    unbinding = 0.3, inf

    hold_growing_end = 1

    hold_shrinking_end = 1

    activity = move
    max_speed = 0
    stall_force = 4

    display = ( size=2; color=green; )
}
```

```
set single motor
{
     hand = plus_motor;
     stiffness = 100;
}

%Define a hand to attach motor head to solid backbone

set hand fixer
{
     binding = 100, 0.1
     unbinding = 0, inf
     display = ( color=blue; size = 4;)
}

set single anchor
{
     hand = fixer
     stiffness = 5000
     activity = fixed
}

%Define the motor backbone

set solid minifilament
{
     display = ( coloring = 1; size = 2; style = 4; );
}

%%%%%%%%%%%%%%%%%%%%%%%%%%%%%%%%%%%%%%%%%%%%
% Crosslinker Definition
%%%%%%%%%%%%%%%%%%%%%%%%%%%%%%%%%%%%%%%%%%%%

% Define crosslinker binding and unbinding behavior

set hand binder
{
     binding = 10, 0.01
     unbinding = 0, 10
     display = ( size=2; color=blue; )

     activity = rescue
     rescue_prob = .1
}

% Create the point like crosslinker couple object

set couple crosslinker
{
     hand1 = binder
     hand2 = binder
     stiffness = 250
     diffusion = 1
```

```
}

%%%%%%%%%%%%%%%%%%%%%%%%%%%%%%%%%%%%%%%%
% Fiber Definition
%%%%%%%%%%%%%%%%%%%%%%%%%%%%%%%%%%%%%%%%

%Define the rigidity, segmentation and dynamics of the fibers

set fiber filament
{
    rigidity = 22
    segmentation = 0.1

    activity = classic
    growing_force    = 1,   1
    growing_speed    = 0.08,   0
    shrinking_speed  = -0.056,  -0.014
    catastrophe_rate = 4, 8
    rescue_rate      = 3.4, 2
    min_length       = 0.03
    max_length       = 5
    persistent       = 1

    binding_key = 1

    display = ( line_width = 1; )
}


%%%%%%%%%%%%%%%%%%%%%%%%%%%%%%%%%%%%%%%%
% Initialize Objects
%%%%%%%%%%%%%%%%%%%%%%%%%%%%%%%%%%%%%%%%

% Specify count and create crosslinkers

new 500 couple crosslinker

% Specify count and create fibers. We show both uniform and exponential
%    length options, as well as an optional equilibrate command to use
%    with flexible fibers.

new 1000 fiber filament
{
%    length = .8, exponential
    length = 1
    plus_end = grow
%    equilibrate = 10
}

% Specify count and create motor backbone with a length from -.4 to 4
% Explicitly attach motor heads at a location specified as percentage
%    along the backbone length away from minus end

new 500 solid minifilament
```

```
{
    point1 = -0.4 0 0, 0.005, motor;
    point2 = +0.4 0 0, 0.005, motor;
    anchor1 = point1, point2, 0.03, motor;
    anchor2 = point1, point2, 0.06, motor;
    anchor3 = point1, point2, 0.09, motor;
    anchor4 = point1, point2, 0.12, motor;
    anchor5 = point1, point2, 0.15, motor;
    anchor6 = point1, point2, 0.18, motor;
    anchor7 = point1, point2, 0.21, motor;
    anchor8 = point1, point2, 0.24, motor;
    anchor9 = point1, point2, 0.27, motor;
    anchor10 = point1, point2, 0.30, motor;
    anchor11 = point1, point2, 0.33, motor;
    anchor12 = point1, point2, 0.66, motor;
    anchor13 = point1, point2, 0.69, motor;
    anchor14 = point1, point2, 0.72, motor;
    anchor15 = point1, point2, 0.75, motor;
    anchor16 = point1, point2, 0.78, motor;
    anchor17 = point1, point2, 0.81, motor;
    anchor18 = point1, point2, 0.84, motor;
    anchor19 = point1, point2, 0.87, motor;
    anchor20 = point1, point2, 0.9, motor;
    anchor21 = point1, point2, 0.93, motor;
    anchor22 = point1, point2, 0.96, motor;

}

%%%%%%%%%%%%%%%%%%%%%%%%%%%%%%%%%%%%%%%%
% Run Simulation
%%%%%%%%%%%%%%%%%%%%%%%%%%%%%%%%%%%%%%%%

% Equilibrate the binding/unbinding of connectors while filaments are not
%    allowed to move:
% This ensures the simulation begins in a physically realistic
%    distribution.

run 2000 simul *
{
    solve = 0
}

% Change the max_speed so motors can walk along fibers

change hand plus_motor
{
    max_speed = 2
}

% Execute simulation for a given number of timesteps.
% Save the specified number of frames starting with frame 0.
% nb_frames must be a divisor of the total frame count to avoid errors.
% Saved frames will be equally spaced over entire simulation.
```

```
run 20000 simul *
{
   nb_frames = 5

}
```